



universität
wien

DISSERTATION

Titel der Dissertation

Characterization of the neuronal mechanisms that mediate temporal control of the courtship behaviour of *Drosophila melanogaster*.

Verfasser

Daniel Bath, BSc. MSc.

angestrebter akademischer Grad

Doctor of Philosophy (PhD)

Wien, 2014

Studienkennzahl lt. Studienblatt: A 094 490
Dissertationsgebiet lt. Studienblatt: Molekulare Biologie
Betreut von: Dr. Barry Dickson

Acknowledgements

I am grateful to a great many people who contributed to this work.

First and foremost I thank Barry Dickson for his support throughout my doctoral work. His guidance and commentary were a great source of inspiration and motivation over the years.

I would also like to thank the members of my advisory committee, Andrew Straw and Manuel Zimmer, for their helpful insight at key moments during this work.

I was lucky to collaborate with many talented people who contributed directly to the work that follows. John Stowers, in particular, was a key driving force behind the technical advancements that we achieved in Chapter 1. John's success was built upon the foundational technologies developed by Andrew Straw. I also express my gratitude to Dorothea Hörmann and Andreas Poehlmann for their valuable contributions to this work.

I thank many members and alumni of the Dickson lab. This work relies heavily on several reagents and resources developed by current and former members. I thank Jai Yu and Tianxiao Liu for their annotation and cataloguing of genetic reagents. I thank Anne von Philipsborn for sharing knowledge and reagents that were crucial to designing this project. I thank Mark Palfreyman and Joshua Lillvis for their insightful discussion.

I am grateful to the Natural Sciences and Engineering Research Council of Canada for their financial support. The work presented here was also supported by basic funding at the Institute for Molecular Pathology by Boeringher Ingelheim Fonds GmbH, and by basic funding at Janelia Research Campus by the Howard Hughes Medical Institute.

Lastly, I would like to thank David Mahringer, Katharina Roseneder, Georg Ammer & Michael Sonntag for their help and kindness during my years in Austria. Their friendship and tremendous hospitality afforded me many opportunities to experience the beautiful mountainous backdrop of my doctoral work, upon which I will look back and remember fondly for years to come.

Table of Contents

ACKNOWLEDGEMENTS	1
SYNOPSIS	4
INTRODUCTION	7
REFERENCES	13
CHAPTER 1: FLYMAD: RAPID THERMOGENETIC CONTROL OF NEURONAL	
ACTIVITY IN FREELY-WALKING <i>DROSOPHILA</i>	17
SUMMARY	17
INTRODUCTION	18
RESULTS.....	20
<i>Implementation of FlyMAD</i>	20
<i>Rapid activation and silencing of neurons</i>	22
<i>Through-the-mirror targeting of specific body parts</i>	26
<i>Temporal properties of courtship song neurons</i>	30
DISCUSSION	34
MATERIALS & METHODS	37
<i>Fly stocks</i>	37
<i>Behaviour assays</i>	38
<i>Statistics and general methods</i>	39
<i>Cameras and optical equipment</i>	40
<i>Realtime tracking and targeting architecture</i>	40
<i>TTM head and body detection</i>	42
<i>Latency and accuracy estimation</i>	43
<i>Alignment and calibration</i>	44
ACKNOWLEDGMENTS	45
REFERENCES	47
SUPPLEMENTARY MATERIAL.....	50
<i>List of supplementary videos</i>	50
<i>Supplementary figures</i>	51
CHAPTER 2: INHIBITORY NEURONS IN THE <i>FRUITLESS</i> CIRCUIT SUPPRESS	
<i>DROSOPHILA</i> COURTSHIP BEHAVIOUR	73
SUMMARY	73
INTRODUCTION	74
RESULTS.....	78

<i>A screen to identify neurons that inhibit courtship</i>	78
<i>aDT2 activity inhibits courtship</i>	80
<i>aDT2 activity is required for response to oenocyte products</i>	84
<i>aDT2 activity affects P1-dependent behaviours</i>	86
DISCUSSION	88
<i>aDT2 inhibits courtship in response to aversive courtship stimuli</i>	88
<i>The role of aDT2 in the courtship circuit</i>	90
EXPERIMENTAL PROCEDURES	93
<i>Fly stocks</i>	93
<i>Co-activation screen</i>	93
<i>Optogenetic assays</i>	93
<i>Silencing assays</i>	94
<i>Thermogenetic assays</i>	95
ACKNOWLEDGMENTS	95
REFERENCES	96
SUPPLEMENTARY MATERIAL.....	100
DISCUSSION	103
REFERENCES	110
CURRICULUM VITAE	111

Synopsis

Complex behaviours require that an animal interpret high-order information from its environment in order to respond appropriately. To generate behaviour, two important tasks of the brain are to stay engaged in the task by integrating information over time, and to select appropriate actions by consolidating sensory information. Courtship behaviour in *Drosophila melanogaster* is a complex behaviour in which a male collects and interprets intermittent sensory stimuli from a potential mate, and chooses whether or not to court. Most aspects of courtship in *Drosophila* can be induced by thermo-genetic activation of a specific class of neuron, known as P1. However, previous methods of thermo-genetic activation lacked the temporal specificity to determine the temporal relationship between P1 activation and induced courtship behaviour. Here, we develop a novel method for acute thermo-genetic manipulation in freely-moving animals, and use the method to acutely activate P1 neurons. We find that courtship persists after P1 activation ceases. We identify an inhibitory neuron, aDT2, whose activity can override the behavioural effects of activating P1 but not downstream command-like neurons. Based on these results, we hypothesize that normal courtship is driven steadily by persistent P1-dependent neuronal activity, and restricted in time by acute suppression from aDT2.

Synopse

Komplexes Verhalten erfordert von Tieren die Interpretation von Informationen höherer Ordnung aus der Umwelt, um darauf angemessen zu reagieren. Um Verhalten zu generieren, müssen zwei wichtige Elemente im Gehirn miteinander verbunden bleiben: die Integration von relevanten, sensorischen Informationen und die Auswahl der angemessenen Reaktion durch die Konsolidierung dieser akkumulierten, sensorischen Informationen.

Das Paarungsverhalten von *Drosophila melanogaster* ist ein komplexes Verhalten, in welchem ein Männchen intermittierende, sensorische Stimuli von einem potentiellen Paarungspartner sammelt und interpretiert und daraufhin entscheidet entweder zu, oder nicht zu werben. Die meisten Aspekte des Paarungsverhaltens von *Drosophila* können durch thermo-genetische Aktivierung einer spezifischen Klasse eines Neurons, bekannt als P1, eingeleitet werden. Der Nachteil früherer Methoden der thermo-genetischen Aktivierung war ein Mangel an zeitlicher Spezifität, um das zeitliche Verhältnis zwischen P1 Aktivierung und der Beibehaltung des Paarungsverhaltens zu determinieren. Hier stellen wir eine neu entwickelte Methode für die akute, thermo-genetische Manipulation in sich frei-bewegenden Tieren vor und verwenden diese Methode um das P1 Neuron akut zu aktivieren. Unsere Resultate zeigen, dass das Paarungsverhalten andauert, nachdem die Aktivierung des P1 Neurons beendet ist. Des weiteren wurde ein Neuron identifiziert, aDT2, dessen die Auswirkung der Aktivität des P1 Neurons auf das Paarungsverhalten außer Kraft setzten kann, jedoch nicht die nach P1 geschalteter Neuronen. Basierend auf diesen Resultaten, postulieren wir die Hypothese, dass das normale Paarungsverhalten durch beständige, P1-abhängige, neuronale Aktivität angetrieben und zeitlich, durch akute Suppression des aDT2 Neurons, begrenzt wird.

- Übersetzung von David Mahringer

Introduction

A fundamental goal in neuroscience is to understand the mechanisms of the neuronal computations behind complex behaviours. One naïve viewpoint (made famous by Aristotle, among others), is to consider all non-human animals to act as *automata*, bodies acting on reflexes through predictable computations of a brain. Over the past decades, however, modern neuroscience would suggest that most, if not all, animals are not *automata*, and animal behaviour is not a result of pure reflexes (Greenspan & van Swinderen, 2004). Rather, animals across phyla apprehend complex, abstract elements in their environments in order to generate appropriate and complex behaviours. Although the neuronal mechanisms are not fully understood, the generation of behaviour can be broken down into several stages from sensory input to motor output.

In order to apprehend relevant information from its environment, the brain must generate high-order representations of its surroundings from elementary information. Elementary information comes in the form of signals from sensory neurons with specialized receptors (light, chemical compounds, mechanical motion, etc). The process by which elementary information is translated to high-order representations is not fully understood, but there is evidence of neuronal representations at several levels, from perceptual, to relational, to conceptual. The best-studied example of perceptual representation is the olfactory system, which associates relevant odours with activity of olfactory receptor neurons through sparse connectivity in a network (Axel, 2005). Relational information, such as location, is also represented by

neurons, such as the hippocampal place cells or cortical grid cells that fire at specific locations in an environment as an animal explores (Fyhn, Molden, Witter, Moser, & Moser, 2004; O'Keefe & Dostrovsky, 1971). Representations of conceptual information have been identified in the human brain, in which single neurons respond selectively to the concept of individual familiar people (Quiñones-Quiroga, Kraskov, Koch, & Fried, 2009; Quiroga, Reddy, Kreiman, Koch, & Fried, 2005).

Complex representation of the environment undoubtedly requires integration of sensory information within and across modalities, as well as across time. Multisensory integration across modalities improves the salience of stimuli (Lippert, Logothetis, & Kayser, 2007; Reig & Silberberg, 2014; Stein, London, Wilkinson, & Price, 1996). Temporal integration enables the brain to relate current information to previous information on a broad range of timescales. Coincidence detectors or time delays (such as the time delay within the Reichardt motion detector (reviewed in Borst, 2014), integrate information over milliseconds. Short-term or working memory (temporary retention of information during tasks) integrates over seconds (Buhusi & Meck, 2005; Eichenbaum, 2014; Rivest, Kalaska, & Bengio, 2014). Long-term memory, as well as its recall, integrate information over longer timescales, from minutes to decades (Kandel, Dudai, & Mayford, 2014). These three examples of temporal integration enable relatively precise comparisons of the past and present.

There is a fourth method of temporal integration, however, that can drastically alter behaviour based on events in the recent past by integrating sensory information with internal state: arousal. The most prominent behaviour

with which arousal is associated is sleep (for example: Crocker & Sehgal, 2008; 2010; Shaw, Cirelli, Greenspan, & Tononi, 2000; van Swinderen, Nitz, & Greenspan, 2004), which is characterized by a reduction in general arousal relative to wakefulness. However, localized arousal plays important roles in driving specific behaviours, including reproductive, feeding, defensive, or thermoregulatory (Watts & Swanson, 2014). Localized arousal enables two important functions of animal behaviour: prolonged activity in response to an acute stimulus, and progression through a sequence of motor patterns or stages of behaviour (Jing, Gillette, & Weiss, 2009). In *Aplysia* for example, acute contact with food initiates a sequence of feeding behaviours including posture changes and gastric pumping. These behavioural changes correspond to persistent activity of an interneuron called the cerebral-pedal regulator, which fires in response to food contact and increases arousal in feeding and locomotion circuitry (Teyke, Weiss, & Kupfermann, 1991). The neuronal mechanisms that mediate arousal states generally involve persistent-acting neuromodulatory components or local circuits with modulatory transmitters (Jing et al., 2009).

Demonstrating a third role for arousal in temporal integration, studies of arousal in rodents and primates have explored the effects of arousal states on decision making in complex tasks. In the mammalian brain, arousal is mediated by the *locus coeruleus*-norepinephrine (LC-NE) system (Jouvet, 1969). In models of the LC-NE system (reviewed in (Aston-Jones & Cohen, 2005)), synchronous activity of neurons from a relevant stimulus leads to phasic release of norepinephrine by the LC neurons, and electrical coupling of LC neurons suppresses response from asynchronous stimuli. Summation of activity of the LC neurons comprises the baseline excitatory drive, which affects the gain of

downstream responding neurons. Above threshold baseline drive, the LC neurons enter a state of tonic activity, and, theoretically, allow the transmission of irrelevant distractor information. During peak performance in these tasks, baseline drive (ie arousal) is optimized such that phasic activity of LC neurons correlates strongly with decision. In monkeys, the tonic mode of LC activity is correlated with a heightened state of arousal, which includes an increased rate of false-positive errors in decision-making tasks (Aston-Jones, Rajkowski, Kubiak, & Alexinsky, 1994). Thus, it seems that state of arousal can also have an important impact on action selection.

So far, we have discussed how sensory information is summarized into a complex representation of the world by incorporating components such as arousal that drive behaviours over long times scales. For the execution of behaviour, however, the task is now inverted. That is, relatively slow-acting high-order representations guide the execution of precisely-coordinated muscle movements. To solve this problem, intricate neural networks called central pattern generators (CPGs) exist to deliver patterned activity to motor neurons from a simpler drive signal (Bässler & Büschges, 1998; Chrachri & Clarac, 1987; Kiehn, 2006). However, patterned activity from CPGs alone cannot explain complex behaviours for two reasons. First, behaviours are dynamic, so CPG-driven motor patterns need to be modified in response to ongoing stimuli. For example, human locomotion patterns are constantly updated by sensory information and drastically affected by disrupting visual or somatosensory inputs (Chien, Eikema, Mukherjee, & Stergiou, 2014). Second, execution of some complex behaviours, such as sequential behaviours, require the coordinated recruitment of sequences of distinct CPGs.

The neural mechanisms behind the execution of coordinated, dynamic behaviours are not understood. Studies of locomotion in insects have identified neurons that initiate turns or backward walking (Bidaye, Machacek, Wu, & Dickson, 2014; Ridgel, Alexander, & Ritzmann, 2007), but the neurons associated with the computation of when and to what degree locomotion should be modified remain elusive. Sequential behaviours have been studied in more depth, but have been limited to stereotyped motor programs that are induced by instantaneous, non-dynamic stimuli. For example, in gastropod escape and feeding behaviour, shared elements between escape, locomotion, and feeding CPGs induce a sequence of escape response followed by feeding (Jing et al., 2009). Consider for comparison, the behaviour of a predator chasing prey. The sequence initiated upon identifying a target as prey might be 'pounce-chase-grasp-kill'. In contrast to the feeding example from gastropods, each step in this sequence is highly variable and requires updates from sensory information. Additionally, at every step in the sequence there is the possibility of failure, which would require the predator to revert to a previous step or abort the hunt. In order to increase our understanding of complex, dynamic behaviours such as these, we focus in this work on the courtship behaviour of the fruit fly, *Drosophila melanogaster* (henceforth 'Drosophila').

Courtship behaviour in *Drosophila* is a series of complex, ritualized motor patterns exhibited by a male fly in order to attract and copulate with a receptive female (Dickson, 2008; Sokolowski, 2001). Over the course of a courtship session, the male directs stereotyped motor patterns toward the female, in a gradual progression from early to late stage behaviours. Execution of courtship behaviour likely requires many elements typically involved in higher-order brain

functions. In particular, the male fly maintains engagement in courtship behaviour despite variation in the strength and salience of stimuli. Maintenance of engagement requires integration of information across time.

In the following chapters, we identify components of behaviour execution mechanisms relating to courtship behaviour in *Drosophila*. First, we improve the temporal specificity of behaviour assays to deliver acute opto- and thermogenetic stimuli. By acutely activating neurons known to be involved in courtship, we demonstrate temporal uncoupling of neuronal activity and behavioural output. We hypothesize that this uncoupling is evidence for arousal driving courtship behaviour. Second, in order to identify neurons that are important for the control or refinement of ongoing courtship behaviour, we conduct an exploratory screen to identify inhibitory neurons involved in courtship.

References

- Aston-Jones, G., & Cohen, J. D. (2005). Adaptive gain and the role of the locus coeruleus-norepinephrine system in optimal performance. *The Journal of Comparative Neurology*, *493*(1), 99–110. doi:10.1002/cne.20723
- Aston-Jones, G., Rajkowski, J., Kubiak, P., & Alexinsky, T. (1994). Locus coeruleus neurons in monkey are selectively activated by attended cues in a vigilance task. *The Journal of Neuroscience : the Official Journal of the Society for Neuroscience*, *14*(7), 4467–4480.
- Axel, R. (2005). Scents and sensibility: a molecular logic of olfactory perception (Nobel lecture). *Angewandte Chemie (International Ed. in English)*, *44*(38), 6110–6127. doi:10.1002/anie.200501726
- Bässler, U., & Büschges, A. (1998). Pattern generation for stick insect walking movements--multisensory control of a locomotor program. *Brain Research. Brain Research Reviews*, *27*(1), 65–88.
- Bidaye, S. S., Machacek, C., Wu, Y., & Dickson, B. J. (2014). Neuronal control of Drosophila walking direction. *Science*, *344*(6179), 97–101. doi:10.1126/science.1249964
- Borst, A. (2014). In search of the holy grail of fly motion vision. *European Journal of Neuroscience*. doi:10.1111/ejn.12731
- Buhusi, C. V., & Meck, W. H. (2005). What makes us tick? Functional and neural mechanisms of interval timing. *Nature Reviews Neuroscience*, *6*(10), 755–765. doi:10.1038/nrn1764
- Chien, J. H., Eikema, D.-J. A., Mukherjee, M., & Stergiou, N. (2014). Locomotor Sensory Organization Test: A Novel Paradigm for the Assessment of Sensory Contributions in Gait. *Annals of Biomedical Engineering*, 1–12. doi:10.1007/s10439-014-1112-7
- Chrachri, A., & Clarac, F. (1987). Induction of rhythmic activity in motoneurons of crayfish thoracic ganglia by cholinergic agonists. *Neuroscience Letters*, *77*(1), 49–54.
- Crocker, A., & Sehgal, A. (2008). Octopamine regulates sleep in drosophila through protein kinase A-dependent mechanisms. *The Journal of Neuroscience : the Official Journal of the Society for Neuroscience*, *28*(38), 9377–9385. doi:10.1523/JNEUROSCI.3072-08a.2008
- Crocker, A., & Sehgal, A. (2010). Genetic analysis of sleep. *Genes & Development*, *24*(12), 1220–1235. doi:10.1101/gad.1913110
- Dickson, B. J. (2008). Wired for sex: the neurobiology of Drosophila mating decisions. *Science*, *322*(5903), 904–909. doi:10.1126/science.1159276

- Eichenbaum, H. (2014). Time cells in the hippocampus: a new dimension for mapping memories. *Nature Reviews Neuroscience*, *15*(11), 732–744. doi:10.1038/nrn3827
- Fyhn, M., Molden, S., Witter, M. P., Moser, E. I., & Moser, M.-B. (2004). Spatial representation in the entorhinal cortex. *Science*, *305*(5688), 1258–1264. doi:10.1126/science.1099901
- Greenspan, R. J., & van Swinderen, B. (2004). Cognitive consonance: complex brain functions in the fruit fly and its relatives. *Trends in Neurosciences*, *27*(12), 707–711. doi:10.1016/j.tins.2004.10.002
- Jing, J., Gillette, R., & Weiss, K. R. (2009). Evolving concepts of arousal: insights from simple model systems. *Reviews in the Neurosciences*, *20*(5-6), 405–427.
- Jouvet, M. (1969). Biogenic amines and the states of sleep. *Science*, *163*(3862), 32–41.
- Kandel, E. R., Dudai, Y., & Mayford, M. R. (2014). The molecular and systems biology of memory. *Cell*, *157*(1), 163–186. doi:10.1016/j.cell.2014.03.001
- Kiehn, O. (2006). Locomotor circuits in the mammalian spinal cord. *Annual Review of Neuroscience*, *29*, 279–306. doi:10.1146/annurev.neuro.29.051605.112910
- Lippert, M., Logothetis, N. K., & Kayser, C. (2007). Improvement of visual contrast detection by a simultaneous sound. *Brain Research*, *1173*, 102–109. doi:10.1016/j.brainres.2007.07.050
- O'Keefe, J., & Dostrovsky, J. (1971). The hippocampus as a spatial map. Preliminary evidence from unit activity in the freely-moving rat. *Brain Research*, *34*(1), 171–175.
- Quian Quiroga, R., Kraskov, A., Koch, C., & Fried, I. (2009). Explicit encoding of multimodal percepts by single neurons in the human brain. *Current Biology : CB*, *19*(15), 1308–1313. doi:10.1016/j.cub.2009.06.060
- Quiroga, R. Q., Reddy, L., Kreiman, G., Koch, C., & Fried, I. (2005). Invariant visual representation by single neurons in the human brain. *Nature*, *435*(7045), 1102–1107. doi:10.1038/nature03687
- Reig, R., & Silberberg, G. (2014). Multisensory integration in the mouse striatum. *Neuron*, *83*(5), 1200–1212. doi:10.1016/j.neuron.2014.07.033
- Ridgel, A. L., Alexander, B. E., & Ritzmann, R. E. (2007). Descending control of turning behavior in the cockroach, *Blaberus discoidalis*. *Journal of Comparative Physiology a: Sensory, Neural, and Behavioral Physiology*, *193*(4), 385–402. doi:10.1007/s00359-006-0193-7

- Rivest, F., Kalaska, J. F., & Bengio, Y. (2014). Conditioning and time representation in long short-term memory networks. *Biological Cybernetics*, *108*(1), 23–48. doi:10.1007/s00422-013-0575-1
- Shaw, P. J., Cirelli, C., Greenspan, R. J., & Tononi, G. (2000). Correlates of sleep and waking in *Drosophila melanogaster*. *Science*, *287*(5459), 1834–1837.
- Sokolowski, M. B. (2001). *Drosophila*: genetics meets behaviour. *Nature Reviews Genetics*, *2*(11), 879–890. doi:10.1038/35098592
- Stein, B. E., London, N., Wilkinson, L. K., & Price, D. D. (1996). Enhancement of perceived visual intensity by auditory stimuli: a psychophysical analysis. *Journal of Cognitive Neuroscience*, *8*(6), 497–506. doi:10.1162/jocn.1996.8.6.497
- Takemura, S.-Y., Bharioke, A., Lu, Z., Nern, A., Vitaladevuni, S., Rivlin, P. K., et al. (2013). A visual motion detection circuit suggested by *Drosophila* connectomics. *Nature*, *500*(7461), 175–181. doi:10.1038/nature12450
- Teyke, T., Weiss, K. R., & Kupfermann, I. (1991). Activity of identified cerebral neuron correlates with food-induced arousal in *Aplysia*. *Neuroscience Letters*, *133*(2), 307–310.
- van Swinderen, B., Nitz, D. A., & Greenspan, R. J. (2004). Uncoupling of brain activity from movement defines arousal States in *Drosophila*. *Current Biology*, *14*(2), 81–87.
- Watts, A. G., & Swanson, L. W. (2014). Anatomy of Motivation. In H. Pashler & R. Gallistel, *Handbook of Experimental Psychology*.

Chapter 1: FlyMAD: Rapid thermogenetic control of neuronal activity in freely-walking *Drosophila*

Summary

Rapidly and selectively modulating the activity of defined neurons in unrestrained animals is a powerful approach in investigating the circuit mechanisms that shape behaviour. In *Drosophila*, temperature-sensitive silencers and activators are widely used to control the activities of genetically-defined neuronal cell types. A limitation of these thermogenetic approaches, however, has been their poor temporal resolution. Here, we introduce FlyMAD (the Fly Mind Altering Device) which allows thermogenetic silencing or activation within seconds or even fractions of a second. Using computer vision, FlyMAD targets an infrared laser to freely-walking flies. As a proof-of-principle, we demonstrate the rapid silencing and activation of neurons involved in locomotion, vision, and courtship. The spatial resolution of the focused beam enables preferential targeting of neurons in the brain or ventral nerve cord. Moreover, the high temporal resolution of FlyMAD allowed us to discover distinct timing relationships for two neuronal cell types previously linked to courtship song.

Introduction

Methods to modulate activity in genetically-defined cell types are essential for establishing relationships between neuronal activity and behaviour. Such methods are most informative when applied to behaving animals with high spatial and temporal resolution. High spatial resolution can generally be provided by genetic methods (Pfeiffer *et al.*, 2008; Jenett *et al.*, 2012), though with considerable limitations. Temporal resolution, however, is constrained by the properties of the genetically-encoded effectors and the external stimuli used to control them. To characterize distinct neuronal types in a common behaviour, it is desirable to have two or more orthogonal systems to independently and acutely modulate activity of multiple cell types in the same animal.

Light-gated optogenetic tools are commonly used to acutely modulate neuronal activity (Lima & Miesenböck, 2005; Boyden *et al.*, 2005). They offer high temporal precision, revolutionizing the functional analysis of neural circuits and behaviour. Nonetheless, using light as an external trigger poses several challenges. Spectral overlap with photoreceptors of the eye (Heisenberg & Buchner, 1977) can cause flash blindness or trigger artifactual visual responses, and surrounding tissue can limit light penetration to the target region. For larger animals, such as rodents, optic fibers can be used to deliver light to deeper tissue without constraining movement (Aravanis *et al.*, 2007). Such fibre optic systems would however disrupt movement of smaller animals, such as adult *Drosophila melanogaster*. This problem may be alleviated by the use of higher light intensities. Red-shifted optogenetic tools provide another solution, with the deeper penetration of longer wavelength light and greater spectral separation

from fly visual sensitivity. While progress in the development of red-shifted channelrhodopsins has been reported (Lin *et al.*, 2013; Inagaki *et al.*, 2013; Klapoetke *et al.*, 2014), independent and bidirectional optogenetic control of multiple cell types in behaving flies is not yet possible.

Fortunately, ectotherms such as *Drosophila* allow the alternative approach of thermogenetics, which exploits temperature-gated ion channels and other proteins to activate or silence neurons (Bernstein, Garrity, & Boyden, 2012). As a trigger, temperature is orthogonal to light, and for small animals, heat can be applied without physical manipulation of the animal. The challenge with thermogenetics, however, has been poor temporal resolution. Typical protocols use convection heating of the environment. Radiant heating with infrared light can greatly improve the kinetics of thermogenetic modulation, but this requires precise targeting of a focused laser beam. Thus far, this method has only been applied to immobilized flies (Keene & Masek, 2012; Marella, Mann & Scott, 2012).

Here we present FlyMAD (Fly Mind-Altering Device) that overcomes this problem by focusing a laser on a freely-walking fly. FlyMAD uses real-time video tracking to determine animal position and target the laser. Using a dichroic mirror, a second camera provides high-resolution videos for behavioural analysis and allows through-the-mirror (TTM) tracking to target the laser to specific body parts. Used with an infrared laser to apply heat, FlyMAD brings high temporal and spatial resolution to the thermogenetic investigation of neuronal activity and behaviour in *Drosophila*. By incorporating an additional visible-light laser, the system is also suitable for optogenetic activation, enabling

rapid and independent activity modulation of distinct cell types in the same animal.

Results

Implementation of FlyMAD

In FlyMAD (**Fig. 1a**, **Supplementary Figs. 1 and 2**, **Supplementary Video 1**), flies walk freely in a 9cm circular chamber with a transparent cover. The chamber is concave (Simon & Dickinson, 2010), so that the fly maintains a constant distance from a galvanometer mounted 10cm above the chamber. The position of the fly is determined by real-time tracking through a camera with a view of the entire arena mounted next to the galvanometer (Straw & Dickinson, 2009) (**Figs. 1b,c**) and these coordinates are used to control galvanometer mirrors that target the laser beam directly at the fly. To facilitate low-latency tracking, image processing is simplified by uniformly illuminating the background (**Supplementary Fig. 2**). The tracking algorithm (described in Online Methods) is capable of tracking multiple flies simultaneously (**Fig. 1c**); the laser is automatically targeted to the first fly detected by default (**Supplementary Fig. 3**). A second camera is aligned with the laser beam, imaging the fly through-the-mirror (TTM; **Fig. 1d**) to provide high-resolution videos for behavioural analysis. These high-resolution images can also be used to further refine the laser position (TTM tracking). An archive of the software is included in the Supplementary Information and can be obtained from <http://flymad.strawlab.org>.

The reliability of the laser targeting depends on the speed and precision with which the tracking system can respond to changes in the fly's motion (**Supplementary Figs. 4 and 5**). Without TTM tracking, we estimated the

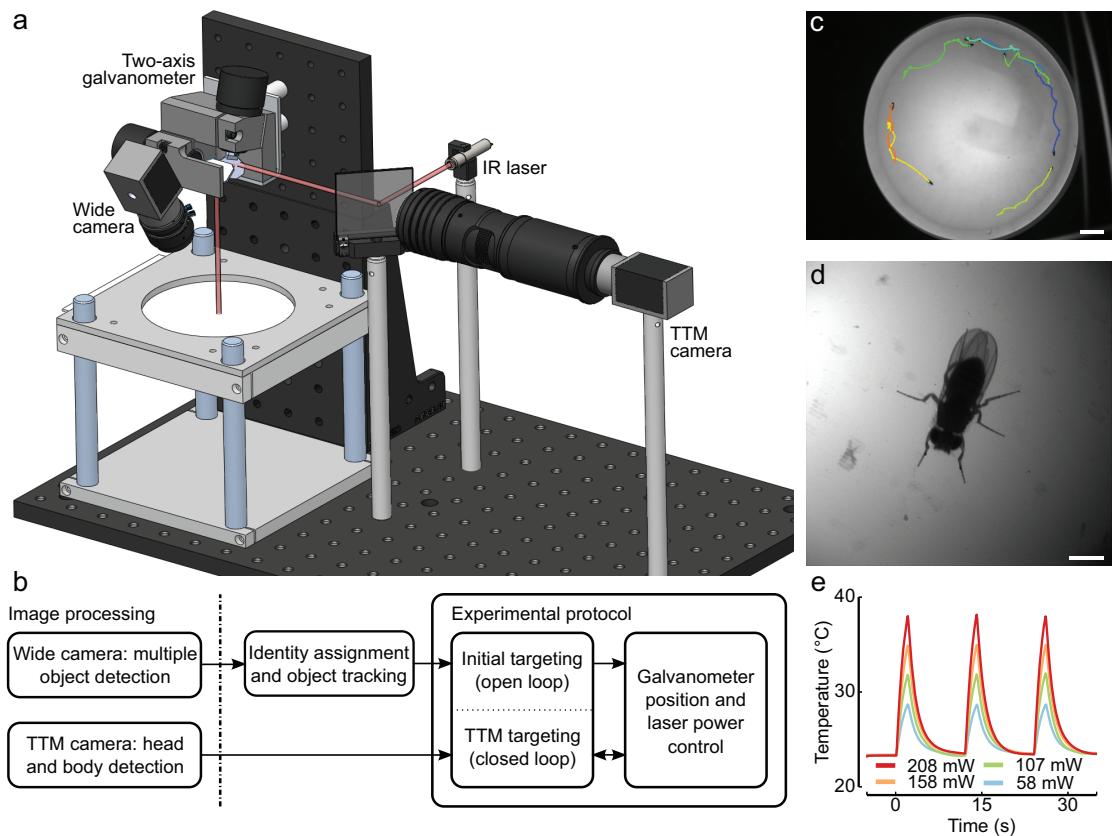


Figure 1 System overview.

- (a)** Drawing of selected components. Red line denotes the optical beam path of the IR laser. (rendering by John R. Stowers)
- (b)** Schematic representation of the information flow within the tracking, galvanometer and laser control systems (schematic by John R. Stowers)
- (c)** Widefield view of the arena through the tracking camera and tracked trajectories of several flies. Scale bar, 1 cm. (photograph by John R. Stowers)
- (d)** Higher magnification TTM (through-the-mirror) view of the targeted fly. Scale bar, 1 mm.
- (e)** Temperature changes inside the thorax of an immobilized fly upon IR stimulation at a range of laser powers (14 day old male fly, unfocused 808 nm laser).

average latency between the software command and the laser illumination to be ~32 msec, and the spatial accuracy to be 0.8 mm (Online Methods). We measured the temperature inside the thorax of an immobilized fly at a range of laser conditions (**Fig. 1e**, **Supplementary Fig. 6**). Using unfocused light, temperatures reached are comparable to thresholds reported in conventional thermogenetic experiments (Pulver *et al.*, 2009). With focused light, the laser powers used in our study deliver greater temperature changes than are typically used in thermogenetic studies. A moving fly may not be as efficiently heated due to residual targeting error (**Supplementary Fig. 5**) and small beam diameter (**Supplementary Fig. 7**); measurements from a stationary fly represent an upper-bound for a mobile fly.

Rapid activation and silencing of neurons

To test the efficacy of FlyMAD for rapid thermogenetic modulation of neuronal activity and behaviour, we first examined locomotor behaviour with wide-field tracking. An 808nm diode laser was slightly defocused to cover the whole body with a ~ 4.0x1.7mm rectangular spot in our video image. We used the GAL4/UAS system (Brand & Perrimon, 1993) to target specific neurons and either silence (using *Shibire^{TS1}*, Kitamoto, 2001; Grigliatti *et al.*, 1973; Poodry & Edgar, 1979) or activate (using *TrpA1*, Viswanath *et al.*, 2003; Hamada *et al.*, 2008) at temperatures above 25°C.

We predicted that silencing all motoneurons should disrupt locomotion. We silenced the motoneurons by expressing *UAS-shi^{ts}* under the control of *DVGlut-GAL4* (*OK371-GAL4*, Mahr & Aberle, 2006). For control flies, we observed an immediate and transient (< 1s) decrease in speed followed by a more

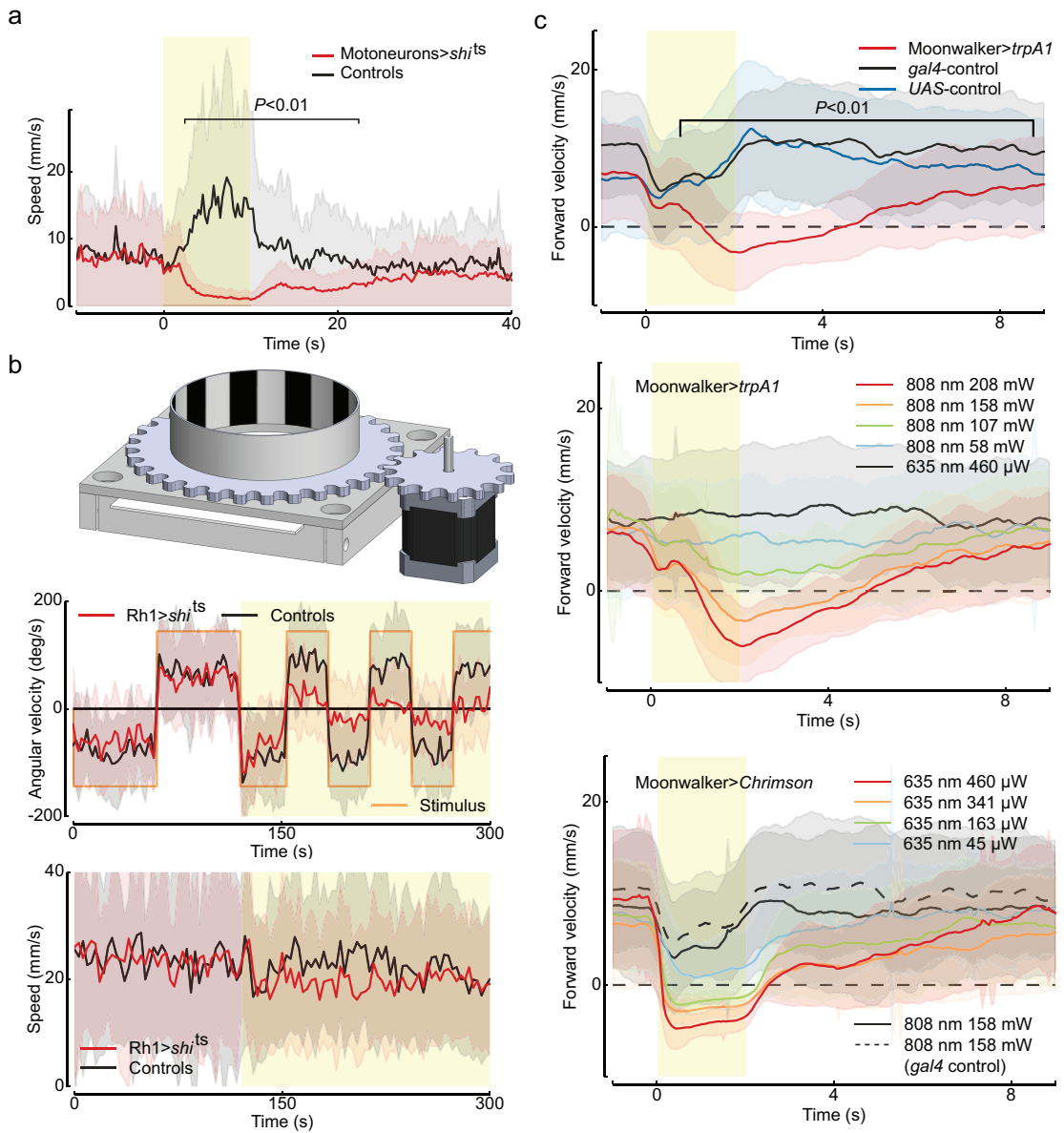
sustained (>10s) and pronounced increase in speed (**Fig. 2a**). We interpret these locomotion effects as aversive reactions to heat. In contrast, in experimental flies, locomotion decreased even further after the immediate aversive response, being significantly slower than control flies within just 2.5 seconds ($P<0.01$, **Supplementary Fig. 8a**, and **Supplementary Video 2**). The locomotion of experimental flies returned to baseline within 12.5 seconds after the laser was turned off.

Next we examined the optomotor response, an innate behaviour in which a fly turns toward visual motion. This response is mediated by the R1-6 photoreceptors (Yamaguchi et al, 2008), so silencing photoreceptors with *Shi^{ts}* should eliminate the optomotor response. Using the *Rh1-Gal4* driver line (Ellis, O'Neill, & Rubin, 1993), we expressed *UAS-shi^{ts1}* in R1-R6 and recorded turning rate as we induced the optomotor response by presenting a high-contrast rotating grating around the edge of the arena (**Fig. 2b**). Prior to laser activation, mean angular velocity of both control and experimental flies correlated with direction of the rotating visual stimulus. Upon stimulation, mean angular velocity of experimental flies was significantly reduced ($P<0.001$, **Supplementary Table 1**, **Supplementary Video 3**), although overall velocity remained unchanged.

For activation experiments, we targeted the “moonwalker” neurons with *VT50660-GAL4* (Bidaye et al., 2014). The activity of these neurons is both necessary and sufficient to trigger backward walking. In control flies lacking the *UAS-trpA1* effector or the *GAL4* driver, laser activation induced a rapid transient decrease followed by an increase in forward velocity, again reflecting the aversive heat response (**Fig. 2c**). By contrast, forward velocity of *VT50660-GAL4 UAS-trpA1* flies continued to decrease and differed from controls within 0.75s of

Figure 2 Behavioral responses to acute neuronal silencing and activation.

- (a)** Silencing motoneurons with *Shi^{ts}*. Speeds of *OK371-GAL4/UAS-shi^{ts}* (red) and *+/UAS-shi^{ts}* (black) flies (n = 25 and 19 flies, respectively, one trial each), 10s stimulation. *P* values computed using two-tailed Kruskal Wallis test.
- (b)** Silencing photoreceptors. Upper panel shows rotating grating apparatus to induce optomotor response. Middle panel shows angular velocity of *Rh1-GAL4/UAS-shi^{ts}* (red) and pooled *Rh1-GAL4/+* and *UAS-shi^{ts}/+* (black) flies presented with a rotating grating (n=18 and 9+12, respectively). Angular velocity of the grating is indicated by the orange square wave. Lower panel shows translational speed before and during stimulus. (by Dorothea Hörmann)
- (c)** Activating moonwalker neurons. Upper panel shows forward velocity of *VT50660-GAL4/UAS-TrpA1* (red, n=11 flies, 10 trials per fly) and *+/UAS-trpA1* (blue, n=10 flies, 10 trials each) and *VT50660-GAL4/+*; (black, n=9 flies, 10 trials each). Forward velocity is the component of locomotion speed toward the fly's head. *P* values computed using two-tailed Kruskal Wallis test. Middle panel shows dose response activation of *VT50660-GAL4/UAS-trpA1* using 808 nm IR laser at varying power (n=10 flies per condition), and 635 nm red laser at high power (n=10). Lower panel shows dose response activation of *VT50660-GAL4/UAS-Chrimson* using 635 nm red laser at varying power (n=10 flies per condition), and 808nm IR laser at 158mW (n=10). In all panels, yellow shaded region indicates time of IR or red stimulation, solid lines indicate mean values, and corresponding color shadings represent s.d.



laser activation ($P < 0.01$, **Supplementary Fig. 8**), becoming negative within 1.0s (**Supplementary Video 4**). Locomotion returned to control velocity within 6.8 s after the laser was turned off. FlyMAD thus allows rapid and reversible neuronal activation with TrpA1.

Recently, acute activation of freely-moving flies has also been demonstrated with optogenetic techniques, using red-shifted channelrhodopsins Chrimson (Klapoetke *et al.*, 2014) and ReaChR (Inagaki *et al.*, 2013). We used the moonwalking assay to test the orthogonality of optogenetic and thermogenetic activation strategies. *VT50660-GAL4 UAS-trpA1* flies showed neither aversive slowing nor backward walking in response to stimulation with 635nm, but walked backwards in response to the 808nm laser (**Fig. 2c** middle, $p < 0.001$, full traces and statistical analyses in **Supplementary Figs. 9-12**). *VT50660-GAL4 UAS-Chrimson* flies walked backwards when exposed to 635nm light (**Fig. 2c** lower, $p < 0.001$). The 808nm IR laser did not induce backward walking in these flies, and the aversive response was not different than control flies (**Fig. 2c** lower, $p > 0.05$, Supplementary Fig. 9e). These data demonstrate the potential for FlyMAD to be used in experiments that combine thermogenetics and optogenetics to independently control the activity of two distinct sets of neurons.

Through-the-mirror targeting of specific body parts

Infrared heating can deliver body region-specific thermogenetic modulation when targeted with a focused beam (Keene & Masek, 2012). For more precise targeting with FlyMAD, we implemented a through-the-mirror (TTM) tracking system, which uses the high-resolution camera axially aligned with the laser beam. In this mode, the laser was focused to a 105 μ m diameter

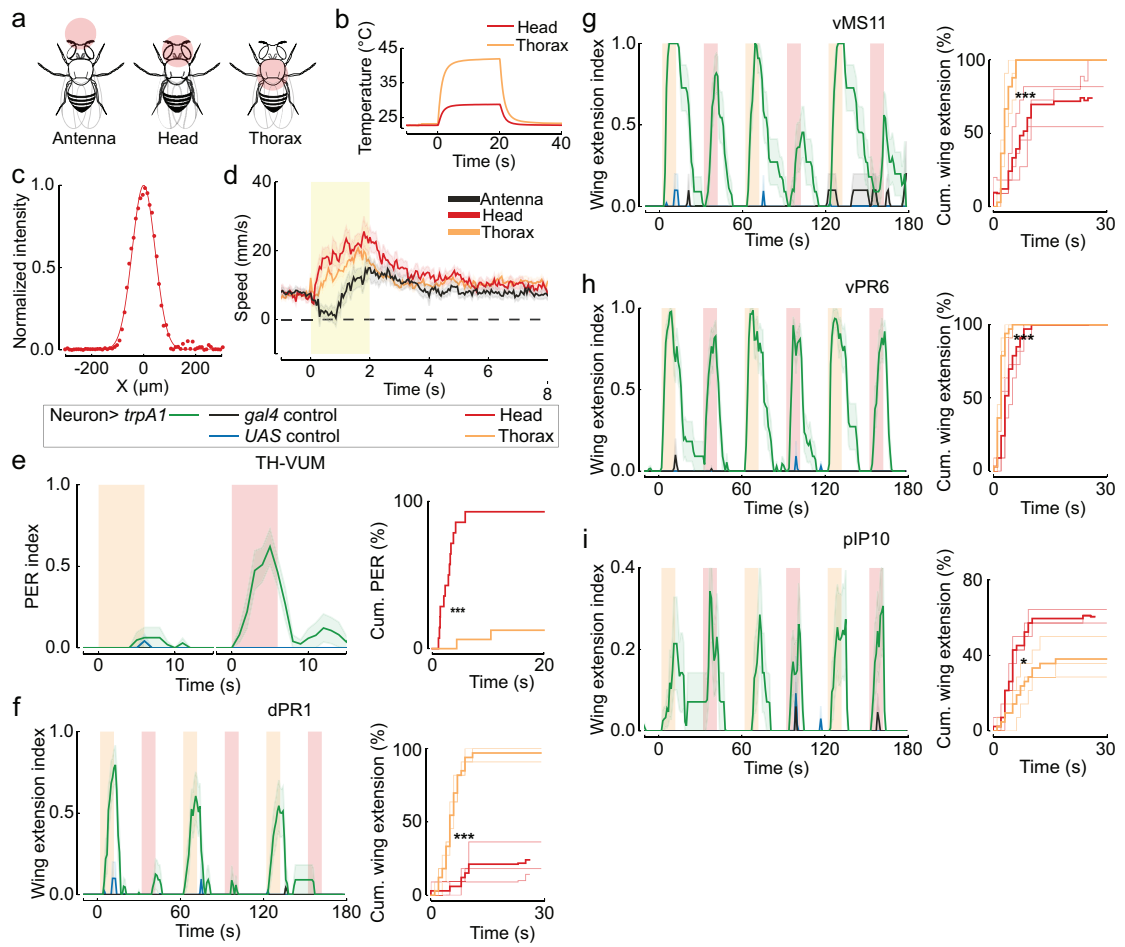
spot (**Fig. 3a-c, Supplementary Fig. 7**). Using template-matching image processing, we could target the laser beam directly at specific body parts – such as antennae, head or thorax (**Supplementary Video 5**). Post-hoc analysis of saved TTM images during thorax targeting showed a mean initial tracking error of 300 μ m at 50ms latency. Upon continual TTM tracking, mean tracking error improved to \sim 100 μ m by 100ms over a range of velocities (**Online Methods and Supplementary Fig. 5**). We compared thorax temperature in stationary head-targeted and thorax-targeted fly bodies (**Fig. 3b**). Due to the size of the thermocouple, we were unable to measure temperature in the head.

We first tested whether TTM targeting could ameliorate the heat aversion response by comparing the effect of TTM-targeting a 2-second laser pulse to the antennae, head, or thorax on the locomotion of wild-type flies. The transient slowing response was observed only upon antennal targeting ($P < 0.05$, **Fig. 3d, Supplementary Fig. 13**), consistent with reports that antennal heat receptors are involved in a rapid heat response (Ni *et al.*, 2013; Tang *et al.*, 2013). The subsequent acceleration was observed in all three TTM conditions, but most pronounced for head targeting. This response might reflect activation of the anterior cell (AC) neurons within the head which express endogenous TrpA1 (Hamada *et al.*, 2008; Gallio *et al.*, 2011).

One potential application of TTM targeting is to preferentially activate neurons in the head or thorax. To explore this possibility, we examined the proboscis extension reflex (PER) and production of courtship song. PER can be elicited by activation of TH-VUM, a dopaminergic neuron in the brain (Marella, Mann & Scott, 2012). Using *TH-GAL4*, which is expressed in dopaminergic neurons of both the brain and VNC, we found that PER was induced more rapidly

Figure 3 Body-part specific targeting using TTM tracking.

- (a) Schematic of laser target location on the fly. Drawing modified from original © 2011 DBCLS Licensed under CC 2.1.
- (b) Temperatures measured in the thorax of a 14 day old male fly during a 20s IR light pulse targeted at the head or thorax.
- (c) Laser spot intensity with Gaussian fit FWHM of 105 μm . (by Andreas Poehlmann)
- (d) Mean and s.e.m. speed of wild-type CantonS flies in response to TTM targeting directed at the antennae, head, or thorax (n=3-5 flies, 10 trials per fly) (by Dorothea Hörmann).
- (e) PER index and cumulative incidence plot of *TH-GAL4 UAS-TrpA1* and pooled *TH-GAL4/+* and *UAS-TrpA1/+* flies exhibiting proboscis extension reflex (PER) during a 6s, 20 mW laser pulse targeted to the head or thorax (n=14-16) (by Dorothea Hörmann).
- (f-i) Wing extension indices and cumulative incidence plots during alternating 10s IR, 20mW pulses directed at the head (red) or thorax (orange). Green traces are experimental genotypes, black traces are the *GAL4* driver alone, and blue traces are *UAS-trpA1* alone. *, $P < 0.05$, *** $P < 0.001$, logrank test. n = 7-17 flies, 3 head and 3 thorax trials each (pooled in thick lines in cumulative wing extension plots). Red lines show head targeting and orange show thorax targeting. For all plots, yellow shaded region indicates time of IR stimulation, solid lines represent mean values, and colored shaded regions represent s.e.m.



and robustly during head targeting than thorax targeting ($P < 0.001$, **Fig. 3e**, **Supplementary Table 2**, **Supplementary Video 6**). Courtship song can be elicited by optogenetic or thermogenetic activation of *fruitless* expressing neurons (Clyne & Miesenböck, 2008) including the descending neuron pIP10, or the VNC neurons dPR1, vPR6 and vMS11 (von Philipsborn *et al.*, 2011). For the thoracic song neurons, we tested using restricted *GAL4* drivers and alternately targeted the laser to the head or thorax (**Figs. 3f-h**). Compared to head targeting, thorax targeting elicited wing extension with lower latency, higher frequency, or both ($P < 0.001$, **Fig. 3f-h**, **Supplementary Table 2**, **Supplementary Video 7**). For the descending neuron pIP10, targeting the head induced a slightly more rapid response ($P < 0.05$, **Fig. 3i**, **Supplementary Table 2**), but overall levels of wing extension were similar in the head- and thorax-targeted trials (**Fig. 3i**). While the resolution of this method is inevitably limited by targeting inaccuracies and gradual transfer of heat from one body part to another, these experiments nonetheless demonstrate that TTM-targeting can localize thermogenetic control to specific regions in a moving fly.

Temporal properties of courtship song neurons

The improved kinetics of thermogenetics afforded by FlyMAD make it possible to distinguish between neuronal activities that relate to persistent behavioural states versus those associated with transient motor actions. We explored this issue in the context of courtship behaviour. Conventional thermogenetic experiments have demonstrated that activating either P1 or pIP10 triggers courtship song (von Philipsborn *et al.*, 2011; Kohatsu, Koganezawa, & Yamamoto, 2011), and that P1 induces other components of

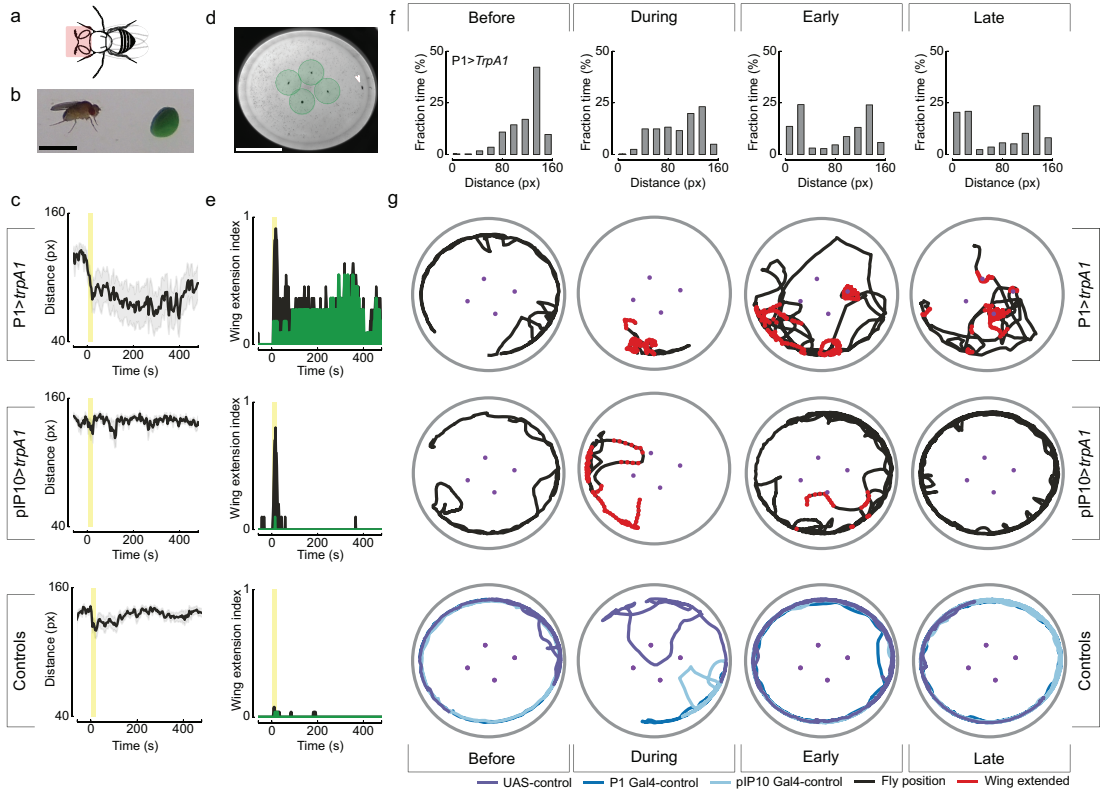
courtship behaviour including following (Kohatsu, Koganezawa, & Yamamoto, 2011). pIP10 neurons are potentially post-synaptic to P1 in the brain and innervate the wing neuropil of the ventral nerve cord (Yu *et al.*, 2010). FlyMAD allowed us to examine whether activation of each cell type induces a courtship-like state, in which song would be triggered by (but temporally uncoupled from) the laser stimulus, or the specific action of singing, in which case song would be time locked to the laser stimulus.

In these experiments, we placed fly-size plasticine targets in the chamber to serve as surrogate courtship targets (**Fig. 4**). P1 neurons were targeted using the genetic intersection of *NP2361-GAL4* and *fru^{FLP}* (Yu *et al.*, 2010) and pIP10 as the intersection of *VT40347-GAL4* and *fru^{FLP}* (**Supplementary Fig. 14**), in both cases driving the combinatorial effector *UAS>stop>trpA1^{myc}* (von Philipsborn *et al.*, 2011; *>stop>* indicates a transcriptional stop cassette that can be excised by FLP recombinase).

As predicted (von Philipsborn *et al.*, 2011; Kohatsu, Koganezawa, & Yamamoto, 2011), acute activation of either P1 or pIP10 in FlyMAD induced wing extension within 5 seconds ($P < 0.05$, **Fig. 4e**, **Supplementary Fig. 15**, and **Supplementary Videos 8** and **9**). In the case of pIP10 activation, wing extension ceased within 10 seconds when the laser was turned off ($P > 0.05$, **Fig. 4e**). In contrast, wing extension triggered by P1 activation persisted intermittently for at least 5 minutes ($P < 0.05$). In both cases, most wing extensions elicited during laser stimulation were not directed towards the targets; the flies generally remained near the periphery of the arena. Indeed, for pIP10 activation, the average distance to the nearest target did not change during the course of the experiment (**Fig. 4c**). Following P1 activation, however, the fly increasingly spent more time

Figure 4 Acute activation of courtship neurons.

- (a)** Location of IR stimulation. Drawing modified from original © 2011 DBCLS Licensed under CC 2.1.
- (b)** Fly approaching a plasticine ball. Scale bar, 3 mm.
- (c)** Mean (solid line) and s.e.m. (shading) of distance to the nearest target. Yellow shaded region represents time of 20 second IR stimulation.
- (d)** The shaded region indicates proximal zone, 50 pixel radius from the plasticine targets. Scale bar, 3 cm.
- (e)** Total (black) and proximal (green) wing extension indices.
- (f)** Distance to nearest target for P1>TrpA1 flies during the 60s period before stimulus (“Before”), the 20s laser pulse (“During”), the first 220s after stimulus (“Early”) and 220 to 440s after stimulus (“Late”)
- (g)** Representative position traces of single flies. Black, purple or blue indicates fly trajectory, red indicates wing extension. Purple points are location of plasticine balls. Genotypes are as follows: P1>TrpA1: *+/UAS>stop>TrpA1^{myc} NP2361-GAL4;fru^{FLP}* (n=11, black); pIP10>TrpA1: *+/UAS>stop>trpA1^{myc};fru^{FLP}/VT40347-GAL4* (n=10, black): Controls: pooled data from *+/UAS>stop>TrpA1^{myc};fru^{FLP}* (n = 9, purple), *+/NP2361-GAL4/+* (n=7, dark blue), and *+/VT40347-GAL4/+* (n=10, light blue).



near the target ($p < 0.01$, **Fig. 4c**, **Supplementary Fig. 15d**). We classified ‘proximal’ and ‘distal’ position using a threshold defined by the bimodal distribution of P1-activated flies relative to targets (**Fig. 4f**). Most wing extensions during the stimulus period occurred when the fly was distant from a target (**Fig. 4c,e**). During the post-stimulus period wing extensions increasingly occurred close to a target ($P < 0.0001$, Chi-squared test, **Supplementary Table 3**) and often appeared to be directed specifically at the target (**Supplementary Video 8**). These data suggest that, just as normal courtship behaviour unfolds as a gradual progression between distinct component actions, the persistent courtship induced by direct activation of P1 is also a dynamic state.

Discussion

FlyMAD directs an infrared laser beam onto freely walking flies using low-latency realtime computer vision, thereby dramatically improving the temporal resolution possible in thermogenetic experiments. Using convection heating, silencing with *Shi^{ts}* has been shown to produce behavioural effects within 60 seconds (Kitamoto, 2001), and *TrpA1* kinetics are tightly correlated with crossing threshold temperatures (Pulver *et al.*, 2009). With FlyMAD, we have drastically reduced these latencies, with behavioural changes occurring within just a few seconds, or even fractions of a second. This time course compares favorably with that normally achieved using optogenetic approaches.

With FlyMAD, neuronal activity can be controlled by either heat or light. This versatility is important for several reasons. First, until long-wavelength optogenetic silencers are developed, FlyMAD and *Shi^{ts}* is the only option for acute silencing in behaving flies. Second, infrared light penetrates deeper,

scatters less, interferes less with visual responses than red light, making fast thermogenetics with FlyMAD an attractive alternative to red-shifted optogenetic tools in experiments where these factors might be critical. Third, and most importantly, in cases where both optogenetics and thermogenetics can be applied, FlyMAD can combine both approaches to independently modulate the activity of distinct cell types in the same experiment. Such dual control will introduce many new possibilities. One can imagine, for example, modulating the activity of one type of neuron contingent upon a behaviour observed upon modulation of a different class of neuron, either in the same fly or another fly in the same arena.

The importance of high temporal resolution in thermogenetic experiments is exemplified here by our analysis of courtship neuron activation. Most complex behaviours, such as courtship, involve the integration of multiple sensory cues and coordinated, timely execution of multiple actions. These actions might unfold over relatively long time scales, during which time the specific sensory cues might be only intermittently present. With no precise temporal coupling between specific sensory cues and motor patterns, it thus becomes imperative to discern whether any neuronal activity is temporally coupled to the presence of specific sensory inputs or the execution of specific actions, or might instead represent a more persistent state that is independent of moment-to-moment sensation and action.

In the context of courtship song, thermogenetic experiments relying on convection heating identified two distinct neuron types – P1 and pIP10 – the activities of which were causally linked to singing. Causation was however only loosely defined, as these experiments lacked the temporal resolution to

discriminate between a long-lasting courtship state and directly-elicited wing extension and vibration. Based on the data we obtained here and recent findings using red-shifted optogenetic tools (Inagaki *et al.*, 2013), we propose that P1 activity more closely correlates with a persistent state of courtship, temporally uncoupled from instantaneous sensory input and motor output, whereas pIP10 activity more closely correlates with the specific action of singing. This model derives from the critical observation that with P1 activation, courtship persisted for several minutes after the laser is turned off whereas with pIP10 activation, song ceased immediately. It will now be of considerable interest to assess how long P1 activity persists after stimuli are removed. Imaging data are not yet available for pIP10 neurons, but their anatomy suggests that they constitute a key descending pathway from P1 neurons to the wing motor centers in the ventral nerve cord.

By enabling fast thermogenetic and optogenetic modulation of neuronal activity in freely walking flies, FlyMAD is a powerful tool for the functional investigation of neuronal circuits in *Drosophila*. We anticipate that FlyMAD will be crucial in studies that address timing, an important and poorly understood aspect of courtship, learning, and other complex behaviours. Future technical developments will further extend its capabilities. For example, the existing tracking software can target a single fly within a group, and the process of selecting a target or modulating laser power could be automated based on spatial location, body posture, sex, or any other detectable physical or behavioural contingency. Time-multiplexing the laser across many flies and integrating automated behaviour recognition (Dankert *et al.*, 2009; Branson *et al.*, 2009) should increase the throughput and experimental sophistication

without sacrificing the precision of FlyMAD. Finally, with adjustable focus optics and improved tracking, FlyMAD could be used with larger and even 3-dimensional arenas, bringing even more of the fly's rich behavioural repertoire into its target.

Materials & Methods

Fly stocks

UAS-TrpA1, *UAS->stop>TrpA1^{myc}*, *UAS-Chrimson*, *UAS-Shi^{ts}* *NP2361-GAL4*, *VT41688-GAL4*, *VT43702-GAL4*, *VT5534-GAL4*, *VT50660-GAL4*, *TH-GAL4*, *Rh1-GAL4* (also called *NinaE-GAL4*) and *OK371-GAL4* lines were previously described (Klapoetke *et al.*, 2014; Marella, Mann & Scott, 2012; Kitamoto, 2001; Hamada *et al.*, 2008; Mahr & Aberle, 2006; Ellis, O'Neill, & Rubin, 1993 ; Bidaye *et al.*, 2014; Gallio *et al.*, 2011; von Philipsborn *et al.*, 2011). *VT40347-GAL4* was generated as part of the VT library (B.J.D., unpublished). *UAS-shi^{ts1}* flies were provided by Julie H. Simpson. Flies were raised at 22°C, and males were collected up to 24 hours after eclosion, and raised at 22°C in groups of 15-20 for 7-9 days (locomotion experiments) or 15-17 days (courtship experiments). For PER and optomotor experiments, female flies were used, age 6-8 days or 4 days, respectively. For moonwalker experiments, flies were raised in 1µM trans-retinal in darkness.

We activated the TH-VUM neurons using *TH-Gal4* (Friggi-Grelin *et al.*, 2003) and vMS11 and dPR1 with *VT43702* and *VT41688*, respectively (von Philipsborn *et al.*, 2011). P1 neurons were targeted using the genetic intersection of *NP2361-GAL4* and *fru^{FLP}* (Yu *et al.*, 2010), pIP10 as the intersection of *VT40347-GAL4* and *fru^{FLP}* (Supplementary Fig. 15) and vPR6 as the intersection of *VT5534* (Yu *et al.*, 2010) and *fru^{FLP}*, in all three cases driving

the combinatorial effector *UAS>stop>TrpA1^{myc}* (Yu *et al.*, 2010; *>stop>* indicates a transcriptional stop cassette that can be excised by FLP recombinase).

Behaviour assays

The surface of the FlyMAD arena is white nylon (Delrin Polyacetylcopolymer). The arena was coated with fly odors by housing 50-100 virgin females overnight. The arena was backlit with diffuse white or 440nm LED light. To prevent flies from walking on the enclosure lid, the glass was coated with a silicon lubricant (SigmaCote). To provide targets for courtship behaviour, four small (approximately 2-3mm) round pieces of plasticine were placed in the center of the arena. Flies were introduced to the FlyMAD arena by gentle aspiration and allowed to acclimatize for minimum 30s before beginning experiments. For head and thorax-targeting experiments, acclimatization was increased to minimum 120s.

For moonwalker experiments, each fly was given repeated stimuli (2 second stimuli at 7 or 12 second intervals, 10 trials), and locomotion data were pooled by trial. For PER and song neuron activation in TTM experiments, the laser was focused to 105 μ m and in the song experiments, each fly was given six 10 second stimuli at 20mW, alternating between thorax and head, with 20 second recoveries. For TTM targeting experiments on wild-type flies (Figure 3c), each fly was given 10 repeated stimuli with 90 seconds rest period and the laser was powered to 46.8 mW. For all other experiments each fly was given only a single stimulus. For experiments with an unfocused beam (Fig 2a,c), the laser was powered as indicated and focused to 4 by 1.7mm beam size as seen in the video camera. For optomotor experiments, flies were stimulated for three

minutes with TTM thorax targeting focused to 105 μ m and 19.3 mW laser power. The visual stimulus (a 42mm wavelength square wave grating laser printed on white paper) changed direction every 30 seconds and rotated at 144°/s about the arena via gear coupling to a stepper motor (Fig 2b).

Some components of fly behaviour were manually scored. For moonwalker experiments, head direction was manually assigned a quadrant, which was applied to the tracked body axis to disambiguate heading. For PER, video frames in which the proboscis was visible in front of the head were scored as positive. Wing extension was defined as extension of one or both wings by more than 15 degrees from their baseline posture, except during righting after a fall and grooming (when the hind legs are stroking the wings or abdomen). The PER index and wing extension index are the fraction of time spent in PER and wing extension, respectively, as defined using these criteria.

Temperature was measured with a Type T (Farnell 8598258) or Type K (Farnell 859-8240) thermocouple after obtaining reference measurements with PT100 temperature probe. Laser power was measured in the arena using an optical power meter (Thorlabs PM100A and Thorlabs S120C).

Statistics and general methods

All experiments were performed on *Drosophila melanogaster*. Our stopping criterion was to end experiments after three working days spent across all genotypes and a particular experimental design. We did not specify an effect size prior to running the experiments. If flies were not moving prior to the experiment or underwent seizures during heating, they were excluded. Within a given experimental design, flies of different genotypes were raised side-by-side

in different vials or bottles. Experiments on different genotypes were performed sequentially. For dose response curves on the same genotype, conditions were tested in sets of one or two and repeated several times until the final sample size was reached for all conditions. The experiments were done with prior knowledge of the genotype. Analysis that required manual scoring was done blindly (no knowledge of the genotype) in random order.

As described in the relevant figure caption and Supplementary Figs. and Tables, we used the Kruskal-Wallis, Mann-Whitney U, Chi-squared and logrank tests, which are not sensitive to the variance of the distributions.

Cameras and optical equipment

Widefield tracking cameras were acA640-120gm (Basler); monochrome 659 pixels x 494 pixels operating at 100 frames per second. Through-the-mirrors cameras were as follows: piA1000-60gm (Basler) at 60 frames per second in courtship experiments and acA640-120gm at 100 frames per second in TTM experiments. Widefield lenses were 2.9-8.2mm 1:1.0 ⅓" CS (Computar). Through-the-mirrors lenses were VS-TC1-220CO (VS Technologies) or 200mm ED AF Nikkor (Nikon). Cameras were connected via gigabit ethernet. Galvanometers were GVS012/M (Thorlabs). Infrared lasers were DB808-350-3(22x65) (Picotronic) and RLMDL-808-1W-5 (Roithner) and red lasers were DA635-1-3(16x58) (Picotronic).

Realtime tracking and targeting architecture

Images were acquired using libcamiface (<https://github.com/motmot/libcamiface>). Detection of fly positions in the

widefield camera, and detection of fly head and body centers in the TTM camera were both implemented as FView (<https://github.com/motmot/fview>) plugins. Both image streams were analyzed in realtime at 100fps. All image processing was implemented using OpenCV (<http://www.opencv.org>) compiled with SSE optimizations.

Processes responsible for the subsequent tracking, targeting, and experimental tasks were implemented as ROS (<http://www.ros.org>) processes and communicated using the ROS inter-process communication protocol. The tracking and data association method was a simplified version of one described previously (Straw *et al.*, 2011). Briefly, putative 2D pixel locations of flies were sent from the realtime tracking FView plugin to a tracker node that assigned these observations to existing models for each fly. If new observations arrived with no corresponding model, a new model was created. Likewise, if a model existed for some time with no observational support, it was destroyed. The model was implemented as a linear Kalman filter with a 4 dimensional state space (x,y, x velocity, y velocity) in pixels. The motion model was a constant velocity model and the observation model was a 2x4 portion of the identity matrix.

Galvanometer positions were set using an analogue reference input between -10V and +10V. Each axis was put into 0.5V/° mode and the reference input generated using a custom printed circuit board (PCB). The PCB contained a ATmega328 based Arduino microprocessor board and analogue reference voltages were generated using DAC714 16-bit digital to analogue converters (Texas Instruments) referenced to +/-12V taken from the galvanometer power supply. Communication between the ROS targeting process on the host computer

and the ATmega328 occurs over USB. Latencies were quantified and shown in Supplementary Fig. 5.

TTM head and body detection

After acquisition, images are downsampled by 4 (Supplementary Fig. 2). An adaptive threshold is applied, followed by a morphological open filter to remove noise, resulting in a binary image. A contour detection step is performed on the binary image to find closed contours. The largest contour is taken to outline the entire fly, and fitted with an ellipse. Using the major axis of the ellipse, an affine transform is applied in order to rotate the contour points so the fly is orientated vertically. Because of the direction ambiguity of the major axis, the fly head may now be above or below the horizontal after the affine transform. A temporary binary image is created, and points contained in the contour in the temporary image are filled with white. The filled and upright fly silhouette is compared with the previously collected template of the fly head in both orientations using a cross correlation template matching strategy to compute a 'difference image'. By the normalized squared difference metric, the best matching template (absolute minimum cross correlation) indicates whether the fly head is above or below the horizontal. The index of the pixel with the minimum value in the difference image is declared the coordinates of the center of the template. An offset ('template fraction' in the GUI shown in Supplementary Fig. 3) relative to the center of the template is added here to target regions along the fly's long axis, before the previous transformation and downsampling is reversed, giving the location of the template target in the original image.

The computationally expensive template operation may also be performed on the GPU if a large template is required, such as if one wishes to define the whole fly body to allow directed targeting within the thorax for example.

The algorithm was implemented with a focus on graceful degradation and efficiency. The relatively expensive affine transform operation was performed only on the contour points (and not on the image pixels). Furthermore, by performing an ellipse fit early in the algorithm, the center of the fly body is returned in addition to the location of the template target; allowing graceful degradation of the control system (by pointing the laser at the body momentarily) for the small number of instances where the template is not matched correctly.

Latency and accuracy estimation

In widefield mode (without TTM), the camera configuration is similar to that previously described (Simon & Dickinson, 2010). As the camera shutter integration time was set to 8 msec and assuming a gigabit Ethernet delay of 5 msec, the predicted latency of images for available for processing is a distribution between 5 and 13 msec, depending on whether a given photon arrived at the beginning or end of the integration period. With image processing times of ~ 8 msec, USB transmission delay of ~ 4 msec, and galvanometer response time of ~ 7 msec, the predicted latency in wide-field mode is 24-32 msec. Indeed, when we measured total latency of the time from the initial target command to the switch to TTM mode, the mode of this distribution was at 32 msec.

Closed loop performance of TTM control is influenced by accuracy of the template matching operation and system latency. Both important image processing operations, ellipse fitting to contour points and template matching via cross-correlation, return estimates without returning quality or confidence. Thus, direct quantification of their accuracy is challenging. Instead, we estimated them in two ways. The first was by performing measurements a single fly whose size we presumed to be constant over the trial (Supplementary Fig. 4). TTM head detection measured contour area between 1400 and 1800 pixels, compared with the true value measured offline of 1544 px. Furthermore, TTM measured distances from head to contour center ranging from 70 to 85 px, with the mode at 77 px, for a true head-contour distance of 74.2 px.

The second way we estimated TTM accuracy was by analyzing the signal sent to control the galvanometers (Supplementary Fig. 4). By definition, this corrective action represents the system's best estimate of spatial error. By aiming the laser in another quadrant of the arena from a fly and then enabling TTM mode, FlyMAD asymptotically approaches the maximal performance of ~100 mm error (thorax targeting mode) or ~200 mm error (head targeting mode) with this value being reached within 200 msec. At 50 msec, mean error \pm standard deviation was 400 ± 200 mm for head targeting and 300 ± 100 μ m for thorax targeting error. Together, these two estimates of TTM accuracy suggest pixel errors < 7 and around 200 mm.

Alignment and calibration

The floor of the arena forms a spherical bowl that was aligned with the galvanometer such that the center of the sphere was coincident with the center

of the galvanometer's secondary axis mirror. The TTM camera and laser beams were aligned with a dichroic mirror such that the transmitted and reflected light paths (respectively) were coaxial before reaching the galvanometer. The wide-angle targeting system was calibrated by delivering a range of known voltages to the galvanometer while widefield tracking with the tracking camera's IR blocking filter removed. Targeting the entire arena was accomplished by interpolating the resultant look-up table of corresponding voltages and tracked positions.

Acknowledgments

The technology presented in this chapter was developed in collaboration with John R. Stowers, Dorothea Hörmann, Andreas Poehlmann, Barry J. Dickson, and Andrew D. Straw. D.E.B., B.J.D. and A.D.S. conceived the project. D.E.B., J.R.S., D.H., A.P. and A.D.S. developed the hardware and software. D.E.B. and D.H. performed experiments. A.D.S. performed statistical analyses. Specific contributions are noted in figure legends. B.J.D. and A.D.S. provided extensive editions to the manuscript.

We thank Salil Bidaye for data on the *VT50660-GAL4* genotype, the IMP workshop for help fabricating the hardware, Mark Palfreyman and Michael Dickinson for insightful discussion, Lisa Fenk for technological support, and Pavel Masek for insight into IR-activation of TrpA1. We thank Julie H Simpson (Howard Hughes Medical Institute, Janelia Farm Research Campus) for providing UAS-Shibire^{TS1} flies. The fruit fly drawings in Fig. 3 are modified from versions made available by Database Center for Life Science (DBCLS) under a CC by 2.1 license. This work was supported by the Natural Sciences and Engineering Research Council of Canada by a postgraduate scholarship to D.E.B., ERC Starting

Grant 281884 and WWTF grant CS2011-029 to A.D.S., ERC Advanced Grant 233306 to B.J.D. and IMP core funding.

References

- Aravanis, A. M. *et al.* (2007). An optical neural interface: in vivo control of rodent motor cortex with integrated fiberoptic and optogenetic technology. *J. Neural Eng.* 4, S143-S156 .
- Bernstein, J. G., Garrity, P. A. & Boyden, E. S. (2012). Optogenetics and thermogenetics: technologies for controlling the activity of targeted cells within intact neural circuits. *Curr. Opin. Neurobiol.* 22, 61-71.
- Bidaye, S. S., Machacek, C., Wu, Y. & Dickson, B. J. (2014). Neuronal control of *Drosophila* walking direction. *Science*.
- Boyden, E. S., Zhang, F., Bamberg, E., Nagel, G. & Deisseroth, K. (2005). Millisecond-timescale, genetically targeted optical control of neural activity. *Nat. Neurosci.* 8, 1263-8.
- Brand, A. & Perrimon, N. (1993). Targeted gene expression as a means of altering cell fates and generating dominant phenotypes. *Development* 118, 401-415.
- Branson, K., Robie, A., Bender, J., Perona, P. & Dickinson, M. H. (2009). High-throughput Ethomics in Large Groups of *Drosophila*. *Nat. Methods* 6, 451-457.
- Clyne, J. D. & Miesenböck, G. (2008). Sex-specific control and tuning of the pattern generator for courtship song in *Drosophila*. *Cell* 133, 354-63.
- Dankert, H., Wang, L., Hoopfer, E. D., Anderson, D. J. & Perona, P. (2009). Automated monitoring and analysis of social behavior in *Drosophila*. *Nat. Methods* 6, 297-303.
- Ellis, M. C., O'Neill, E. M. & Rubin, G. M. (1993). Expression of *Drosophila* glass protein and evidence for negative regulation of its activity in non-neuronal cells by another DNA-binding protein. *Development* 119, 855-65.
- Friggi-Grelin, F. *et al.* (2003). Targeted gene expression in *Drosophila* dopaminergic cells using regulatory sequences from tyrosine hydroxylase. *J. Neurobiol.* 54, 618-27.
- Gallio, M., Ofstad, T. A., Macpherson, L. J., Wang, J. W. & Zuker, C. S. (2011). The Coding of Temperature in the *Drosophila* Brain. *Cell* 144, 614-624.
- Grigliatti, T. A., Hall, L., Rosenbluth, R. & Suzuki, D. T. (1973). Temperature-Sensitive Mutations in *Drosophila melanogaster*. *Molec. gen. Genet.* 120, 107-114.
- Hamada, F. N. *et al.* (2008). An internal thermal sensor controlling temperature preference in *Drosophila*. *Nature* 454, 217-20.

- Heisenberg, M. & Buchner, E. (1977). The role of retinula cell types in visual behavior of *Drosophila melanogaster*. *J. Comp. Physiol. A* 117, 127-162.
- Inagaki, H. K. *et al.* (2013). Optogenetic control of *Drosophila* using a red-shifted channelrhodopsin reveals experience-dependent influences on courtship. *Nat. Methods* 11, 325-332.
- Jenett, A. *et al.* (2012). A GAL4-driver line resource for *Drosophila* neurobiology. *Cell Rep.* 2, 991-1001.
- Keene, A. C. & Masek, P. (2012). Optogenetic induction of aversive taste memory. *Neuroscience* 222, 173-180.
- Kitamoto, T. (2001). Conditional modification of behavior in *Drosophila* by targeted expression of a temperature-sensitive shibire allele in defined neurons. *J. Neurobiol.* 47, 81-92,
- Klapoetke, N. C. *et al.* (2014). Independent optical excitation of distinct neural populations. *Nat. Methods* 11, 338-346.
- Kohatsu, S., Koganezawa, M. & Yamamoto, D. (2011). Female Contact Activates Male-Specific Interneurons that Trigger Stereotypic Courtship Behavior in *Drosophila*. *Neuron* 69, 498-508.
- Lima, S. & Miesenböck, G. (2005). Remote Control of Behavior through Genetically Targeted Photostimulation of Neurons. *Cell* 121, 141-152.
- Lin, J. Y., Knutsen, P. M., Muller, A., Kleinfeld, D. & Tsien, R. Y. (2013). ReaChR: a red-shifted variant of channelrhodopsin enables deep transcranial optogenetic excitation. *Nat. Neurosci.* 16, 1499-508.
- Mahr, A. & Aberle, H. (2006). The expression pattern of the *Drosophila* vesicular glutamate transporter: a marker protein for motoneurons and glutamatergic centers in the brain. *Gene Expr. Patterns* 6, 299-309.
- Marella, S., Mann, K. & Scott, K. (2012). Dopaminergic modulation of sucrose acceptance behavior in *Drosophila*. *Neuron* 73, 941-50.
- Ni, L. *et al.* (2013). A gustatory receptor paralogue controls rapid warmth avoidance in *Drosophila*. *Nature* 500, 580-584.
- Pfeiffer, B. D. *et al.* (2008). Tools for neuroanatomy and neurogenetics in *Drosophila*. *PNAS* 105, 9715-20.
- Poodry, C. A. & Edgar, L. (1979). Reversible alterations in the neuromuscular junctions of *Drosophila melanogaster* bearing a temperature-sensitive mutation, shibire. *J. Cell Biol.* 81, 520-527.
- Pulver, S. R., Pashkovski, S. L., Hornstein, N. J., Garrity, P. a & Griffith, L. C. (2009). Temporal dynamics of neuronal activation by Channelrhodopsin-2 and

- TRPA1 determine behavioral output in *Drosophila* larvae. *J. Neurophysiol.* 101, 3075-88.
- Simon, J. C. & Dickinson, M. H. (2010). A new chamber for studying the behavior of *Drosophila*. *PLoS One* 5, e8793.
- Straw, A. D. & Dickinson, M. H. (2009). Motmot, an open-source toolkit for realtime video acquisition and analysis. *Source Code Biol. Med.* 4, 1-20.
- Straw, A. D., Branson, K., Neumann, T. R. & Dickinson, M. H. (2011). Multi-camera Realtime 3D Tracking of Multiple Flying Animals. *J R Soc Interface* 8, 395-409.
- Tang, X., Platt, M. D., Lagnese, C. M., Leslie, J. R. & Hamada, F. N. (2013). Temperature integration at the AC thermosensory neurons in *Drosophila*. *J. Neurosci.* 33, 894-901.
- Viswanath, V. *et al.* (2003). Opposite thermosensor in fruitfly and mouse. *Nature* 423, 822-3.
- Von Philipsborn, A. C. *et al.* (2011). Neuronal Control of *Drosophila* Courtship Song. *Neuron* 69, 509-522.
- Yamaguchi, S., Wolf, R., Desplan, C. & Heisenberg, M. (2008). Motion vision is independent of color in *Drosophila*. *PNAS* 105, 4910-5.
- Yu, J. Y., Kanai, M. I., Demir, E., Jefferis, G. S. X. E. & Dickson, B. J. (2010). Cellular Organization of the Neural Circuit that Drives *Drosophila* Courtship Behavior. *Curr Biol* 20, 1602-1614.

Supplementary material

List of supplementary videos

Videos are available on the accompanying compact disc, or online at:

nature.com/nmeth/journal/v11/n7/full/nmeth.2973.html

Video 1: FlyMAD: Rapid thermogenetic control of neuronal activity in freely-walking *Drosophila* (10.19 MB). Summary of FlyMAD objectives, operation and results including thermogenetic silencing and activation.

Video 2: Silencing motoneurons with ShibireTS (523 KB). Thermogenetic silencing of motoneurons reversibly disrupts locomotion. Genotype was +; OK371-Gal4/uas-ShibireTS1.

Video 3: Silencing photoreceptors blocks the optomotor response (4.38 MB). Thermogenetic silencing of visual neurons disrupts optomotor response. Genotype was Rh1-Gal4; UAS-ShibireTS.

Video 4: Activating Moonwalker neurons with TrpA1 (865 KB). Thermogenetic activation of moonwalker neurons induces backwards walking. Genotype was VT50660-Gal4; UAS-TrpA1.

Video 5: Estimating the error of Through-The-Mirror (TTM) Tracking (2.57 MB). In TTM tracking, the mirror movement command signal is proportional to the tracking error. The lower panel of this video shows the error in X and Y directions over time, while the upper panels show the wide and TTM camera views.

Video 6: Head-targeted heating induces proboscis extension from dopaminergic activation (19.04 MB). Thermogenetic activation of flies with genotype TH-Gal4; UAS-TrpA1 causes proboscis extension.

Video 7: Activating song neurons in the VNC is stronger when targeting thorax than head (18.5 MB). Thermogenetic activation of flies expressing TrpA1 in thoracic song neurons induces lower latency and more frequent singing when targeting the thorax than the head.

Video 8: P1-dependent courtship persists after stimulus ceases (3.5 MB). A fly expressing TrpA1 in P1 performs courtship towards plasticine balls during and long after the thermogenetic stimulus is applied. Genotype is NP2361-Gal4; UAS>stop>TrpA1myc; fruFLP.

Video 9: pIP10-dependent courtship is closely linked to artificial activation (688 KB). A fly expressing TrpA1 in pIP10 extends wings only when the thermogenetic stimulus is applied. Genotype is VT40347-Gal4; UAS>stop>TrpA1myc; fruFLP.

Supplementary figures

Supplementary Figure 1. Photograph of FlyMAD apparatus.

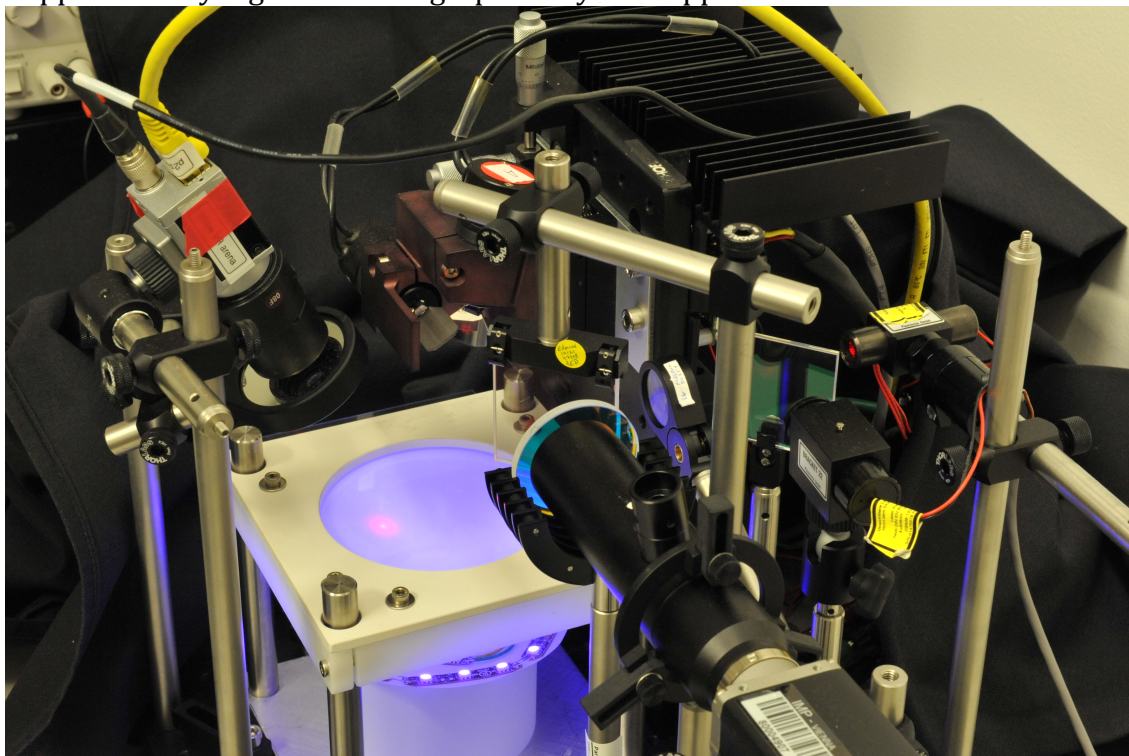
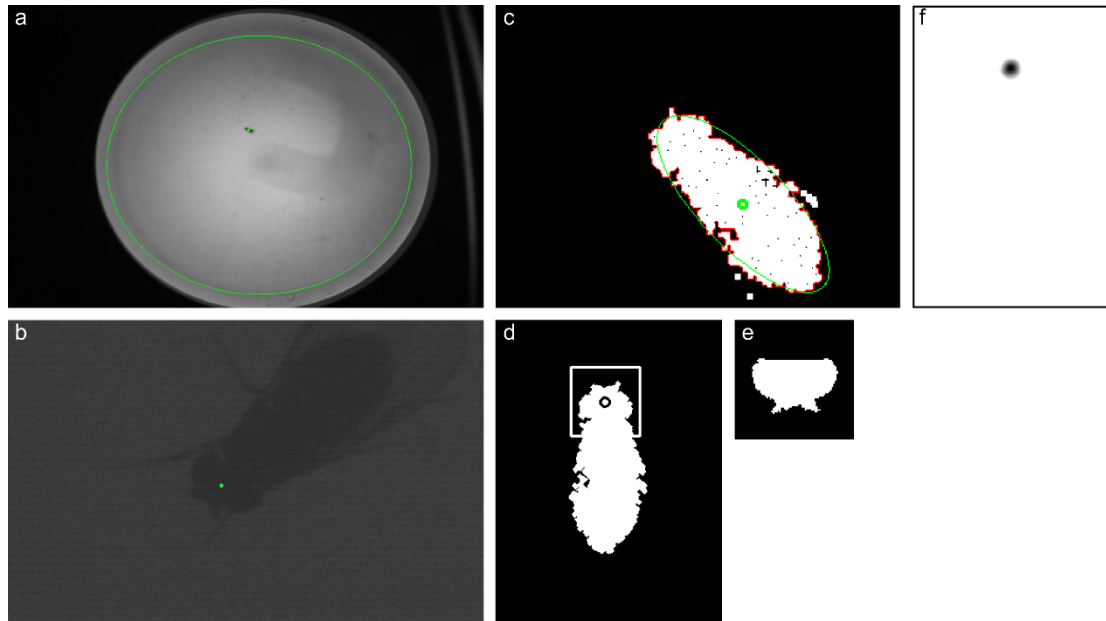


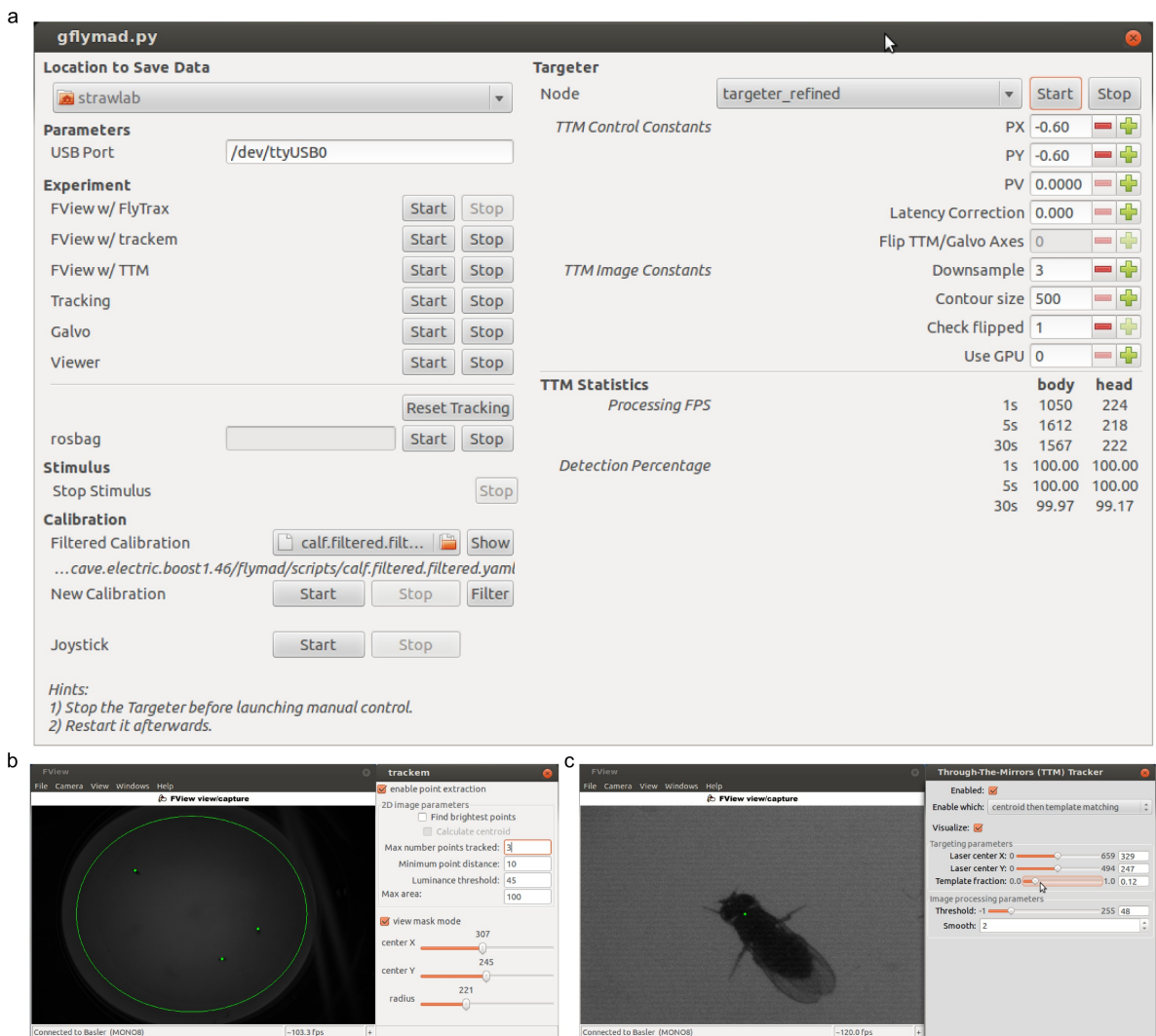
(Photo by Matt Staley.)

Supplementary Figure 2. Realtime image processing (by John Stowers).



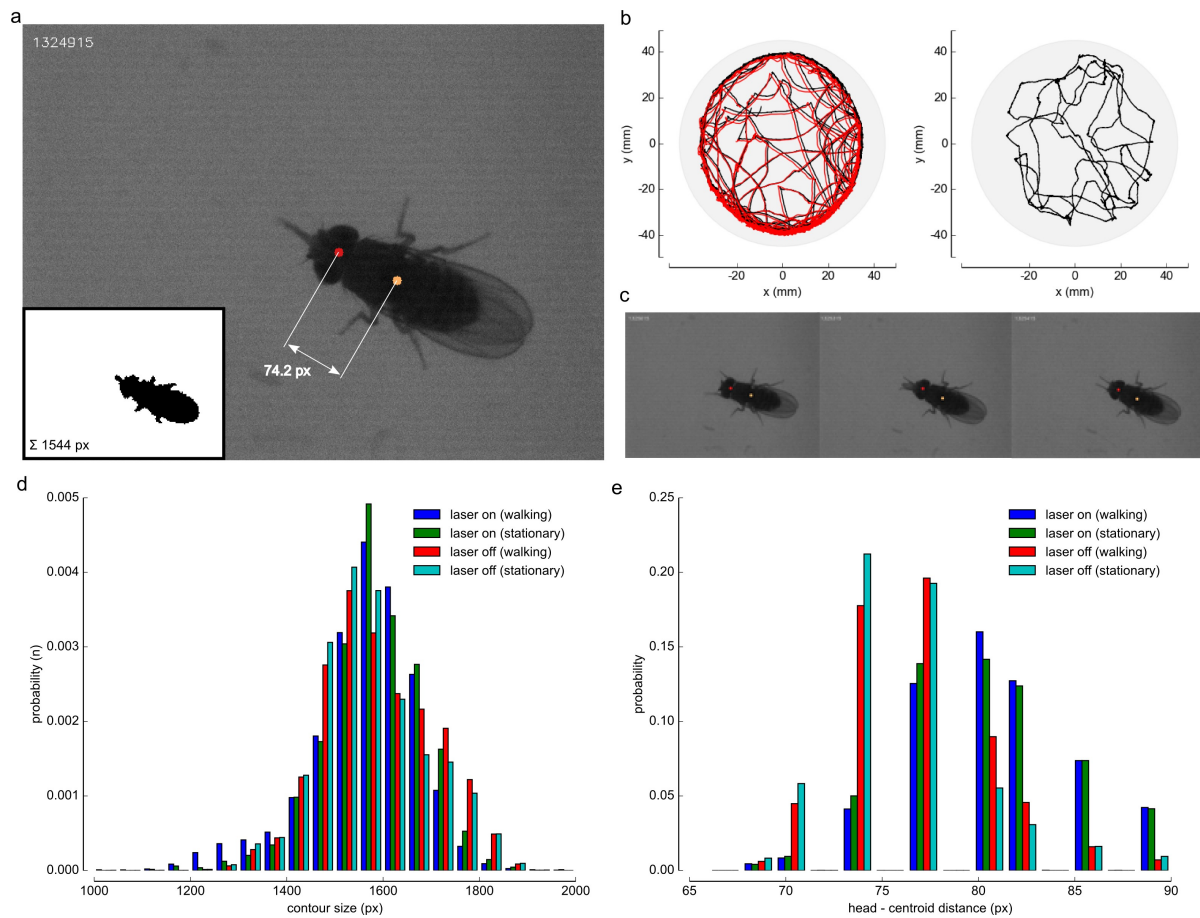
(a) View of arena from wide-field tracking camera showing tracking region (green circle) and tracked fly (green point). **(b)** View of fly from TTM camera and identified head projected onto raw image. **(c)** Downsampled, thresholded and filtered TTM image showing the fly contour (red line outlining white thresholded pixels) and best fit ellipse (green line, and center green circle). **(d)** Affine transformed upright fly image and location identified as head (circle). **(e)** Template used for detecting the fly head. **(f)** Normalized cross correlation result image between upright fly image and fly head template.

Supplementary Figure 3. Graphical user interfaces for controlling FlyMAD.



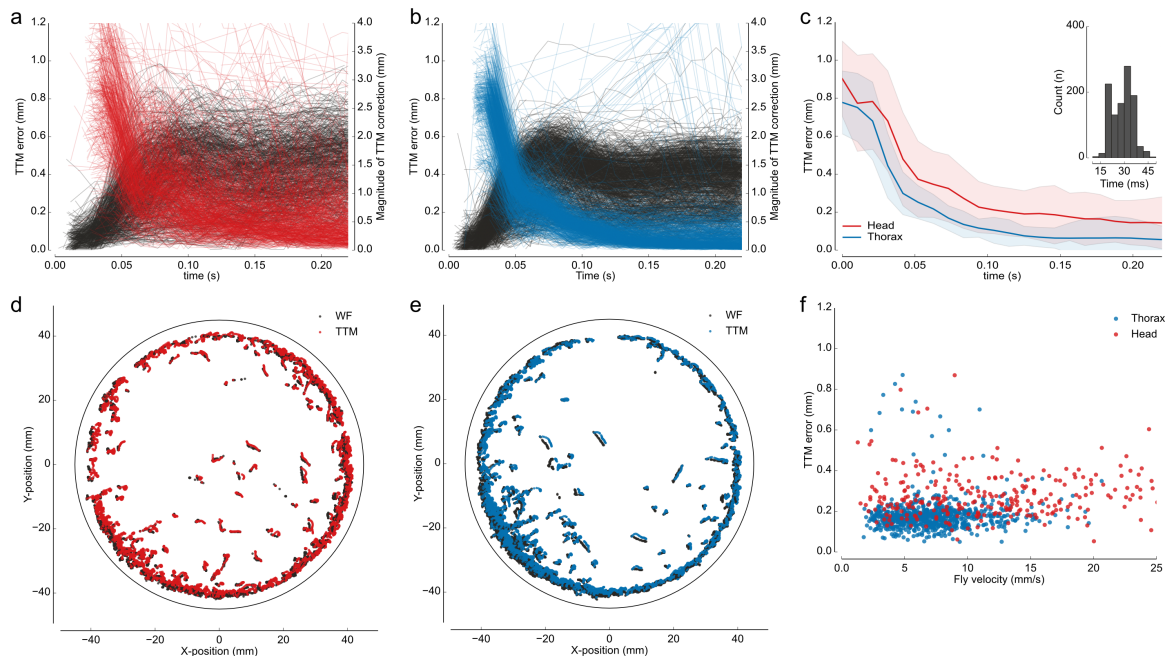
(a) gFlyMAD GUI for launching the major components of the system (targeter, tracker, etc), visualization, recording data, and adjusting control gains. (b) Wide-field tracking software (FView with Trackem plugin) and associated configuration interface for adjusting the number of flies tracked. (c) TTM tracking software (FView with TTM head detection plugin) and associated GUI for adjusting targeting and image processing parameters. gFlyMAD displays realtime statistics showing the effect of any change on tracking accuracy.

Supplementary Figure 4. Measurements of spatial accuracy of head and body detection (by John R. Stowers).



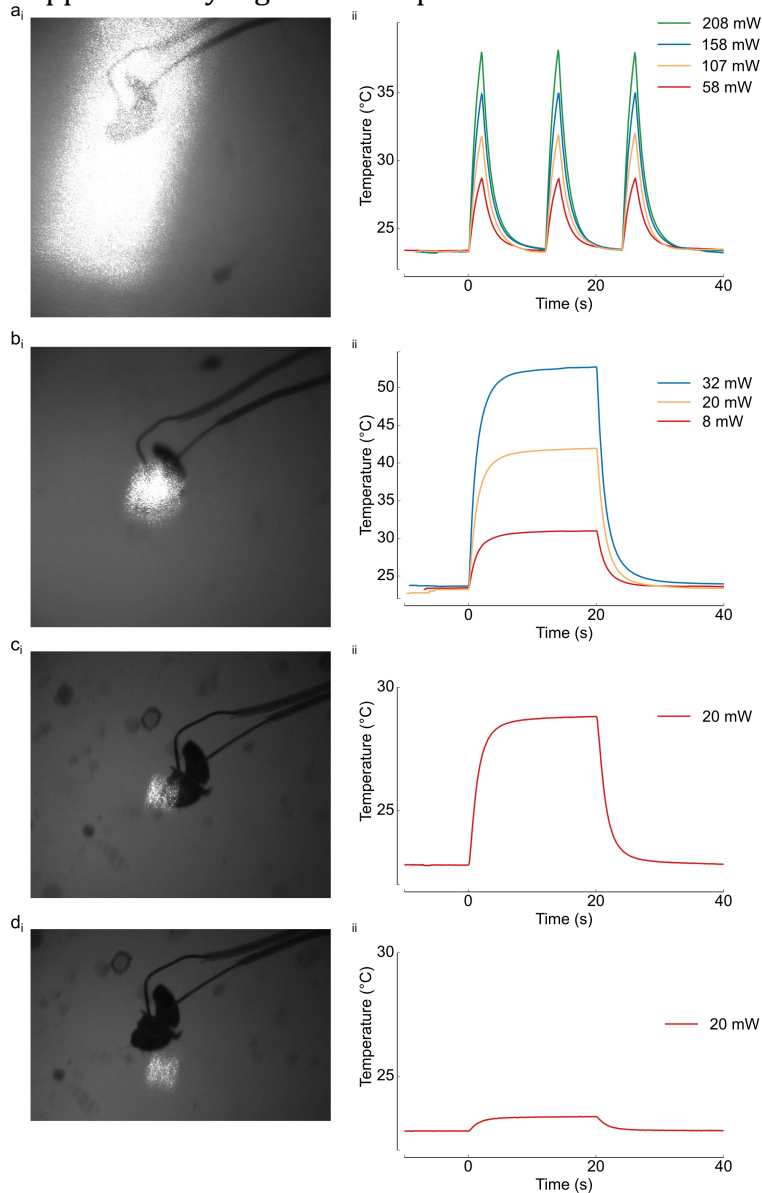
(a) Image of the fly from the TTM camera with the true distance from head to centroid (white dimensions) and fly body contour length (inset, black). **(b)** Trajectories (black) and associated periods of laser stimulation (red) for two 5 minute trials of the same fly. The fly was head targeted for the duration of the experiment with the laser powered ('laser on') or not ('laser off') respectively. **(c)** Representative images from both trials showing head detection. **(d)** Distribution of estimated centroid area for the two trials, split into stationary and walking (< 5mm/s) groups. **(e)** Estimated distance between fly body centroid and head for the same experiments.

Supplementary Figure 5. Measurements of spatial and temporal performance (by John R. Stowers).



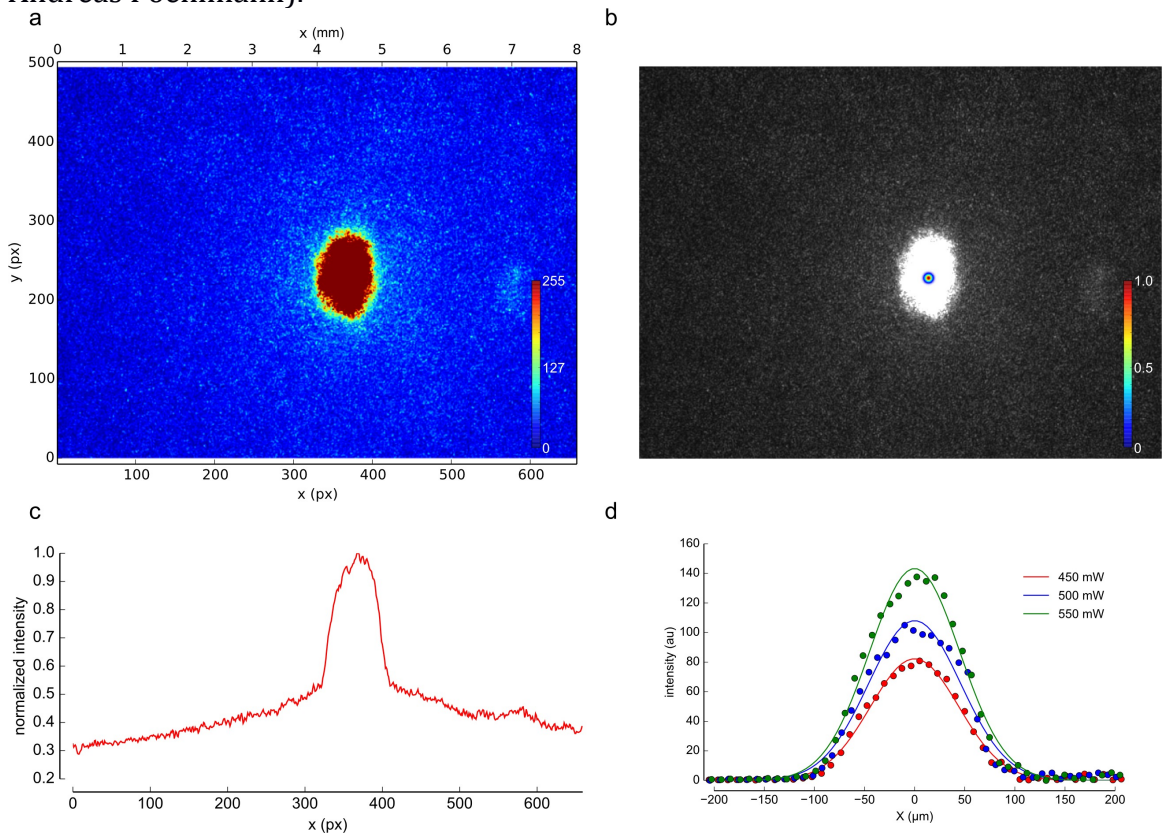
(a-c) Measurement of error (distance between optical path center and targeted location) as a function of time since commanding a switch to the targeted fly. Individual trials in head targeting mode **(a)** and thorax targeting mode **(b)** showing distance between optical path center and targeted location (red, blue) and magnitude of TTM-correction command (black). Average error **(c)** (mean \pm standard deviation). Inset shows histogram of latency of time to switch to TTM targeting. **(d-e)** Top view of fly position estimate from wide-field (WF) camera compared with actual position required to hit the target using TTM refinement for head **(d)**, red) and thorax **(e)**, blue). In both panels, only periods where the laser was on are plotted. **(f)** TTM error as a function of fly velocity for head (red) and thorax (blue) targeting.

Supplementary Figure 6. Temperature measurements.



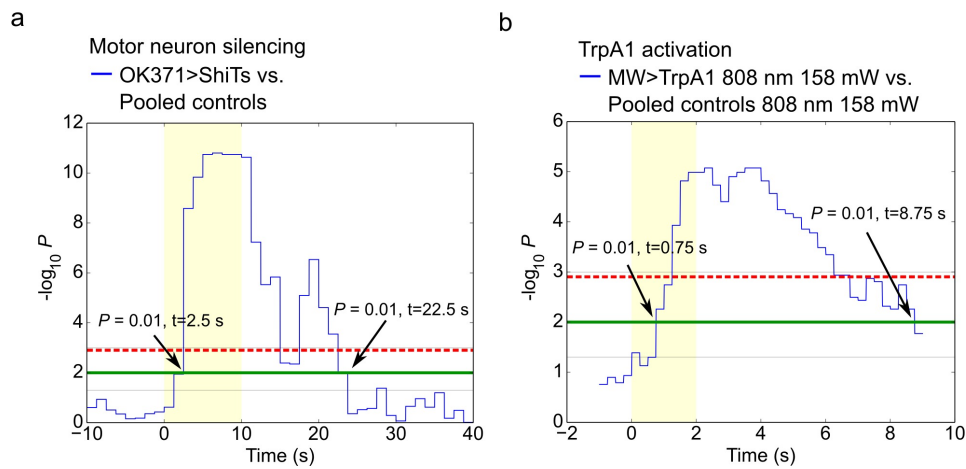
Temperatures measured by a thermocouple in 14-day old male fly with thermocouple inserted in thorax. **(a)** Unfocused laser. **(b)** Focused laser aimed at thorax. **(c)** Focused laser aimed at head. **(d)** Laser focused off-target. Laser powers and wavelengths as specified. All traces from 808nm IR laser.

Supplementary Figure 7. Measurement of laser spot size and optical power (by Andreas Poehlmann).



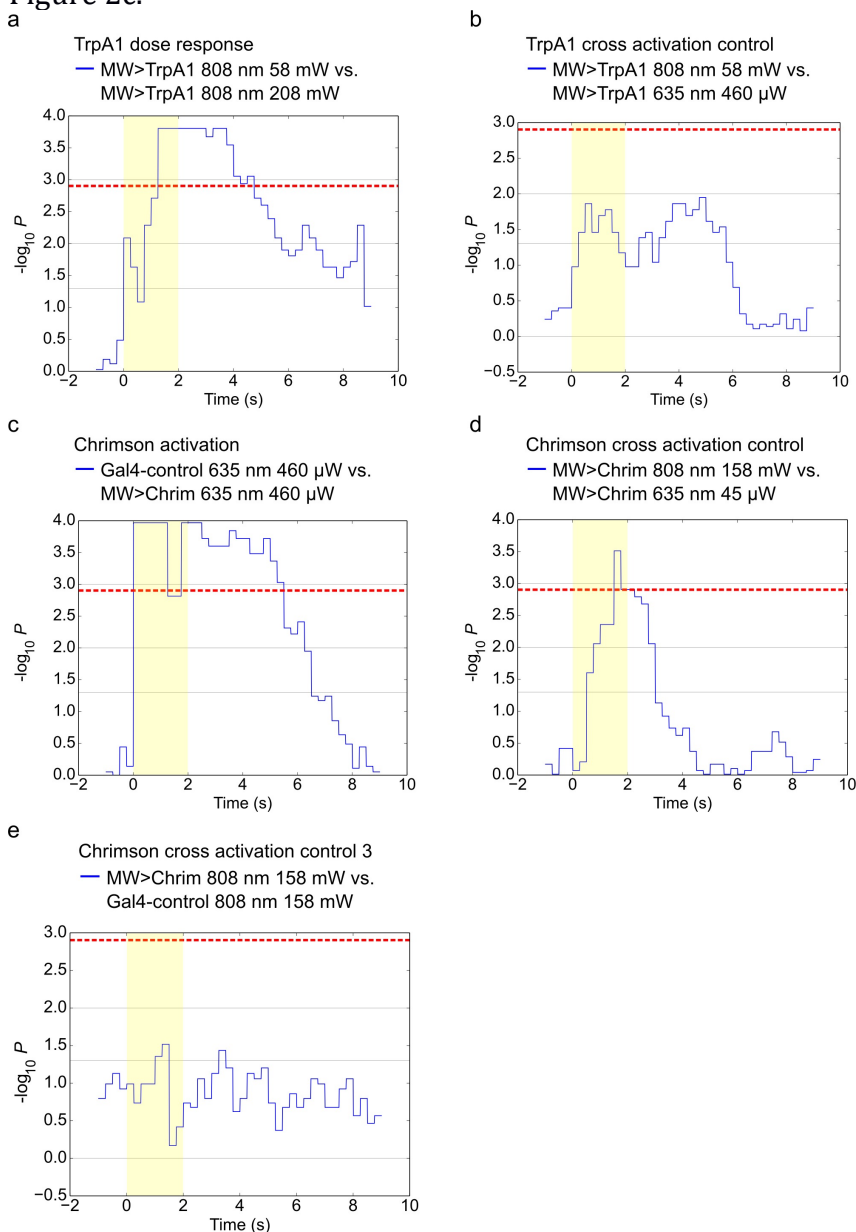
(a) Laser spot viewed from the TTM camera displayed in false color. **(b)** Comparison of the laser spot size as seen in the TTM camera (greyscale image) and the real spot size (false color point). **(c-d)** Laser spot intensity profile from the TTM camera view **(c)** and the real profile **(d)** with Gaussian fit FWHM of 105 μm . The laser intensity was measured using a power meter by partially blocking the beam with a razorblade mounted on a motorized stage moving in the focal plane. Blade position was changed incrementally from non-blocking to fully-blocking, to allow measurement of the spatial integral of the beam. The derivative of this measurement is plotted as the spot profile and fit with a Gaussian.

Supplementary Figure 8. Statistical analysis for Figure 2a and upper panel of Figure 2c.



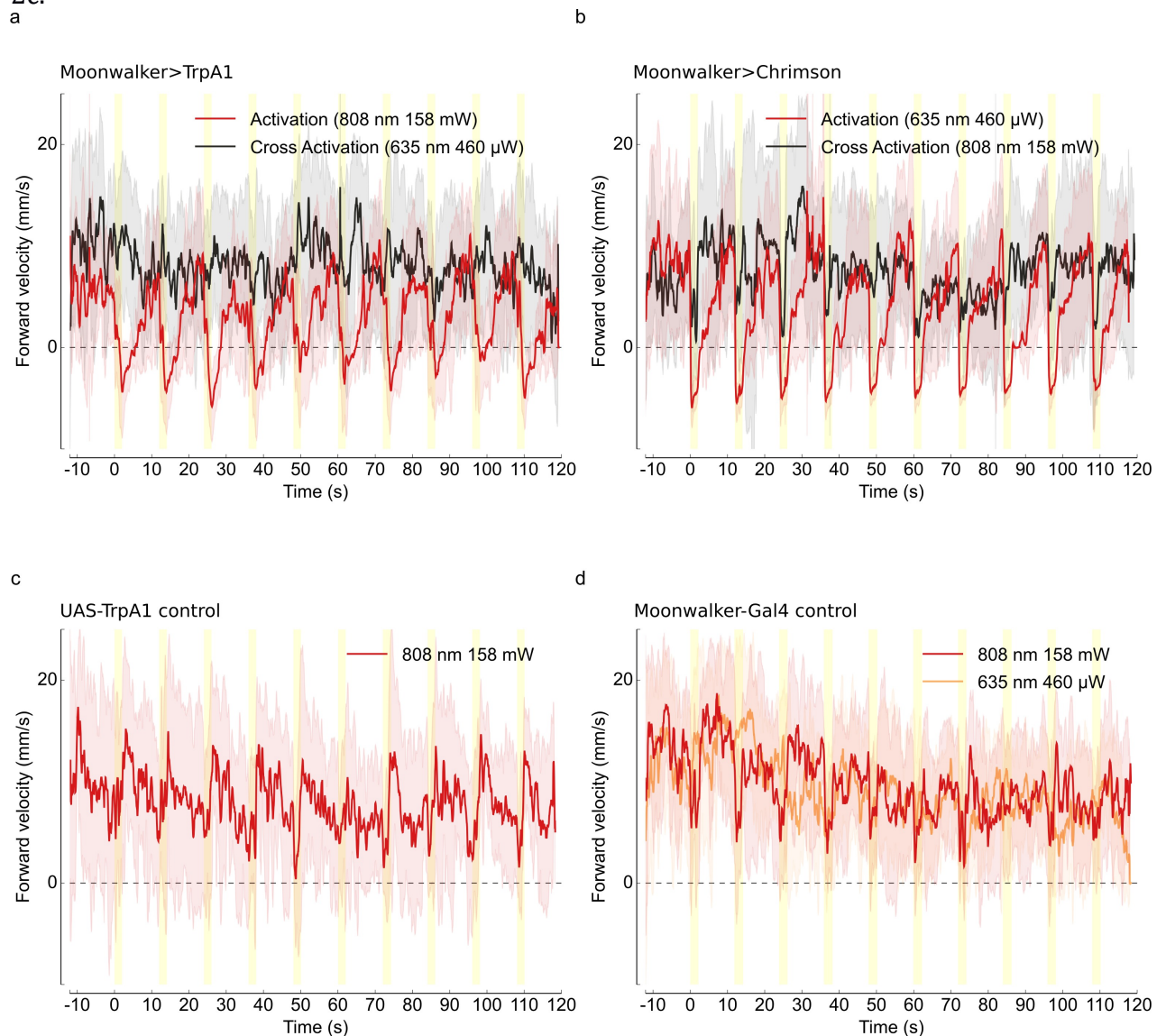
P values are shown on a negative \log_{10} scale. Bonferroni-corrected significance level was computed by dividing significance level (0.05) by number of bins and is indicated by red a dashed line. To measure on- and off- time of the thermogenetic tools, we used a threshold of $P=0.01$ rather than using a more conservative Bonferroni corrected value. For both panels **(a)** Kruskal-Wallis tests applied to data of Fig. 2a. P values cross $P=0.01$ threshold (green line) at 2.5s after the onset of laser stimulation, returning at 22.5s (12.5s after laser off). **(b)** Kruskal-Wallis tests applied to data of Fig. 2ci. **b** shows data from repeated trials where controls were pooled into a single analysis. P values cross $P=0.01$ threshold (green line) at 0.75s after the onset of laser stimulation, returning above this threshold at 8.8s (6.8s after laser off). For both panels, thin horizontal lines correspond to P values of 0.05, 0.001. (by Andrew Straw)

Supplementary Figure 9. Statistical analysis for middle and lower panels of Figure 2c.



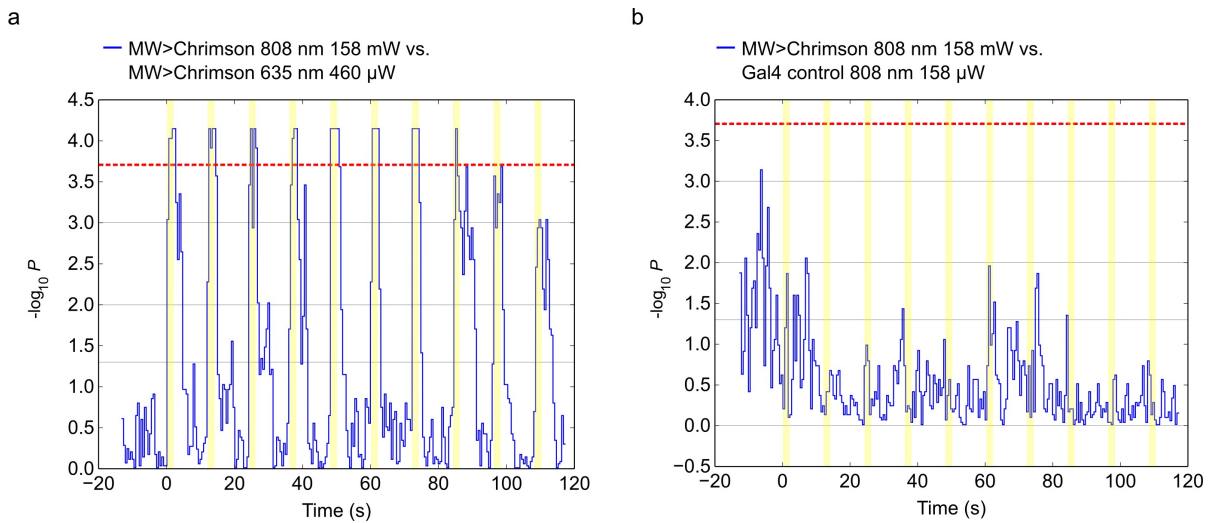
P values are shown on a negative \log_{10} scale. Kruskal-Wallis test was used for all tests. Bonferroni-corrected significance level was computed by dividing significance level (0.05) by number of bins and is indicated by a red dashed line. In all panels, data from repeated trials were pooled into a single analysis. **(a-b)** Kruskal-Wallis tests applied to the data of Fig. 2c (middle panel). **a** compares responses of Moonwalker>*trpA1* flies to low (58mW) and high (208mW) IR laser. **b** compares responses of Moonwalker>*trpA1* to 58 mW IR light and 460 μ W red light. **(c-f)** Kruskal-Wallis tests applied to the data of Fig. 2c (lower panel). **c** compares responses of MW>*Chrimson* flies with MW-Gal4 controls, both to 460 μ W red light. **d** compares responses of MW>*Chrimson* flies to 158 mW IR light and 45 μ W red light. **e** compares responses of MW>*Chrimson* flies and MW-Gal4 control flies exposed to 158 mW IR light. For all panels, thin horizontal lines correspond to P values of 1.0, 0.05, 0.01, 0.001. (by Andrew Straw)

Supplementary Figure 10. Replotted data of middle and lower panels of Figure 2c.



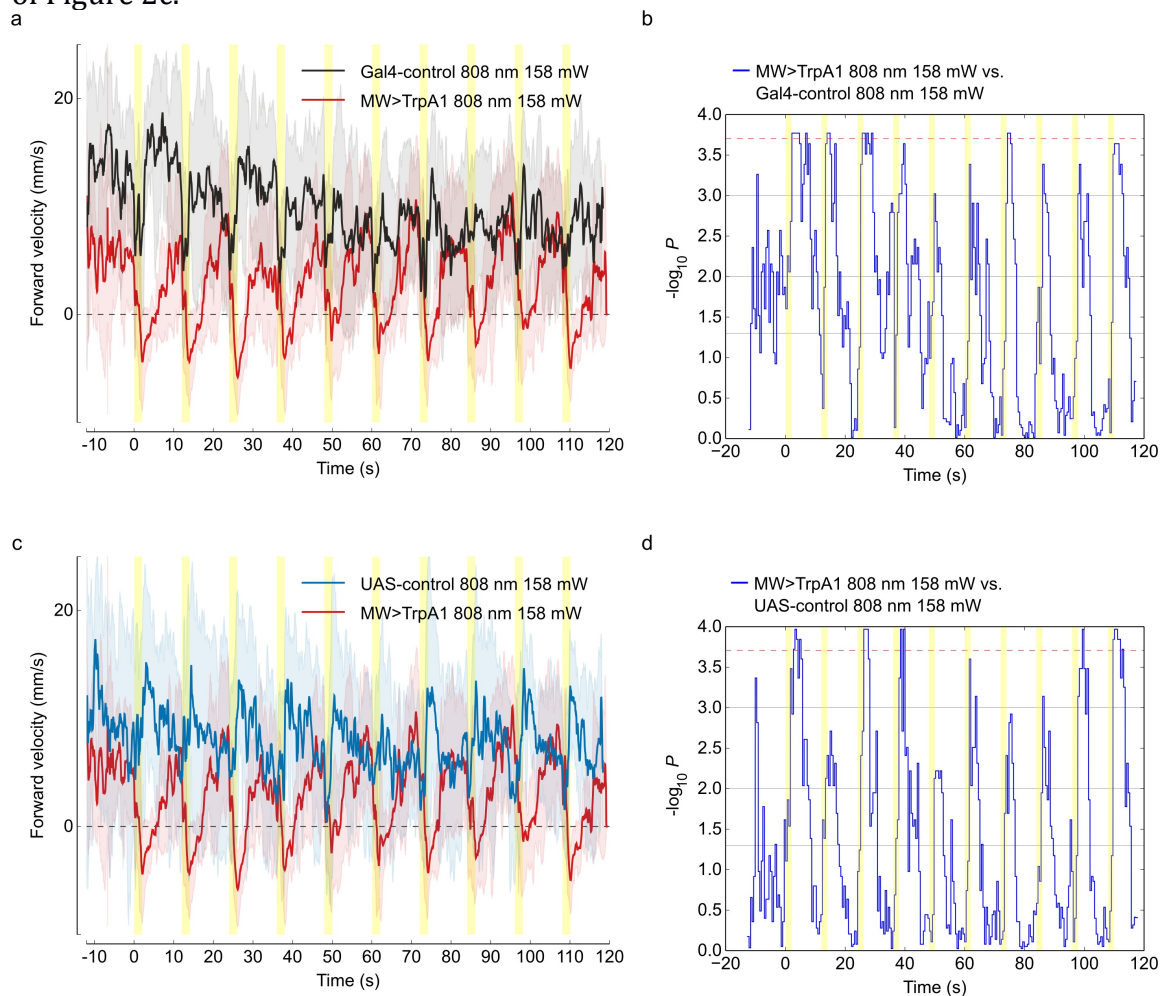
(a) Moonwalker>*trpA1* traces shown without pooling across repeated trials. **(b)** Moonwalker>*Chrimson* traces shown without pooling across repeated trials. **(c)** *UAS>trpA1* trace shown without pooling across repeated trials. **(d)** Moonwalker-Gal4 trace shown without pooling across repeated trials.

Supplementary Figure 11. Statistical analysis of lower panel of Figure 2c.



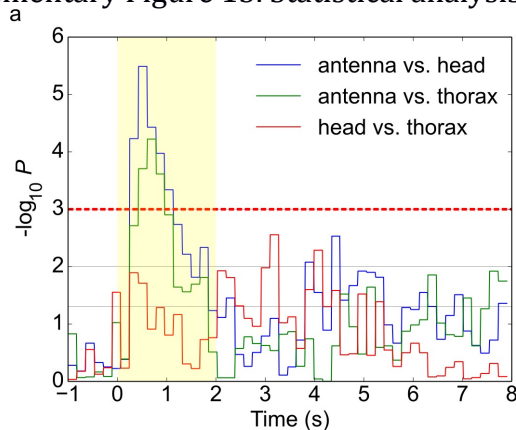
Kruskal-Wallis test was used for all tests. Bonferroni-corrected significance level was computed by dividing significance level (0.05) by number of bins and is indicated by a red dashed line. In both panels, traces are shown without pooling across repeated trials (original data shown in Supplemental Figure 10). **(a)** Comparison between data in Supplementary Figure 10b, Moonwalker>*Chrimson* flies in response to IR and red light. **(b)** Comparison between Moonwalker>*Chrimson* and Moonwalker-GAL4 flies in response to IR light. For all panels, thin horizontal lines correspond to P values of 1.0, 0.05, 0.01, 0.001. (by Andrew Straw)

Supplementary Figure 12. Replotted data and statistical analysis for upper panel of Figure 2c.



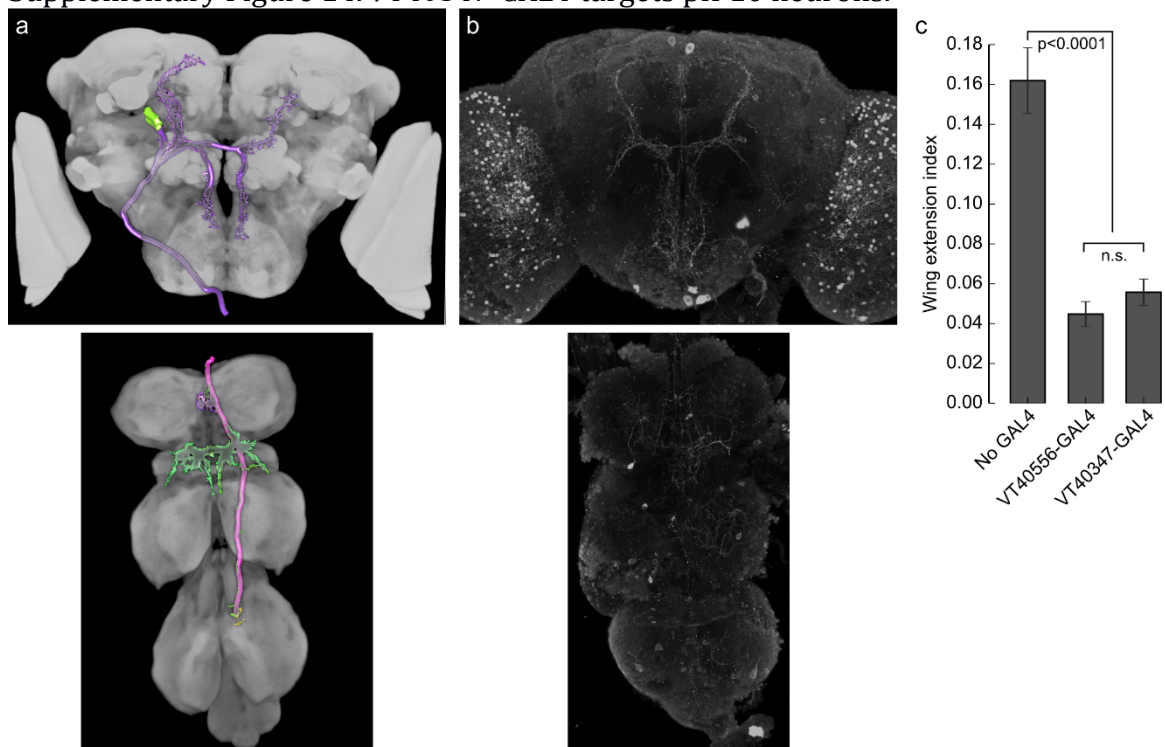
(a) Experimental and Gal4 control traces shown without pooling across repeated trials. **(b)** Kruskal-Wallis test for comparison shown in **a**. **(c)** Experimental and UAS control traces shown without pooling across repeated trials. **(d)** Kruskal-Wallis test for comparison shown in **c**. For panels **b** and **d**, P values are shown on a negative \log_{10} scale, Bonferroni-corrected significance level was computed by dividing significance level (0.05) by number of bins and is indicated by a red dashed line, and thin horizontal lines correspond to P values of 0.05, 0.01, 0.001. (by Andrew Straw)

Supplementary Figure 13. Statistical analysis for Figure 3c.



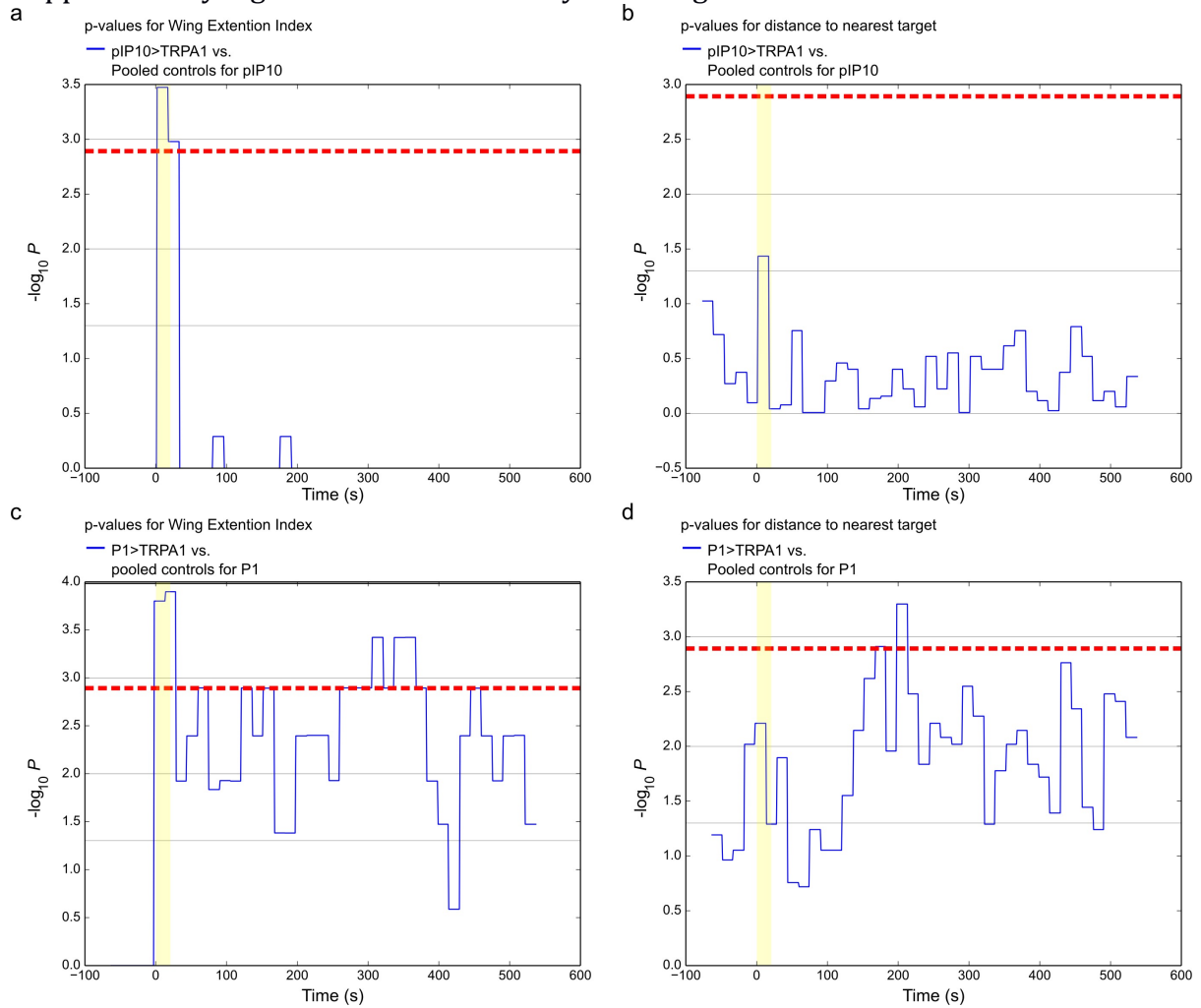
(a) P values are shown on a negative \log_{10} scale. Kruskal-Wallis test was used. Bonferroni-corrected significance level was computed by dividing significance level (0.05) by number of bins and is indicated by a red dashed line. Thin horizontal lines correspond to P values of 0.05, 0.01, 0.001. (by Andrew Straw)

Supplementary Figure 14. *VT40347-GAL4* targets pIP10 neurons.



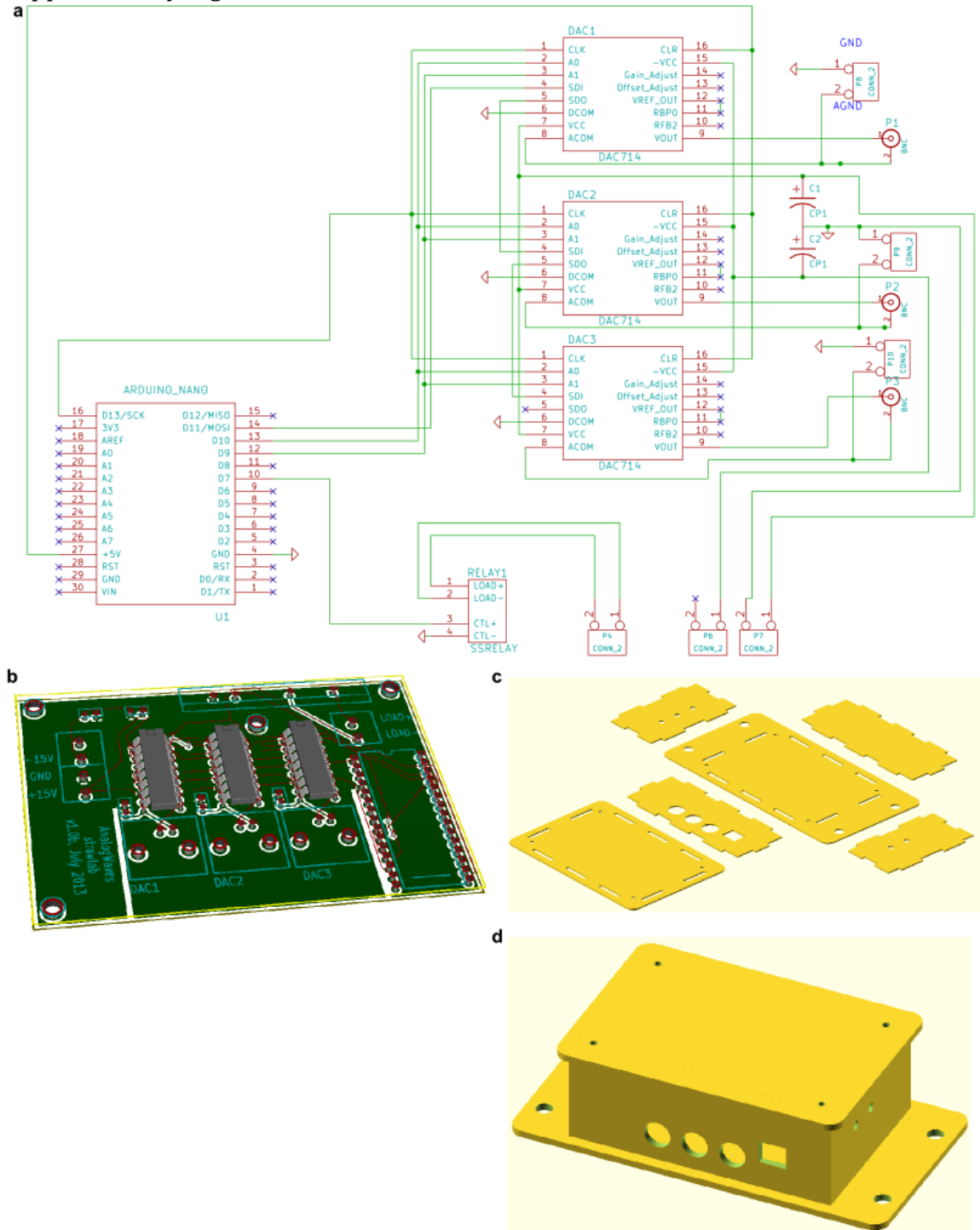
(a) 3D View of segmented representation of pIP10. (b) Maximum intensity Z-projection of brain (top) and ventral nerve cord (bottom) of a *VT40347-GAL4 UAS-mCD8GFP* male, stained with rabbit polyclonal anti-GFP (1:6,000; Torrey Pines, Fisher Catalog No.: NC9589665), and Alexa488-conjugated goat anti-rabbit IgG (1:1000; Life Technologies catalog no. A-11001). (c) Wing extension indices of males carrying the indicated *GAL4* driver and *fru^{FLP} UAS>stop>Kir2.1*, in single pair assays with wild-type virgin females. Comparable reductions in courtship song were observed upon silencing pIP10 with either *VT40556-GAL4* (ref. 30) or the more restricted *VT40347-GAL4*. $n = 18$ for no *GAL4* and *VT40556*; $n = 36$ for *VT40347*; $*p < 0.0001$, Kruskal-Wallis test.

Supplementary Figure 15. Statistical analysis for Figure 4.



P values are shown on a negative log scale. Kruskal-Wallis test was used for all tests. Bonferroni-corrected significance level was computed by dividing significance level (0.05) by number of bins and is indicated by a red dashed line. For all panels, thin horizontal lines corresponding to *P* values of 1.0, 0.05, 0.01, 0.001. (by Andrew Straw)

Supplementary Figure 16. Mirror control electronics.



(a-b) Schematic (a) and rendering (b) of printed circuit board (PCB) used to generate analog voltages to control the galvanometer and a solid-state relay to control laser power. (c-d) Renderings of the enclosure to hold the PCB, including flat layout as used for laser cutting (c) and assembled (d). (by John R. Stowers and Andrew Straw)

Supplementary Table 1. Statistical analysis of data in Figure 2b.

start time (seconds)	stop time (seconds)	<i>P</i> (angular velocity <i>Rh1>shi^{ts}</i> vs. controls)	<i>P</i> (angular velocity <i>Rh1>shi^{ts}</i> vs. zero)	<i>P</i> (linear velocity <i>Rh1>shi^{ts}</i> vs. controls)	<i>P</i> (<i>Rh1>shi^{ts}</i> vs <i>Rh1>shi^{ts}</i> pre-stim)	<i>P</i> (controls vs controls pre-stim)	Laser on
0	60	0.050	*** 7.0e-08	0.81	-	-	no
60	120	0.21	*** 5.4e-10	0.83	-	-	no
120	154	* 0.041	*** 6.7e-09	0.92	0.62	0.28	yes
154	184	*** 9.1e-06	*** 0.00010	** 0.0036	*** 0.00014	0.11	yes
184	214	*** 3.6e-06	** 0.0076	** 0.0027	*** 0.00033	0.15	yes
214	244	*** 6.1e-06	0.13	* 0.016	*** 1.2e-05	0.21	yes
244	274	*** 0.00024	** 0.0068	0.24	*** 0.00067	0.82	yes
274	304	*** 0.00014	0.29	0.83	*** 7.6e-06	0.30	yes

A two-tailed Mann-Whitney U test was used to calculate “P (angular velocity *Rh1>shi^{ts}* vs. controls)” and “P (linear velocity *Rh1>shi^{ts}* vs. controls)”. These tests were used to compare the effect of IR heating on the experimental and control genotypes. A t-test was used to compute “P (angular velocity *Rh1>shi^{ts}* vs. zero)”, which tested whether mean angular velocity differed significantly from zero. “P (*Rh1>shi^{ts}* vs *Rh1>shi^{ts}* pre-stim)” was performed with a two-tailed Mann-Whitney U test to compare angular velocity between the pre-stimulus period and the stimulus period for *Rh1>shi^{ts}* flies. Likewise, “P (controls vs controls pre-stim)” is a similar test for control flies. All tests done with *Rh1-GAL4/UAS-shi^{ts}* and pooled *Rh1-GAL4/+* and *UAS-shi^{ts}/+* flies (n=18 and 9+12, respectively). (by Andrew Straw)

Supplementary Table 2. Statistical analysis of data in Figure 3d.

genotype	<i>P</i> (head vs. thorax)
TH> <i>trpA1</i>	*** 2.1e-07
dPR1> <i>trpA1</i>	*** 9.3e-12
vMS11> <i>trpA1</i>	*** 3.4e-07
vPR6> <i>trpA1</i>	*** 9.4e-05
pIP10> <i>trpA1</i>	* 0.031

All analyses done using the log-rank test. (by Andrew Straw)

Supplementary Table 3. Statistical analysis of proximal and distal wing extension indices.

Test	<i>P</i> (early vs. during)	<i>P</i> (late vs. during)	<i>P</i> (early vs. late)
Total W.E.I.	*** 1.9e-47	*** 2.9e-50	0.60
Proximal W.E.I.	*** 3.0e-41	*** 7.4e-59	*** 2.3e-04
Proximal visit frequency	*** 1.3e-102	*** 5.2e-110	0.29

Wing extension indices are abbreviated W.E.I. Pearson’s Chi-squared test (1 degree of freedom) was used to test the null hypotheses that total and proximal W.E.I. and proximal visit frequency do not differ among different stages of the P1-activation experiment shown in figure 4. “During” refers to the time when the laser stimulus is on (t=0-20s), “early” refers to the first 220 seconds post-stimulus (t=20-240s), and “late” refers to the the 220 seconds immediately after “early” (t=240-460s). “Proximal” refers to a distance less than 50 pixels from a target. “Proximal visits” are defined as a 2 second period in which the fly entered a proximal area. (by Andrew Straw)

Supplementary Table 4. Parts list, (with alternatives from Dorothea Hörmann).

	Quantity	Part numbers	alternative
Arena			
Arena	1	custom, see accompanying specifications	
Arena mount	1	custom, see accompanying specifications	
Arena cover glass	1	custom, see accompanying specifications	
backlight LED	2	Superbright LEDs: NFLS-UV30x3-DI	or comparable
backlight LED, center	6	Mouser Electronics 604-WP710A10MBCK	or comparable
Wide field tracking system			
Wide field camera	1	Basler acA640-120gm Computar 2.9-8.2mm 1:1.0	
Wide field camera lens	1	1/3"	
camera post mount	1	Giottos MH1004	
Hot mirrors	2	Edmund Optics 43-955	
Galvanometer and TTM system			
Galvanometer	1	Thorlabs GVS012/M	
Galvanometer power supply	1	Thorlabs GPS011	
Galvanometer control circuit board	1	custom, see accompanying specifications	
TTM camera	1	Basler piA 1000-60gm VS Technologies VS-TC1-220CO	Basler acA640-120gm Nikon 200mm ED
TTM camera lens	1		AF Nikkor Thorlabs BA2T2/M
TTM lens mount	1	Thorlabs LH1/M	
Bandpass filter, 435nm	1	Edmund Optics 86-360	
Mounting cell 50mm	1	Edmund Optics 55-007	
Short-pass filter 750nm	1	Thorlabs FES0750	
Galvanometer mounting common			
Breadboard – base	1	Thorlabs MB3045/M	or larger
Breadboard – right angle bracket	1	Thorlabs AP90RL/M	
Breadboard – Galvo base	1	Thorlabs MB1515/M	
Vibration isolators, set of 4	1	Thorlabs AV1/M	
Galvanometer			

mounting option A

Pitch and Yaw
mounting platform 1 Thorlabs PY003/M

Galvanometer**mounting option B**

Cage system cube 1 Thorlabs C6W
Cage adapter for
Galvanometer 1 Thorlabs GCM012/M
Cage cube platform 1 Thorlabs B3C/M
Cage assembly rod – ½" 4 Thorlabs ER05-P4
Cage assembly rod – 2" 6 Thorlabs ER2-P4
Cage assembly rod – 8" 8 Thorlabs ER8-P4

Laser system**Option A: two coaxial lasers**

Infrared (808nm) laser 1 Picotronic DB808-350-3(22x65)
Infrared laser mount 1 Picotronic BALLHEAD-MOUNT-22(25x80)
Red (635nm) laser 1 Picotronic DA635-1-3(16x58)
Red laser mount 1 Picotronic BALLHEAD-MOUNT-16(25x75)
Short-pass 700nm dichroic mirror 1 Edmund Optics NT43-957
Short-pass 600nm dichroic mirror 1 Edmund Optics 69-216
IR filter 1 Thorlabs FGB37S
Filter mount 3 Thorlabs SFH2
Beam-focusing lens, f=250mm 1 Thorlabs LB1056
Beam-focusing lens mount 1 Thorlabs LMR1/M

Option B: small spotsize

Infrared (808nm) laser 1 Roithner RLTM DL-808-1W-5
Short-pass filter mount 1 Thorlabs CP02T/M
Short-pass 700nm dichroic mirror 1 Edmund Optics 43955
Collimation Package 1 Thorlabs F810SMA-780
Dichroic mirror mount 1 Thorlabs B5C
Infrared laser mount 2 Thorlabs CP02/M, AD15F
IR filter 1 Thorlabs FGS900S
Filter mount 1 Thorlabs SFH2
Beam-focusing lens, f=100mm 1 Thorlabs LA1509
Beam-focusing lens, 1 Thorlabs LA1708

Supplementary Table 5. Software used.

Name	Version	URL	Usage
Robot Operating System (ROS)	Electric	http://ros.org	Inter-process communication
FView, FlyTrax, Trackem	2013-11-01 git master	http://code.astraw.com/projects/mot/fview.html	Realtime image acquisition and analysis framework
OpenCV	2.4	http://opencv.org/	Realtime image analysis
Kicad	0.0.20110616-1	http://www.kicad-pcb.org/	Printed Circuit Board (PCB) design
py2scad	23:54eadbba357d	http://hg.iorodeo.com/py2scad	PCB enclosure
Aravis	0.1.13	https://wiki.gnome.org/Aravis	Camera drivers
libcamiface	0.8.4	http://code.astraw.com/projects/mot/libcamiface.html	Camera interaction
Ubuntu GNU/Linux	12.04 LTS	http://ubuntu.com/	Operating system
Python	2.7.3	http://python.org/	Primary programming language
Scipy	0.9.0	http://scipy.org/	Kruskal-Wallis and Mann Whitney U statistics
Lifelines	0.2.3.0.3	http://lifelines.readthedocs.org/	Log-rank statistics
Numpy	1.6.1	http://numpy.org/	Numerical computation
Pandas	0.12.0	http://pandas.pydata.org/	Data analysis package
adskalman	0.3.3	http://github.com/astraw/adskalman	Kalman filtering
OpenSCAD	2011.09	http://openscad.org/	CAD modeller
SolidWorks	2010	http://www.solidworks.com/	CAD modeller

Chapter 2: Inhibitory neurons in the *Fruitless* circuit suppress *Drosophila* courtship behaviour

Summary

Complex behaviour is made up of a suite of actions that are orchestrated by selecting appropriate actions with appropriate timing. To accomplish this task, the animal must stay engaged over time on a relatively large scale, while selecting actions based on immediate sensory information. The neuronal mechanisms behind this orchestration are not understood. Toward this goal, previous studies of the courtship behaviour of *Drosophila melanogaster* have characterized 'general' neurons (known as P1), which are involved in the execution of a broad range of actions, and 'specific' neurons (known as pIP10), whose activity effects only a narrow range of actions. Reasoning that action selection likely occurs somewhere between general and specific neurons, we predict that a key point of inhibition for action selection lies downstream of P1. Here we screen for neurons that override P1-dependent courtship. We identify and characterize a class of neurons that process inhibitory gustatory signals and may integrate with courtship circuitry between P1 and pIP10, the key point defined in our model.

Introduction

Animal behaviour requires complex computation by neuronal networks in order to carry out the variable and dynamic computations that relate sensory input to motor output. In order to generate coordinated and appropriate motor output, the animal brain must be capable of inducing motor patterns as well as suppressing them. Behaviour suppression may occur for many reasons, including prioritization of mutually exclusive behaviours (Bullock, 2004; Seeds et al., 2014), or suppression of behaviour by specific cues (Jallon, 1984; Lacaille et al., 2007). In addition, lateral inhibition is necessary for sensory discrimination, to suppress noise and improve perception of stimuli (Hamilton et al., 2005; Kuffler, 1953; Reig & Silberberg, 2014). Computational models of complex neuronal networks (based on the mammalian cerebral cortex) have suggested an essential role for inhibition in sensory processing (Abbott & Chance, 2005). In these models, balanced excitatory and inhibitory inputs enable the filtering of sensory information either by suppressing irrelevant information (Vogels & Abbott, 2005) or by relaying relevant information (Vogels & Abbott, 2009). Balanced excitation and inhibition are also essential for gain control (Chance, Abbott, & Reyes, 2002), providing a potential mechanism for variation in responsiveness (including arousal) in vertebrates and invertebrates (Baca, Marin-Burgin, Wagenaar, & Kristan, 2008). Thus, inhibition plays a prominent role in controlling complex behaviours across phyla.

Courtship behaviour in *Drosophila melanogaster* is a complex behaviour; it requires that a male fly interpret complex information and execute stereotyped motor patterns. Environmental inputs help determine the existence of a

potential mate, and whether that mate is suitable with respect to its gender and mating status. The behavioural output is also complex, involving several intricate component behaviours. Perhaps the greatest complexity of courtship behaviour is the temporal relationship between sensory input and motor output. Both sensory inputs and motor outputs are varied and intermittent, but they are temporally uncoupled from one another. Furthermore, the fly remains engaged in courtship between bouts of intermittent stimuli. We recently demonstrated that acute activation of the P1 neurons induces persistent courtship directed toward targets (Bath et al., 2014; Inagaki et al., 2013), suggesting that the solution to temporal uncoupling and engagement may involve the induction of a heightened state of arousal for courtship.

During the state of courtship arousal, motor output needs to be controlled on several broad levels, including target selection, action selection, and action direction. Target selection is perhaps the best-studied aspect of the control of courtship behaviour, though our understanding is still limited to sensory inputs and basic neuronal processing. Discrimination between receptive and non-receptive mates relies primarily on chemosensory inputs (Jallon, 1984; Lacaille et al., 2007). *cis*-vaccenyl acetate (cVA) is a male-specific olfactory pheromone contained within the ejaculate (Brieger & Butterworth, 1970; Jallon, 1984). Present on males and mated females, but absent on virgin females, it serves as a reliable indicator of non-receptivity, a fact that flies acquire through both innate and learned regimes. In addition to cVA, there are gustatory pheromones within the cuticular hydrocarbons that inhibit male courtship. The most prominent male-specific cuticular hydrocarbon is (z)-7-Tricosene (Everaerts, Farine, Cobb, & Ferveur, 2010; Lacaille et al., 2007), which has an innate aversive effect on

courtship.

In addition to target selection, components of courtship behaviour are temporally controlled by an unknown mechanism, here referred to as action selection. Courtship behaviour consists of a suite of semi-discrete component actions (reviewed in (Sokolowski, 2001)) including orienting (turning the body toward the target), following (chasing behind the target), wing song (extension and vibration of a wing to produce a stereotyped sound), tapping and licking of the target's genitalia, and finally abdominal bending to achieve copulation. A courting session usually follows a tendency from early to late components, though the progression is not absolute. For each component behaviour, execution of motor output is likely derived from integration of information with a distinct set of parameters (inclusion/exclusion, thresholds, etc), though the nature of the integration and the relevant parameters are unknown.

A third level of refinement of courtship behaviour is direction selection. Many components of courtship are executed toward a particular direction, the most tractable example of which is the laterality of wing song. Typical courtship song is performed unilaterally, with the male extending the wing on the side nearest to the female. Direction selection of wing song is performed with tremendous accuracy, updating even as the male turns and the target quickly crosses his field of view. One study proposed a model in which gustatory inputs influence the laterality of wing song (Koganezawa, Haba, Matsuo, & Yamamoto, 2010), although the accuracy of wing extension direction even without contact is evidence against this model.

Towards understanding this complex behaviour, the neuronal processes

that underlie courtship have been an area of intense study. In general, though with notable exceptions, courtship neurons tend to express sex-specific genes *fruitless* and/or *doublesex* (Demir & Dickson, 2005; Kimura, Hachiya, Koganezawa, Tazawa, & Yamamoto, 2008). Some sensory inputs, particularly cVA, have been mapped to specific neurons, including first-, second-, and third-order neurons (Cachero, Ostrovsky, Yu, Dickson, & Jefferis, 2010; Kohl, Ostrovsky, Frechter, & Jefferis, 2013; Ruta et al., 2010). Similarly, some motor outputs have been mapped, primarily for wing song (Kohatsu, Koganezawa, & Yamamoto, 2011; Philipsborn et al., 2011). This consists of a central brain neuron, P1, a descending neuron, pIP10, and three neurons in the ventral nerve cord. However, it is still unknown how sensory input relates to motor output and how the behaviour is refined.

Given the prominence of inhibition in higher-order brain functions in other species, the control of *Drosophila* courtship behaviour (at any or all of the levels discussed above) likely requires inhibition. Despite the extensive characterization of neurons involved in courtship, so far only one class of inhibitory neurons, the median bundle, has been linked to behaviour (Manoli & Baker, 2004), and the precise role of the median bundle neurons remains unclear. Here, we present a screen targeted at identifying inhibitory components of the courtship circuit. We characterize one class of inhibitory neuron, aDT2, and propose that it is an essential inhibitory component involved in the control of courtship.

Results

A screen to identify neurons that inhibit courtship

The courtship neurons P1 and pIP10 were identified in an activation screen of Fru+ neurons. In this screen, flies expressing TRPA1 in subsets of Fru+ neurons were screened for wing extension at 30°C. By its design, this activation screen identified only neurons whose activity is positively correlated with courtship behaviour. In order to identify neurons whose activity is negatively correlated with courtship, we designed a second screen in which we co-activated P1 alongside candidate neurons. In cases where the candidate neuron is an important inhibitory component, the activity of the candidate neuron should override or interrupt the P1-dependent neuronal activity and disrupt P1-dependent wing song. Thus, positive results from this screen were flies that showed reduced wing extension at 30°C (**Fig. 1a**).

We selected candidate *fru*+ neurons based on predicted anatomical overlap with pIP10 (Bruckner et al., 2009; Yu, Kanai, Demir, Jefferis, & Dickson, 2010), and found 11 neuronal classes (**Fig. 1b**). We restricted expression to *fru* neurons using a FLP-out approach, in which FLP recombinase is expressed in *fru* neurons (*fru^{FLP}* (Yu et al., 2010)) and excises a transcriptional stop cassette from the reporter (>*stop*>). We selected 142 GAL4 driver lines (VT library, publicly available from the Vienna Drosophila RNAi Center) whose *fru^{FLP}*-restricted expression pattern contained a candidate neuron and not more than two other neuronal classes. In order to co-activate P1 and candidate neurons, we tested males with the genotype *+ ; NP2361-GAL4, UAS>stop>TRPA1::MYC / + ; fru^{FLP} / VT-GAL4* in a male-male courtship assay. Co-activation of candidate neurons

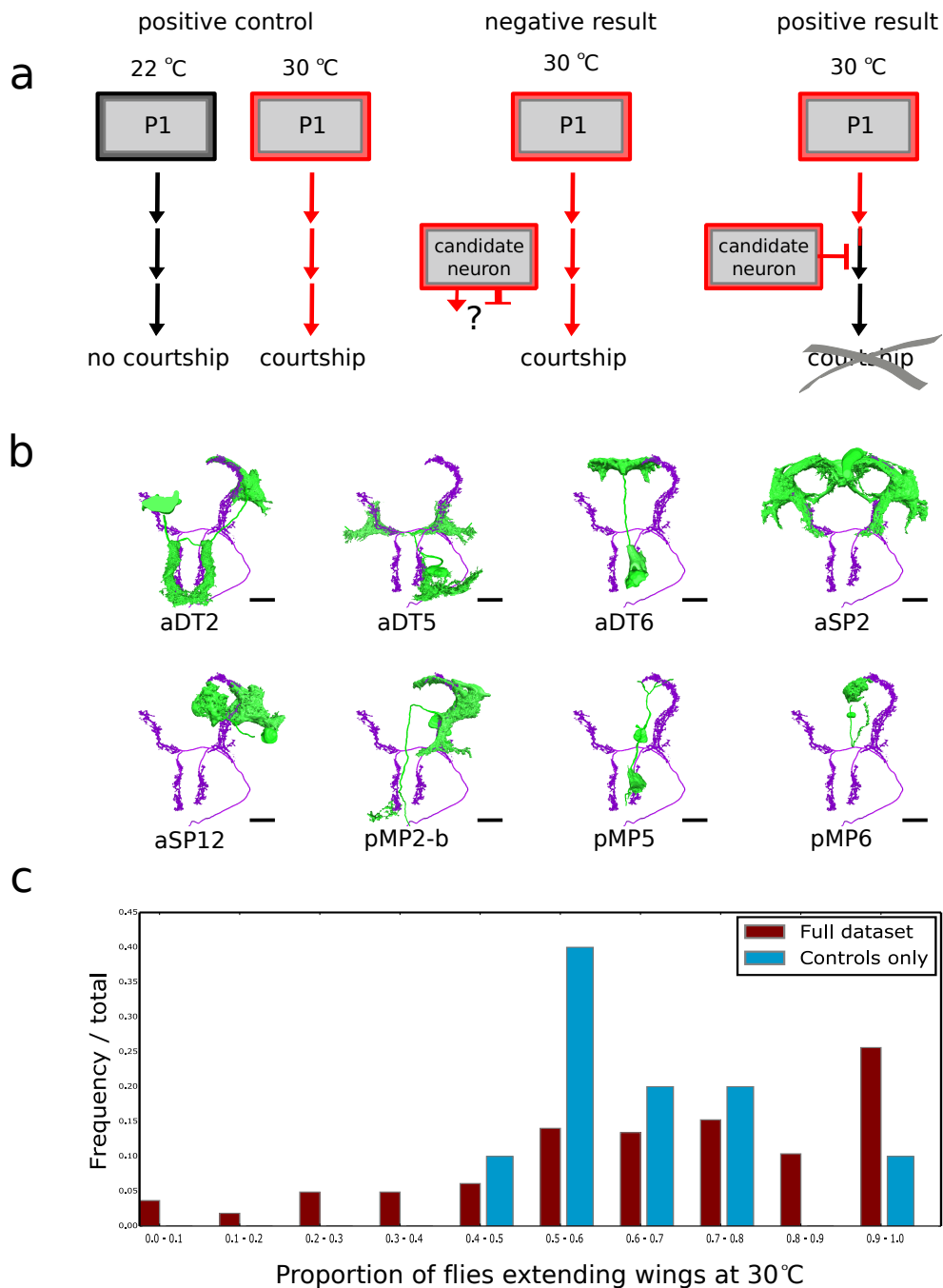


Figure 1. P1 Co-activation screen

- (a) Schematic representation of screening strategy. Red outlines and arrows represent TrpA1-dependent neural activity. Arrows represent excitatory transmission, flat bars represent inhibitory transmission.
- (b) Examples of computer-rendered models of candidate neurons (green) whose arborisations are predicted to overlap with pIP10 (magenta). Scale bars (black) represent 50µM.
- (c) Frequency histogram of proportion of flies exhibiting unilateral wing extension at 30°C for positive controls (blue) and the entire screen dataset (red).

caused both increases and decreases in the proportion of flies extending wings at 30°C relative to activation of P1 alone (**Fig. 1c**). There were five lines in which wing extension was completely abolished.

aDT2 activity inhibits courtship

Two GAL4 lines which were strong positives in the co-activation screen, *VT26992-GAL4* and *VT38210-GAL4*, express strongly in a specific neuronal class, aDT2, with only sparse expression in the rest of the central nervous system (**Fig. 2a,b**). aDT2, also known as mAL, is a FRU-expressing neuron cluster that has been well characterized for its sexual dimorphism, and is at least partially GABAergic (Kimura, Ote, Tazawa, & Yamamoto, 2005). aDT2 has been implicated in controlling the laterality of wing song by transmitting lateralized signals from male-specific pheromone receptors in the forelegs (Koganezawa et al., 2010).

Co-staining with anti-GABA antibody confirmed that the aDT2 neurons labelled by *VT26992-GAL4 UAS-mCD8GFP* are GABAergic (**Fig. 2c,d**). To determine which subtype(s) of aDT2 are labelled by the GAL4 drivers, we used stochastic labelling with Flybow2.0 and *fru^{FLP}* (Hadjieconomou et al., 2011). *VT26992-GAL4* expresses in both male-specific and unisex subtypes of aDT2 (**Fig. 2e,f**), and *VT38210-GAL4* expresses only in the male-specific subtype (**Fig. 2g**, n=11 unilaterally labelled brains).

The reduced wing extension observed during co-activation of P1 with either *VT26992-GAL4* or *VT38210-GAL4*, suggested that aDT2 is a strong inhibitor of courtship. To explore this further, we acutely activated aDT2 using *UAS-CsCHRIMSON::mVENUS* (Klapoetke et al., 2014). aDT2 activation caused a sudden decrease in all courtship behaviours toward virgin females, including

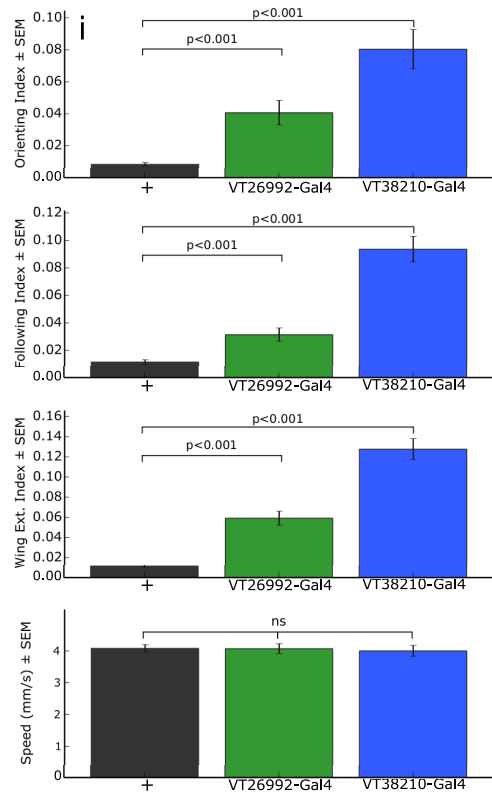
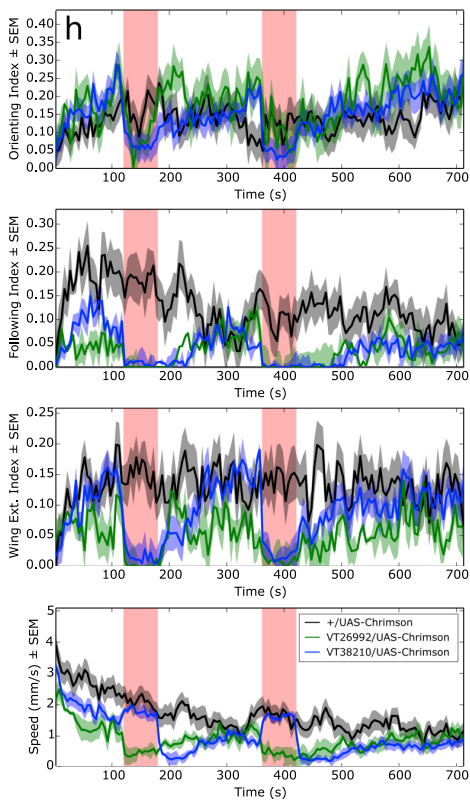
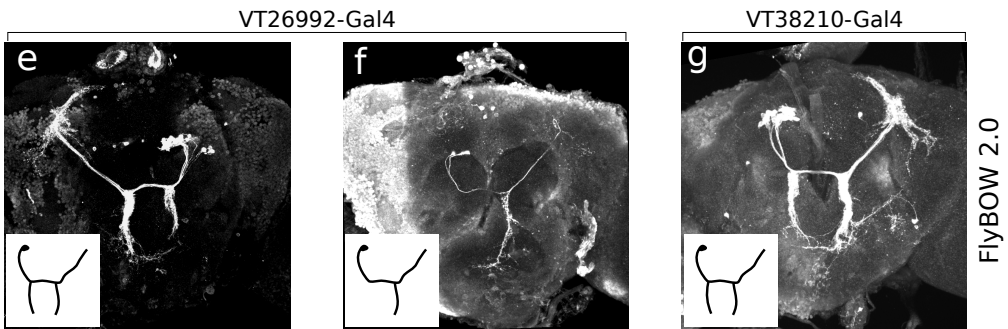
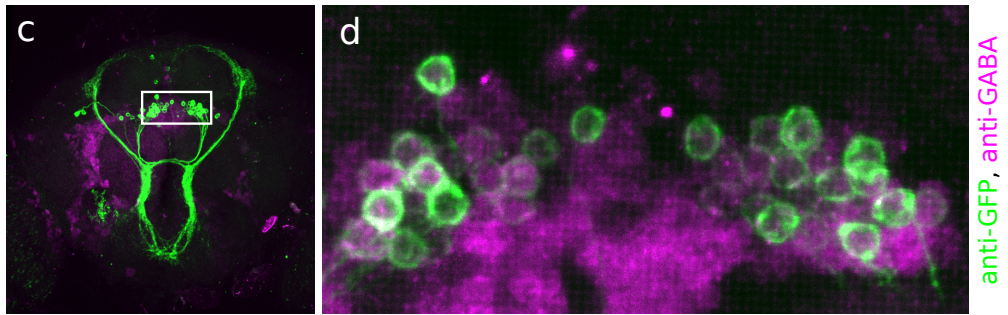
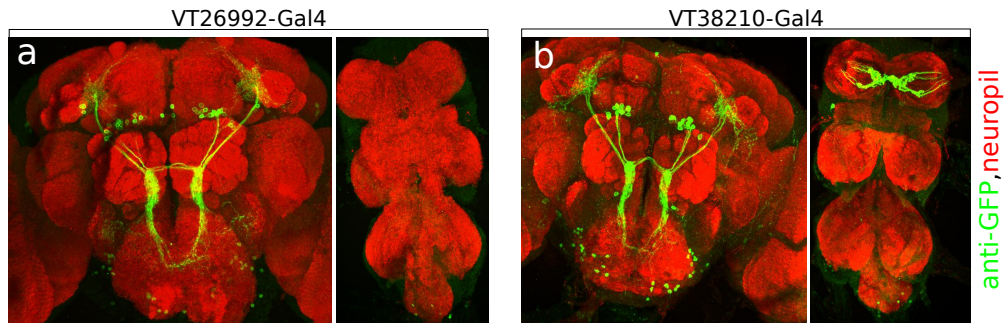
orienting, following, and wing extension (**Fig. 2h**). Both aDT2 lines also exhibited locomotion defects: *VT26992-GAL4/UAS-CsCHRIMSON::mVENUS* flies showed acute slowing, whereas *VT38210-GAL4/UAS-CsCHRIMSON::mVENUS* showed erratic locomotion during the stimulus, followed by immediate slowing afterward.

It is unclear from the optogenetic activation whether or not the courtship defects are secondary effects of locomotion defects. To distinguish between locomotion- and courtship-specific effects, and to determine whether aDT2 is required for courtship inhibition, we silenced aDT2 using Kir2.1 (Hardie et al., 2001), expressed in the *fru^{FLP}*-restricted patterns of *VT26992-GAL4* and *VT38210-GAL4*. Courtship toward male targets was very low in control flies, but was increased in aDT2-silenced flies (**Fig. 2i**). No changes in locomotion were observed. We silenced aDT2 with Kir2.1 using several drivers, and found that courtship toward male targets was lower with drivers that label fewer aDT2 cells (**Supplementary Fig. 1**). Previous studies have implicated aDT2 in influencing the laterality of wing song, based on an increase in bilateral wing extension upon silencing aDT2 (Koganezawa et al., 2010). In contrast, we observed no increase in bilateral wing extension, but a significant increase in unilateral wing extension upon silencing (**Supplementary Fig. 2**).

Taking together activation and silencing experiments, we conclude that aDT2 is important for inhibition of several courtship behaviours. It is unclear, however, what sensory information is processed by aDT2, and how aDT2 integrates with other known circuitry.

Figure 2. aDT2 inhibits courtship.

- (a, b) Expression patterns in the brain (left) and ventral nerve cord (right) of + ; *UAS>stop>mcd8GFP* ; *fru^{FLP} / VT-GAL4* flies, with *VT26992-GAL4*(a) and *VT38210-GAL4*(b), stained with anti-GFP (green) and synaptic marker mAb nc82 (red).
- (c,d) Whole brain (c) and aDT2 cell bodies (d, inset from c) from a + ; *UAS>stop>mcd8GFP*; *fru^{FLP} / VT26992-GAL4* fly stained with anti-GFP (green) and anti-GABA (magenta).
- (e-g) Unilateral labelling of aDT2 with FlyBow2.0. FlyBow expression under *VT26992-GAL4* labelled male-specific (e, n=2) and unisex (f, n=2) subtypes of aDT2. Expression under *VT38210-GAL4* labelled only the male-specific subtype (g, n=11). Cartoons in the bottom left corner of each panel show the typical subtype morphology.
- (h) Quantification of fly behaviours (orienting, following, wing extension, and speed) before, during and after activation of aDT2 using *UAS-CsChrimson^{mVenus}* by *VT26992-GAL4* (green) or *VT38210-GAL4* (blue) or controls (black) in a male-female courtship assay. Red shaded region indicates the time of red light stimulus. n=33-71.
- (i) Quantification of behaviours in flies expressing Kir2.1 in aDT2 (drivers indicated) in a male-male courtship assay. n=69-122. p-values are derived from the Mann-Whitney rank sums test.



aDT2 activity is required for response to oenocyte products

To determine whether aDT2 is involved in processing sensory information, we asked whether aDT2 activity is required for courtship inhibition by male pheromones: cVA or cuticular hydrocarbons. We once again tested aDT2-silenced flies, presenting different targets with altered pheromone profiles. To assess cVA response, we presented male flies with virgin females perfumed with various quantities of cVA. In this experiment, control flies exhibit reduced courtship toward virgin females with greater quantities of cVA, and this effect is less prominent in naïve males than in males pre-conditioned to cVA by exposure to mated females (**Fig. 3a**). We observed no difference between aDT2-silenced flies versus controls for all quantities of cVA applied, in both naïve and experienced conditions.

To assess response to cuticular hydrocarbons, we first paired males with either control target males (*oe+*), or target males in which the cuticular hydrocarbons were abolished by ablation of the oenocytes (*oe-*, (Billeter, Atallah, Krupp, Millar, & Levine, 2010)). Control flies courted *oe-* targets more than *oe+* targets (**Fig. 3b**), whereas aDT2-silenced flies courted *oe+* and *oe-* targets equally, with a courtship index similar to that of control flies paired with *oe-* flies. These results suggest that ablating the oenocytes of male targets had an effect similar to and redundant with silencing aDT2. Consistent with this result, pairing males with pre-mated females (which exhibit male pheromones transferred to the abdomen during mating) caused reduced courtship in controls, but not in aDT2 silenced males. Lastly, we sought to determine whether the increased courtship toward males and mated females upon

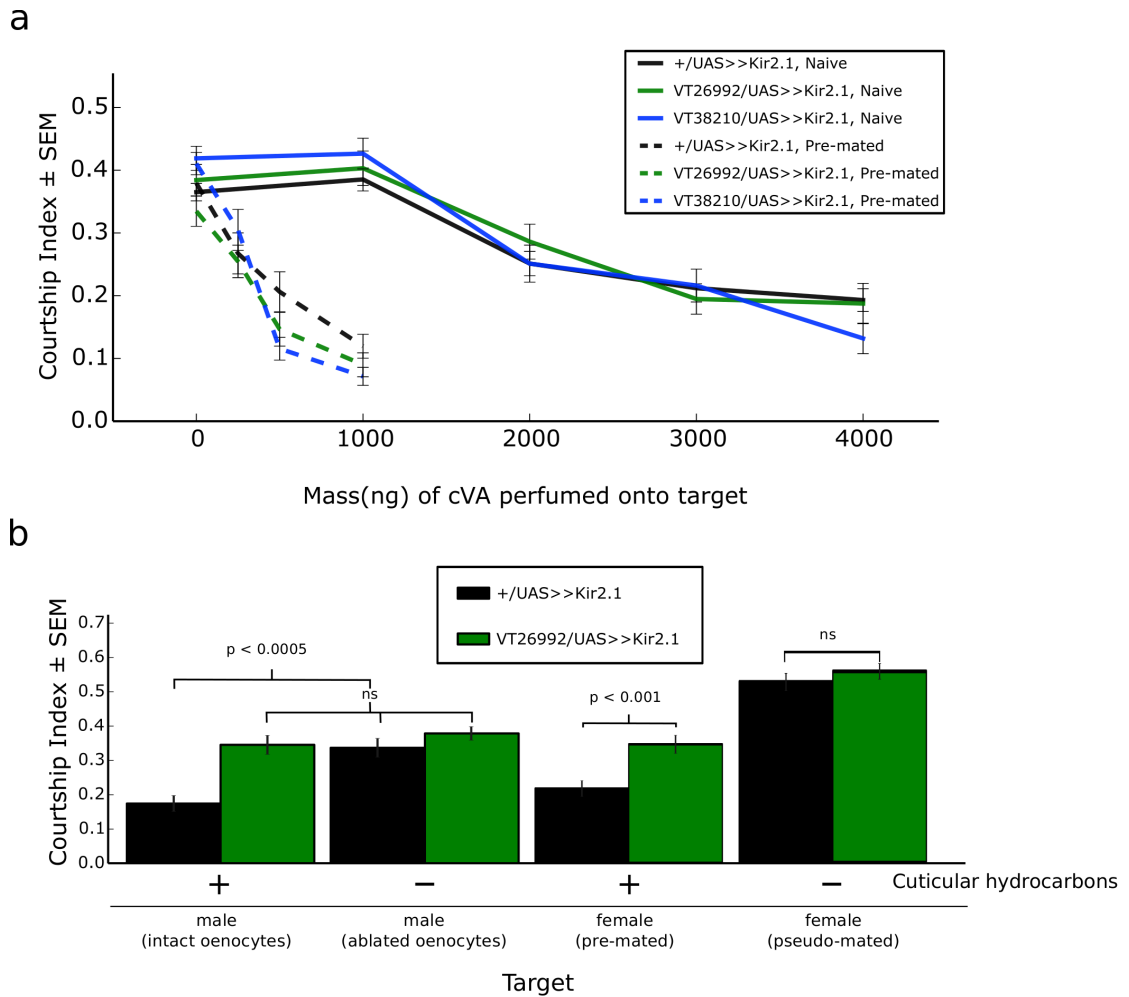


Figure 3. aDT2 is required for sensing male oenocyte products.

- (a) Courtship index of flies courting virgin females perfumed with cVA, for naïve (solid line) and experienced (dashed line) males. Comparison of control flies (black) to flies expressing Kir2.1 in aDT2 using VT26992-GAL4 (green) and VT38210 (blue) showed no significant difference for all quantities of cVA tested (Mann-Whitney test). n=31-65.
- (b) Courtship index of aDT2-silenced flies (green) versus controls (black) paired with targets that present altered pheromone profiles. The theoretical presence (+) or absence (-) of male-specific cuticular hydrocarbons is indicated below the graph. *p*-values are derived from the Mann-Whitney rank sums test. n=35-57.

silencing aDT2 is due to a defect in response to rejection behaviour by the target. To distinguish these possibilities, we paired aDT2-silenced and control males with pseudomated females, which reject but exhibit no male pheromones (Keleman et al., 2012; Nakayama, Kaiser, & Aigaki, 1997). We observed no significant difference between genotypes when paired with pseudomated females. Thus, we conclude that aDT2 is necessary for the inhibitory effects of male oenocyte products, but not cVA.

aDT2 activity affects P1-dependent behaviours

The results of our aDT2 activation and silencing experiments suggest that aDT2 plays an important role in courtship behaviour. The screen by which we identified aDT2 suggested that its activity can override P1. It remains to be determined, however, whether aDT2 functions in the same neural pathway as P1 or in a parallel, competitive pathway. In order to determine the neural epistasis of aDT2 with known courtship circuitry, we co-activated or co-silenced aDT2 with P1 or pIP10.

Based on the initial screening result in which we co-activated aDT2 and P1 by expressing TRPA1::MYC, we expected co-activation of aDT2 to override the P1-induced wing extension. We repeated this experiment, this time slowly increasing the temperature from ambient to 33°C, and pooled temporal data by temperature to determine temperature-specific courtship indices (**Fig. 4a**). Flies expressing TRPA1 in P1 alone (+ ; *NP2361-GAL4, UAS>stop>TRPA1::MYC ; fru^{FLP}*) exhibited a temperature-dependent increase in male-male courtship above 30°C. Flies expressing TRPA1 in aDT2 alone (+ ; *UAS>stop>TRPA1::MYC ; fru^{FLP} /VT26992-GAL4*) showed little or no courtship throughout the assay. Flies

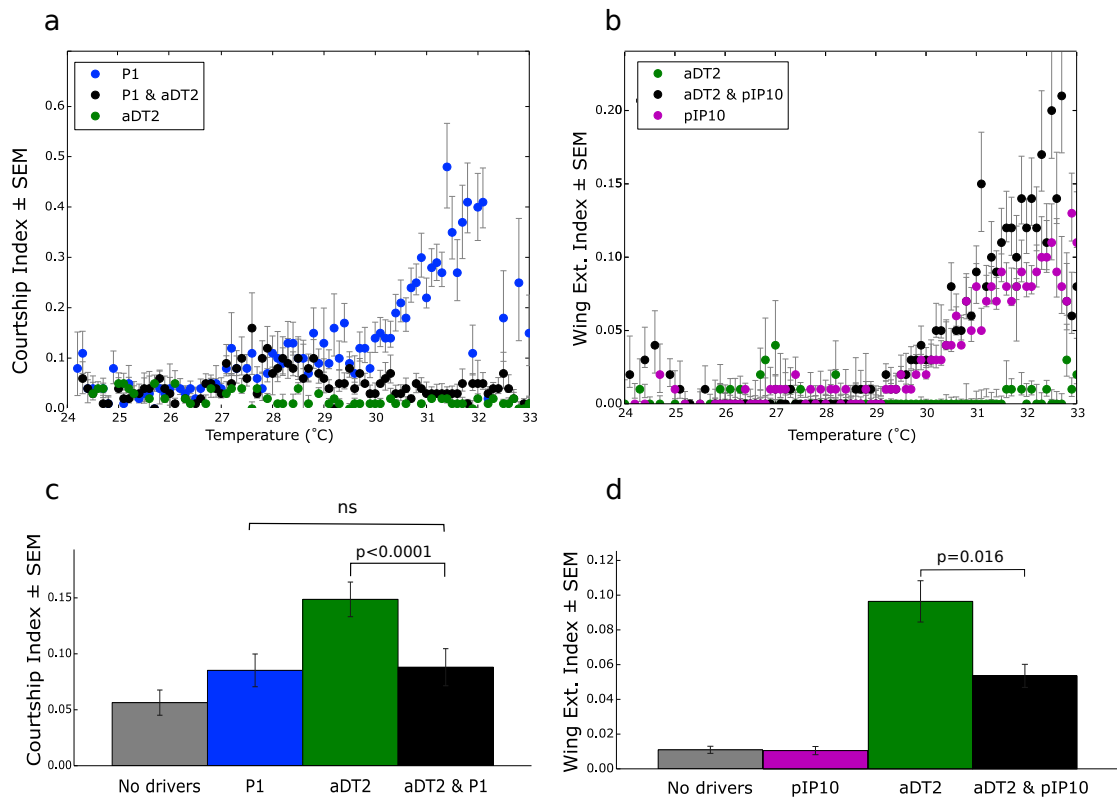


Figure 4. Behavioural epistasis of aDT2 with P1 and piP10.

- (a) Courtship index at various temperatures of flies in which P1 is activated (blue, + ; *NP2361-GAL4,UAS>stop>TrpA1::myc ; fruFLP*), aDT2 is activated (green, + ; *UAS>stop>TrpA1::myc ; fruFLP / VT26992-GAL4*), or the co-activation of P1 and aDT2 (black, + ; *NP2361-GAL4, UAS>stop>TrpA1::myc; fruFLP/ VT26992-GAL4*). Dots represent mean, error bars represent standard error of the mean. n=32-53.
- (b) Wing extension index at various temperatures of flies in which piP10 is activated (purple, + ; *UAS>stop>TrpA1::myc ; fruFLP / VT40556-GAL4*), aDT2 is activated (green, + ; *UAS>stop>TrpA1::myc ; fruFLP / VT26992-GAL4*), or the co-activation of piP10 and aDT2 (black, + ; *UAS>stop>TrpA1::myc; fruFLP, VT26992-GAL4/ VT40556-GAL4*). Dots represent mean, error bars represent standard error of the mean. n=58-73.
- (c) Courtship index toward male targets of flies in which P1 is silenced (blue, + ; *NP2361-GAL4 / UAS>stop>Kir2.1 ; fruFLP*), aDT2 is silenced (green, + ; *UAS>stop>Kir2.1 ; fruFLP / VT26992-GAL4*), no-driver control (grey, + ; *UAS>stop>Kir2.1 ; FruFLP*), or co-silencing of P1 and aDT2 (black, + ; *NP2361-GAL4 / UAS>stop>Kir2.1; fruFLP/ VT26992-GAL4*). Plotted mean and standard error of the mean. n=60-72. *p*-values are derived from Mann-Whitney rank sums test.
- (d) Courtship index toward male targets of flies in which piP10 is silenced (blue, + ; *UAS>stop>Kir2.1 ; fruFLP/ 40556-GAL4*), aDT2 is silenced (green, + ; *UAS>stop>Kir2.1 ; fruFLP / VT26992-GAL4*), no-driver control (grey, + ; *UAS>stop>Kir2.1 ; FruFLP*), or co-silencing of piP10 and aDT2 (black, + ; *UAS>stop>Kir2.1; fruFLP, VT26992-GAL4/ VT40556-GAL4*). Plotted mean and standard error of the mean. n=32-46. *p*-values are derived from Mann-Whitney rank sums test.

expressing TRPA1 in both P1 and aDT2 also showed little to no courtship above 30°C, closely resembling flies expressing TRPA1 in aDT2 alone.

Using the same logic, we conducted a similar experiment in which we activated pIP10, aDT2, or both neurons with TRPA1 (**Fig. 4b**). Activation of pIP10 alone (+ ; *UAS>stop>TRPA1::MYC* ; *fru^{FLP} /VT40556-GAL4*) caused a temperature-dependent increase in wing extension index above 29°C. Again, activation of aDT2 alone (+ ; *UAS>stop>TRPA1::MYC* ; *fru^{FLP} /VT26992-GAL4*) caused little to no wing extension across the entire temperature range. In contrast to the previous experiment, co-activation of aDT2 and pIP10 (+ ; *UAS>stop>TRPA1::MYC* ; *VT26992-Gal4, fru^{FLP} /VT40556-GAL4*) caused temperature-dependent wing extension similar to activation of pIP10 alone.

The co-activation of P1 or pIP10 with aDT2 suggested that aDT2 is epistatic to P1 but not pIP10. However, we could not rule out the possibility that aDT2 functions in a separate, parallel pathway. To test this hypothesis, we asked whether the aberrant male-male courtship that we observed upon silencing aDT2 (**Fig. 2i**) is still observable when the activity of P1 or pIP10 is silenced. Co-silencing of P1 and aDT2 abolished aDT2-dependent male-male courtship (**Fig. 4c**). Similarly, co-silencing pIP10 and aDT2 reduced aDT2-dependent wing extension (**Fig. 4d**).

Discussion

aDT2 inhibits courtship in response to aversive courtship stimuli

In this chapter, we have characterized an inhibitory neuron in the central brain, aDT2. We identified aDT2 in a screen for neurons that counteract the courtship-promoting effects of a previously-identified class of neurons, P1.

Through activation and silencing experiments, we determined that aDT2 activity is sufficient to inhibit courtship toward courtship-promoting targets, and necessary to inhibit courtship toward courtship-inhibiting targets. The effects of aDT2 were evident in all components of courtship behaviour that we measured. We further refined the requirement of aDT2 to discrimination of the presence or absence of oenocytes on male targets, and to inhibit courtship toward mated females but not rejecting virgin females.

We hypothesize that aDT2 is required for the response to male-specific gustatory pheromones. The most likely candidate is 7(Z)-Tricosene (7-T), a cuticular hydrocarbon that is produced in the oenocytes, prominent in males and mated females but not virgin females (Everaerts et al., 2010). It has previously been suggested that the gustatory receptor for 7-T is Gr32a (Wang et al., 2011). The Gr32a receptor neurons arborize in the sub-oesophageal ganglion, and may innervate the arborizations of aDT2 (Koganezawa et al., 2010). Consistent with this hypothesis, *Gr32a* mutant males show elevated courtship toward males and mated females (Miyamoto & Amrein, 2008). We attempted to address whether aDT2 is necessary for 7-T signalling by perfuming 7-T onto targets and silencing aDT2. Unfortunately, our attempts to reproduce published 7-T perfuming results were unsuccessful (data not shown), though we are currently preparing a functional imaging-based approach.

Despite its importance for inhibiting courtship toward male targets, the activity of aDT2 is not required to respond to cVA. The neural processing of cVA has been studied in detail (Cachero et al., 2010; Kohl et al., 2013; Ruta et al., 2010), although no inhibitory neuron has been reported.

The temporal relevance of olfactory (volatile) and gustatory (non-volatile) cues differs strongly. Volatile cues are sampled passively and may be either relevant to the object of attention, or they may represent a factor in the environment that is not immediately relevant. Non-volatile cues, however, are derived from contact (active sampling), and are more likely to represent the object of attention. This difference in temporal relevance should therefore be represented in the neural processing of olfactory and gustatory cues. It would be interesting to determine whether differential processing of volatile and non-volatile modalities reflects their respective influence on the temporal control of behaviour. This hypothesis could be explored by observing the courtship behaviour of flies in which components of the gustatory or olfactory inhibitory pathways were acutely activated.

The role of aDT2 in the courtship circuit

Currently, two classes of inhibitory neurons have been functionally implicated in courtship: aDT2 and the median bundle neurons. Median bundle neurons may prevent the premature activation of later components of the courtship repertoire (Manoli & Baker, 2004), although the mechanism remains unknown. Here, we identified a role for aDT2 for the inhibition of all components of courtship behaviour that we measured. The addition of an inhibitory component to the growing list of circuit components enabled us to induce opposing manipulations to neuronal activity and conduct neuronal epistasis experiments. We characterized the epistatic relationships of aDT2 with P1 and pIP10. The increased male-male courtship observed upon silencing aDT2 is abolished by co-silencing either P1 or pIP10, though the latter is limited only to

wing extension. The requirement of P1 and pIP10 activity suggests that aDT2 inhibits neuronal activity that, at some point, transmits through both P1 and pIP10. Co-activation of aDT2 and P1 abolished P1-induced courtship, suggesting that aDT2 is epistatic to P1. Co-activating aDT2 and pIP10, however, had no effect on pIP10-dependent wing extension, suggesting that pIP10 is epistatic to aDT2. Taken together, co-silencing and co-activation experiments suggest that the inhibitory effects of aDT2 are integrated with courtship circuitry between P1 and pIP10.

Behavioural epistasis experiments cannot determine whether aDT2 has synaptic connections with either P1 or pIP10. Two approaches are currently possible to address this question. First, electrophysiological whole-cell recording from P1 or pIP10 during optogenetic stimulation of aDT2 would result in inhibitory post-synaptic potentials (IPSPs) if aDT2 synapses directly onto the recorded neuron. Second, RNAi-mediated knockdown of GABA receptors in aDT2's target downstream neuron(s) would render the fly less sensitive to inhibition by aDT2, and thus increase wing extension both during male-male courtship and during optogenetic activation of aDT2.

We assigned three broad hypothetical categories for the suppression of courtship: target selection (initiation or cessation of the arousal state), action selection (inhibiting inappropriate actions to ensure the coordination of a progression through the courtship ritual), or direction selection (to control the direction or laterality of courtship behaviours). Which, if any, category of suppression involves aDT2? We observed no defects in laterality of wing song during aDT2 silencing experiments, suggesting that aDT2 is not required for

direction-selection, at least for the generation of unilateral wing song. However, our experiments do not preclude a role for aDT2 in either target- or action-selection due to the low temporal resolution of our co-activation experiments. Acute optogenetic activation of aDT2 led to an acute decrease in courtship toward females, however the chronic positive courtship stimulus (the target female) confounds any conclusions we might draw with respect to the temporal effects of aDT2 activation. To address this question, it will be crucial to determine the effect of acute aDT2 activation during P1-induced persistent courtship. We hope to address this question by the sequential thermo- and optogenetic activation of P1 and aDT2 using FlyMAD. An acute suppression of courtship by aDT2 activation may suggest a role for aDT2 in action selection, whereas a persistent suppression of P1-dependent courtship may suggest a more transitional role for aDT2 in target-selection or cessation of courtship.

The prominent and comprehensive role of aDT2 in courtship suppression supports the general requirement for inhibition in higher-brain function. Although its precise role remains elusive, our discovery of aDT2's important role in aversive cue response will enable further characterization of information processing in the fly brain. Here we found only one neuron, aDT2, that inhibits courtship. It is not surprising that we pinpoint its activity to be between P1 & pIP10, because we selected candidate neurons based on overlap with pIP10. In order to identify a greater diversity of inhibitory neurons in courtship, it may be necessary to conduct additional screens. With greater potential for control of courtship suppression, we hope to elucidate how an animal interprets a complex, dynamic environment to orchestrate a rich display of behaviour.

Experimental Procedures

Fly stocks

Reporter construct lines were from the following sources: *UAS>stop>TrpA1^{myc}* (Philipsborn et al., 2011), *UAS-CsChrimson^{mVenus}* (Klapoetke et al., 2014), *UAS>stop>Kir2.1*, *fru^{FLP}* and *UAS>stop>mCD8-GFP* (Yu et al., 2010), FlyBow2.0 (Hadjieconomou et al., 2011). VT driver lines were generated using the strategy of (Pfeiffer et al., 2008) (B.J.D. unpublished data). *NP2361-GAL4* was obtained from the *Drosophila* Genetics Resource Centre, Japan. Virgin female targets were CantonS. White-eyed male targets were *w¹¹¹⁸*. Oenocyteless targets were generated using the strategy of (Billeter et al., 2010).

Co-activation screen

Male flies from 142 *VT-GAL4* driver lines (VT collection, VDRC) were crossed to virgins of the genotype *+ ; NP2361-GAL4, UAS>stop>TRPA1::MYC / + ; fru^{FLP} / +*. Flies were raised at 22°C and aged for 10-12 days at 22°C on a 12:12 hour day:night cycle. Test flies were paired with white-eyed (*w¹¹¹⁸*) males in 10mm diameter chambers. The upper wall of the chamber was made of high-resistance conducting glass. To heat the chamber, constant voltage (8V) was passed through the glass until the temperature inside the chamber reached 33°C. Temperature was recorded with a Testo® 176T4 thermocouple. Videos of each experiment were scored manually. Wing extension was defined as unilateral or bilateral wing extension greater than 30° and lasting more than one second.

Optogenetic assays

Flies were raised in the dark at 25°C and aged under blue light (470nm,

less than $1\mu\text{W}/\text{mm}^2$) on a 12:12 hour day:night cycle at 25°C . During larval and adult stages, flies were maintained on food containing 0.1mM *trans*-retinal (Sigma-Aldrich). Test males were paired with 2-4 day old virgin females in 10mm diameter chambers. Experiments were conducted in a dark room with less than $1\mu\text{W}/\text{mm}^2$ of blue light (470nm). The chambers were backlit with RGB LEDs (SuperBright LEDs Inc). Constant illumination with the blue channel (470nm, $1.53\pm 0.25\mu\text{W}/\text{mm}^2$) enabled visually-guided behaviours and provided input to video recording equipment. Stimuli were given through the red channel (626nm, $26.75\pm 2.54\mu\text{W}/\text{mm}^2$), pulsed at 20Hz with 25ms pulse width. Stimulus light was controlled using an ArduinoUno microcontroller (Arduino Inc.) with custom software and electronics, and blocked from the camera with a blue dichroic filter (Edmund Optics #52-531). Courtship behaviours were quantified using automated analysis software (Machacek & Dickson, unpublished).

Silencing assays

Flies were raised and aged for 7-10 days on a 12:12 hour day:night cycle at 25°C . Adult males were selected within 24 hours of eclosion and raised in isolation. Test flies were paired with targets in 10mm diameter chambers and observed for 10 minutes. Courtship behaviours were quantified using a custom automated analysis software (Machacek & Dickson, unpublished).

Male targets were *w¹¹¹⁸* (age 7-14 days). Mated females were *w¹¹¹⁸*, raised for 7 days in dense 1:1 male:female populations. Oenocyteless targets were generated using the strategy of (Billeter et al., 2010). Pseudomated females were generated using the strategy of (Keleman et al., 2012).

cVA perfuming was performed with minor modifications from previous

descriptions (Keleman et al., 2012). Briefly: 2-4 day old CantonS virgins were anaesthetized on ice, and 0.5mL of acetone solution with various concentrations of cVA was applied to the abdomen. Flies were allowed to recover for 3-4 hours before assays.

Thermogenetic assays

Flies were raised at 22°C and aged for 10-12 days at 22°C on a 12:12 hour day:night cycle. Test flies were paired with white-eyed (w^{1118}) males in 10mm diameter chambers. The upper wall of the chamber was made of high-resistance conducting glass. Chambers were heated with a constant voltage (7,2V) passed through the glass for 25 minutes or until the chamber reached 33°C. Temperature was recorded with a Testo® 176T4 thermocouple every 10 seconds. Courtship behaviours were quantified using a custom automated analysis software (Machacek & Dickson, unpublished), and data was binned into 30 second bins. Temperature and video were synchronized by Unix time stamps recorded for both video and thermocouple.

Acknowledgments

We thank T. Liu for detailed annotation of VT-GAL4 driver lines, K. Keleman for helpful advice for perfuming and pseudo-mated assays, and C. Schusterreiter and C. Machacek for developing behaviour-tracking software, and J. Lillvis for insightful discussion. This work was funded in part by a Natural Sciences and Engineering Research Council (NSERC) Scholarship. Basic research at the I.M.P is funded in part by Boehringer Ingelheim GmbH. Basic research at J.F.R.C. is funded by the Howard Hughes Medical Institute.

References

- Abbott, L. F., & Chance, F. S. (2005). Drivers and modulators from push-pull and balanced synaptic input. *Progress in Brain Research*, *149*, 147–155. doi:10.1016/S0079-6123(05)49011-1
- Baca, S. M., Marin-Burgin, A., Wagenaar, D. A., & Kristan, W. B. (2008). Widespread inhibition proportional to excitation controls the gain of a leech behavioral circuit. *Neuron*, *57*(2), 276–289. doi:10.1016/j.neuron.2007.11.028
- Bath, D. E., Stowers, J. R., Hörmann, D., Poehlmann, A., Dickson, B. J., & Straw, A. D. (2014). FlyMAD: rapid thermogenetic control of neuronal activity in freely walking *Drosophila*. *Nature Methods*, *11*(7), 756–762. doi:10.1038/nmeth.2973
- Billeter, J.-C., Atallah, J., Krupp, J. J., Millar, J. G., & Levine, J. D. (2010). Specialized cells tag sexual and species identity in *Drosophila melanogaster*. *Nature*, *461*(7266), 987–991. doi:10.1038/nature08495
- Brieger, G., & Butterworth, F. M. (1970). *Drosophila melanogaster*: identity of male lipid in reproductive system. *Science*, *167*(3922), 1262.
- Bruckner, S., Soltészová, V., Gröller, M. E., Hladůvka, J., Bühler, K., Yu, J. Y., & Dickson, B. J. (2009). BrainGazer--visual queries for neurobiology research. *IEEE Transactions on Visualization and Computer Graphics*, *15*(6), 1497–1504. doi:10.1109/TVCG.2009.121
- Bullock, D. (2004). Adaptive neural models of queuing and timing in fluent action. *Trends in Cognitive Sciences*, *8*(9), 426–433. doi:10.1016/j.tics.2004.07.003
- Cachero, S., Ostrovsky, A. D., Yu, J. Y., Dickson, B. J., & Jefferis, G. S. X. E. (2010). Sexual Dimorphism in the Fly Brain. *Current Biology*, *20*(18), 1589–1601. doi:10.1016/j.cub.2010.07.045
- Chance, F. S., Abbott, L. F., & Reyes, A. D. (2002). Gain modulation from background synaptic input. *Neuron*, *35*(4), 773–782.
- Demir, E., & Dickson, B. J. (2005). fruitless Splicing Specifies Male Courtship Behavior in *Drosophila*. *Cell*, *121*(5), 785–794. doi:10.1016/j.cell.2005.04.027
- Everaerts, C., Farine, J.-P., Cobb, M., & Ferveur, J.-F. (2010). *Drosophila* Cuticular Hydrocarbons Revisited: Mating Status Alters Cuticular Profiles. *PLoS ONE*, *5*(3), e9607. doi:10.1371/journal.pone.0009607

- Hadjieconomou, D., Rotkopf, S., Alexandre, C., Bell, D. M., Dickson, B. J., & Salecker, I. (2011). Flybow: genetic multicolor cell labeling for neural circuit analysis in *Drosophila melanogaster*. *Nature Methods*, *8*(3), 260–266. doi:10.1038/nmeth.1567
- Hamilton, K. A., Heinbockel, T., Ennis, M., Szabo, G., Erdélyi, F., & Hayar, A. (2005). Properties of external plexiform layer interneurons in mouse olfactory bulb slices. *Neuroscience*, *133*(3), 819–829. doi:10.1016/j.neuroscience.2005.03.008
- Hardie, R. C., Raghu, P., Moore, S., Juusola, M., Baines, R. A., & Sweeney, S. T. (2001). Calcium influx via TRP channels is required to maintain PIP2 levels in *Drosophila* photoreceptors. *Neuron*, *30*(1), 149–159.
- Inagaki, H. K., Jung, Y., Hoopfer, E. D., Wong, A. M., Mishra, N., Lin, J. Y., et al. (2013). Optogenetic control of *Drosophila* using a red-shifted channelrhodopsin reveals experience-dependent influences on courtship. *Nature Methods*, 1–11. doi:10.1038/nmeth.2765
- Jallon, J. M. (1984). A few chemical words exchanged by *Drosophila* during courtship and mating. *Behavior Genetics*, *14*(5), 441–478.
- Keleman, K., Vrontou, E., Krüttner, S., Yu, J. Y., Kurtovic-Kozaric, A., & Dickson, B. J. (2012). Dopamine neurons modulate pheromone responses in *Drosophila* courtship learning. *Nature*, 1–6. doi:10.1038/nature11345
- Kimura, K.-I., Hachiya, T., Koganezawa, M., Tazawa, T., & Yamamoto, D. (2008). Fruitless and Doublesex Coordinate to Generate Male-Specific Neurons that Can Initiate Courtship. *Neuron*, *59*(5), 759–769. doi:10.1016/j.neuron.2008.06.007
- Kimura, K.-I., Ote, M., Tazawa, T., & Yamamoto, D. (2005). Fruitless specifies sexually dimorphic neural circuitry in the *Drosophila* brain. *Nature*, *438*(7065), 229–233. doi:10.1038/nature04229
- Klapoetke, N. C., Murata, Y., Kim, S. S., Pulver, S. R., Birdsey-Benson, A., Cho, Y. K., et al. (2014). Independent optical excitation of distinct neural populations. *Nature Methods*, *11*(3), 338–346. doi:10.1038/nmeth.2836
- Koganezawa, M., Haba, D., Matsuo, T., & Yamamoto, D. (2010). The Shaping of Male Courtship Posture by Lateralized Gustatory Inputs to Male-Specific Interneurons. *Current Biology*, *20*(1), 1–8. doi:10.1016/j.cub.2009.11.038
- Kohatsu, S., Koganezawa, M., & Yamamoto, D. (2011). Female Contact Activates Male-Specific Interneurons that Trigger Stereotypic Courtship Behavior in *Drosophila*. *Neuron*, *69*(3), 498–508. doi:10.1016/j.neuron.2010.12.017

- Kohl, J., Ostrovsky, A. D., Frechter, S., & Jefferis, G. S. X. E. (2013). A bidirectional circuit switch reroutes pheromone signals in male and female brains. *Cell*, *155*(7), 1610–1623. doi:10.1016/j.cell.2013.11.025
- Kuffler, S. W. (1953). Discharge patterns and functional organization of mammalian retina. *Journal of Neurophysiology*, *16*(1), 37–68.
- Lacaille, F., Hiroi, M., Twele, R., Inoshita, T., Umemoto, D., Manière, G., et al. (2007). An Inhibitory Sex Pheromone Tastes Bitter for *Drosophila* Males. *PLoS ONE*, *2*(8), e661. doi:10.1371/journal.pone.0000661
- Manoli, D. S., & Baker, B. S. (2004). Median bundle neurons coordinate behaviours during *Drosophila* male courtship. *Nature*, *430*(6999), 564–569. doi:10.1038/nature02713
- Miyamoto, T., & Amrein, H. (2008). Suppression of male courtship by a *Drosophila* pheromone receptor. *Nature Neuroscience*, *11*(8), 874–876. doi:10.1038/nn.2161
- Nakayama, S., Kaiser, K., & Aigaki, T. (1997). Ectopic expression of sex-peptide in a variety of tissues in *Drosophila* females using the P[GAL4] enhancer-trap system. *Molecular & General Genetics : MGG*, *254*(4), 449–455.
- Pfeiffer, B. D., Jenett, A., Hammonds, A. S., Ngo, T.-T. B., Misra, S., Murphy, C., et al. (2008). Tools for neuroanatomy and neurogenetics in *Drosophila*. *Proceedings of the National Academy of Sciences of the United States of America*, *105*(28), 9715–9720. doi:10.1073/pnas.0803697105
- Philipsborn, von, A. C., Liu, T., Yu, J. Y., Masser, C., Bidaye, S. S., & Dickson, B. J. (2011). Neuronal Control of *Drosophila* Courtship Song. *Neuron*, *69*(3), 509–522. doi:10.1016/j.neuron.2011.01.011
- Reig, R., & Silberberg, G. (2014). Multisensory integration in the mouse striatum. *Neuron*, *83*(5), 1200–1212. doi:10.1016/j.neuron.2014.07.033
- Ruta, V., Datta, S. R., Vasconcelos, M. L., Freeland, J., Looger, L. L., & Axel, R. (2010). A dimorphic pheromone circuit in *Drosophila* from sensory input to descending output. *Nature*, *468*(7324), 686–690. doi:10.1038/nature09554
- Seeds, A. M., Ravbar, P., Chung, P., Hampel, S., Midgley, F. M., Mensh, B. D., & Simpson, J. H. (2014). A suppression hierarchy among competing motor programs drives sequential grooming in *Drosophila*. *eLife*, *3*, e02951.
- Sokolowski, M. B. (2001). *Drosophila*: genetics meets behaviour. *Nature Reviews Genetics*, *2*(11), 879–890. doi:10.1038/35098592
- Vogels, T. P., & Abbott, L. F. (2005). Signal propagation and logic gating in

networks of integrate-and-fire neurons. *The Journal of Neuroscience : the Official Journal of the Society for Neuroscience*, 25(46), 10786–10795.
doi:10.1523/JNEUROSCI.3508-05.2005

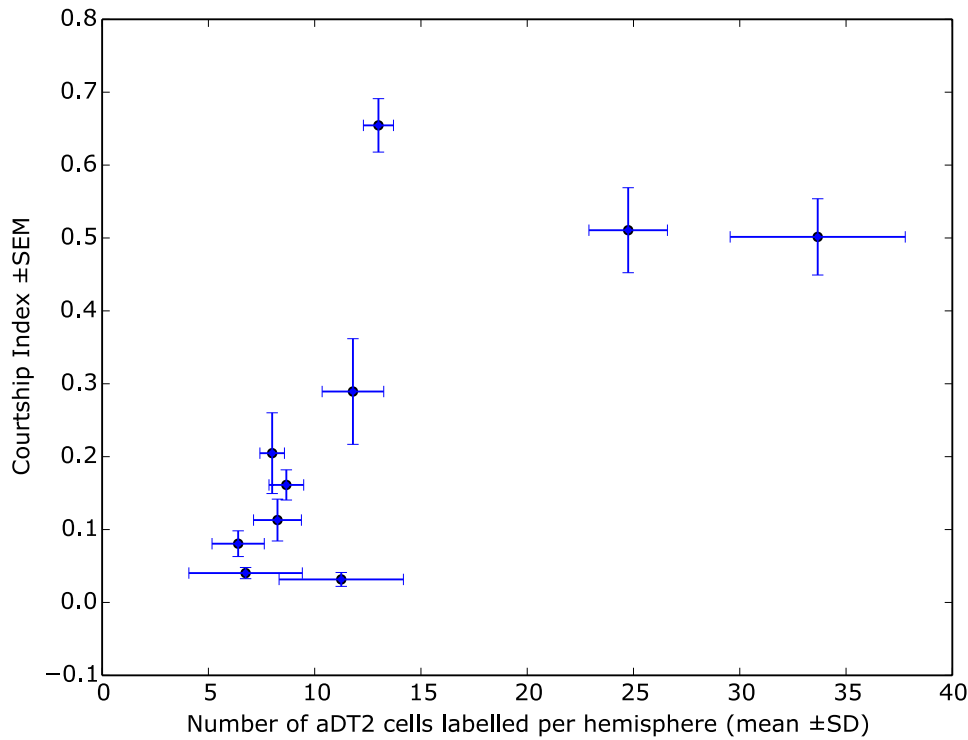
Vogels, T. P., & Abbott, L. F. (2009). Gating multiple signals through detailed balance of excitation and inhibition in spiking networks. *Nature Neuroscience*, 12(4), 483–491. doi:10.1038/nn.2276

Wang, L., Han, X., Mehren, J., Hiroi, M., Billeter, J.-C., Miyamoto, T., et al. (2011). Hierarchical chemosensory regulation of male-male social interactions in *Drosophila*. *Nature Neuroscience*, 14(6), 757–762. doi:10.1038/nn.2800

Yu, J. Y., Kanai, M. I., Demir, E., Jefferis, G. S. X. E., & Dickson, B. J. (2010). Cellular Organization of the Neural Circuit that Drives *Drosophila* Courtship Behavior. *Current Biology*, 20(18), 1602–1614.
doi:10.1016/j.cub.2010.08.025

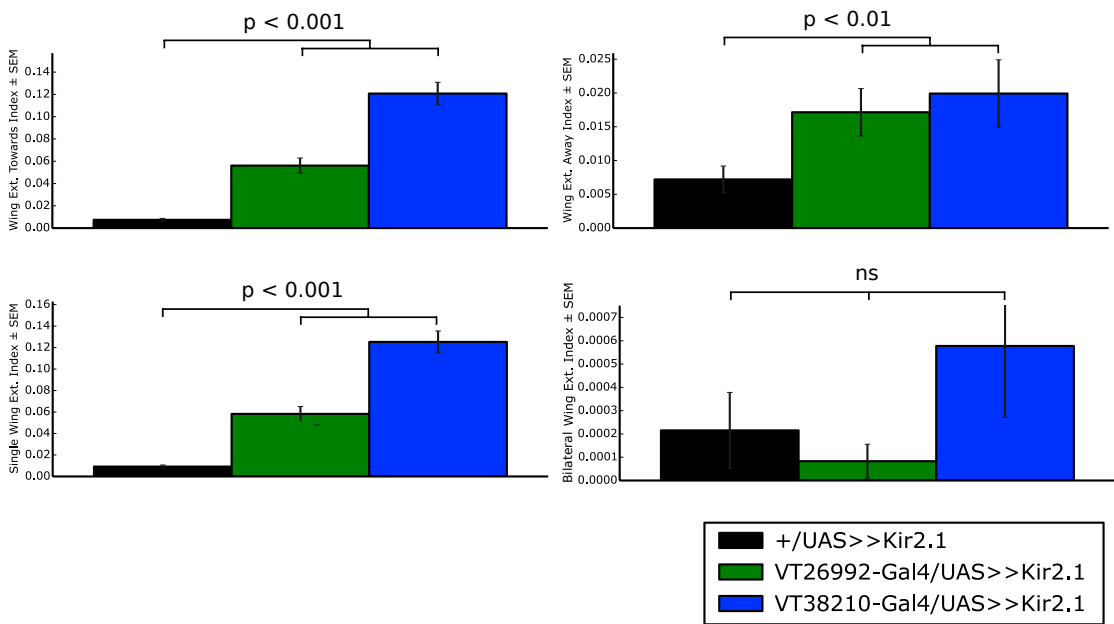
Supplementary material

Supplementary figure 1. aDT2 silencing using weak drivers.



Courtship index of aDT2-silenced flies (+ ; *UAS>stop>Kir2.1; fru^{FLP} / VT-GAL4*) using several drivers versus the average number of aDT2 cells labelled per hemisphere when the same driver is used to express GFP (+ ; *UAS>stop>mcd8GFP; fru^{FLP} / VT-GAL4*). Each blue marker represents mean values for a single driver line. Grey bars represent standard deviation (x-axis) and standard error of the mean (y-axis). 18<n<36 flies per line for courtship indices, and 8<n<16 brain hemispheres per line for cell counts.

Supplementary figure 2. Laterality of wing extension during aDT2 silencing.



Wing extension indices of aDT2-silenced flies (+ ; *UAS>stop>Kir2.1*; *fru^{FLP} / VT-GAL4*), where wing extension is toward the target (top left), away from the target (top right), unilateral (bottom left), or bilateral (bottom right). Dataset is identical to the data shown in Figure 2i. *p*-values are derived from a Mann-Whitney rank sums test.

Discussion

We developed a method, FlyMAD, to deliver acute stimuli for both thermo- and opto-genetic manipulation of neural activity in freely-moving fruit flies. Using FlyMAD, we delivered acute activation stimuli to neurons and observed the temporal relationship between neuronal activation and behaviour in greater detail than was previously possible with conventional activation methods. With the ability to deliver acute stimuli, we were able to address questions about high-order brain functions in which neuronal activity is uncoupled from behaviour. Specifically, we tested hypotheses concerning arousal.

From acute activation of P1 and pIP10, we learned that P1-activation is sufficient to induce a behavioural state change in which flies frequently court inanimate objects. The frequent, aberrant courtship is, in other words, a high rate of false positives in the selection of appropriate courtship targets. This high false positive rate resulting from P1 activation is analogous to the high error rate observed during mammalian hyper-arousal states, driven by increased excitatory drive (and tonic activity) of LC neurons ((Aston-Jones, Rajkowski, Kubiak, & Alexinsky, 1994)). The similarity of the behavioural phenotypes resulting from activation of LC neurons and P1 neurons suggests that activating P1 may have induced a state of courtship hyper-arousal. If this is true, similar behavioural defects during hyper-arousal would suggest that mammals and invertebrates both make use of arousal states during decision making. In a natural environment, evoking courtship arousal upon contact with a receptive female would be necessary to induce and maintain engagement in courtship as the female moves away.

Normal courtship and the behaviour observed during P1-induced hyper-arousal are not constant, but intermittent. It is not yet clear how neuronal activity mediates intermittent behavioural output during P1-induced hyper-arousal. One possibility is that, similar to heightened arousal in the LC-NE system in mammals, courtship arousal erroneously biases behavioural output toward courtship. With this model, the courtship observed during P1-dependent courtship hyper-arousal occurs when the hyper-aroused fly approaches an object while the system is biased toward courtship, erroneously identifying either the inanimate object as an appropriate courtship target, or courtship as an appropriate behaviour toward the inanimate object. A second possible mechanism for intermittent courtship during arousal is that arousal (or hyper-arousal) is insufficient to induce courtship in the absence of additional acute stimuli. In this model, courtship during arousal is gated by the necessity for an acute stimulus, such as an approaching object or a novel chemosensory input. These are two possibilities among several potential processing strategies.

Our experiments do not provide information about the neuronal activity that underlies courtship arousal. Many other known arousal states involve tonic or persistent neural activity (Jing, Gillette, & Weiss, 2009). In mammalian arousal, tonic activity of LC neurons is sufficient to induce hyper-arousal during decision-making tasks (Aston-Jones et al., 1994). In some cases, arousal is mediated by bistable neurons, such as the serotonin-dependent activity of the R15 neuron in *Aplysia*, which exhibit tonic activity for up to tens of minutes from a short depolarization (Lechner, Baxter, Clark, & Byrne, 1996). Also in *Aplysia*,

the cerebral-pedal regulator neuron fires persistently in response to food contact and increases arousal in feeding and locomotion circuitry (Teyke, Weiss, & Kupfermann, 1991). In most cases, and all three examples given here, persistent activity is mediated by neuromodulators.

Though extensive studies are still forthcoming, functional imaging of P1 neurons (Inagaki et al., 2013; Kohatsu, Koganezawa, & Yamamoto, 2011) has thus far shown only acute (or “phasic”) activity of P1. This does not preclude the existence of tonic P1 activity, because the stimuli or experimental conditions during P1 imaging may have been insufficient or non-conducive to induce tonic activity. Further imaging and electrophysiological studies will be crucial to understand the neural activity during persistent courtship. In particular, electrophysiological studies would expose tonic and/or phasic activity, identity of neurotransmitter or neuromodulator released by P1, and whether neighbouring P1 cells are electrically coupled. A caveat of physiology and imaging experiments, especially when observing tonic versus phasic activity, is the use of saline solutions. Reverberating and recurrent networks can be extraordinarily sensitive to local external concentration of calcium ions (Lau & Bi, 2009), which can be disrupted in non-intact assays. Therefore, it will be crucial to also perform behaviour experiments using intact animals. To determine whether the P1-dependent courting state requires persistent activity (synaptic release or depolarization) of P1, we are currently preparing experiments in which we first acutely activate P1 using optogenetic activators or TrpA1, and then acutely silence it with ShibireTS (Kitamoto, 2001) or optogenetic silencers (Chuong et al., 2014).

We posited above that intermittent courtship is mediated by arousal and hypothesized mechanisms for how courtship is turned on and off. Even during a single bout of courtship, the fly transitions between actions (such as wing song, following, or orienting). Therefore, there must be additional control of behavioural output to coordinate different actions during courtship. But how are individual actions controlled? Although several mechanisms are possible, we favour models in which P1 leads to the excitation of distinct command-like neurons that are specific to component behaviours. We favour this model based on the observation that activity of pIP10, a descending neuron, is necessary and sufficient for wing extension, but not other actions. We hypothesize that several other command-like neurons exist, each dedicated to a specific action (or subset of actions). Assuming that action selection is indeed mediated by specific command-like neurons, what mechanisms determine which command-like neurons are activated? We can imagine three distinct models for action selection:

First, action selection may function by a mechanism similar to sequential behaviours observed in other organisms. In some sequential behaviours, the execution of an action inhibits the previous action and/or promotes the next action. In *Drosophila* grooming behaviour, for example, a fly covered in dust will clean its body in a stereotyped, prioritized order, because it cannot clean two parts simultaneously (Seeds et al., 2014). In this case, the stimulus to groom all body parts is present at the onset and sequentially eliminated from body parts as the body is cleaned. In contrast with grooming, however, courtship actions are not mutually exclusive, but are executed in a general progression from early to late actions. In other sequential behaviours, an acute stimulus initiates a

sequence of actions. Feeding behaviour in *Aplysia*, for example, involves a progression through a series including posture adjustment, chewing, and gastric pumping actions, all of which are initiated by contact with food (Teyke et al., 1991). With a stationary target (food), initiating such a stereotyped program is sufficient; however courtship is a two-body behaviour with a moving, changing target, where the beginning of the sequence is not absolutely predictive of the end. It is therefore unlikely that the sequence of courtship behaviours is guided by neuronal activity that follows either of these sequential models, although we cannot exclude some lateral influence of actions to promote/suppress others in favour of a progression through the suite.

In a second, relatively simple model, each command-like neuron is activated during a limited range of arousal levels, with neurons that induce early actions responding to lower arousal levels than neurons that induce late actions. These ranges would likely overlap, because flies frequently execute multiple courtship actions simultaneously. It is unlikely, however, that a model based only on level of arousal is correct, because it would suggest an absolute pattern of actions that always begin and end at predictable moments. That is, two actions that occur at overlapping arousal levels would be expected to always occur simultaneously during a transition from the first action to the second. Courtship behaviour is variable, and such absolute transition states are not observed.

In a third model of action selection, P1-dependent courtship arousal biases action selection toward courtship, but execution of actions is gated by the activity of the target. This model is an extension of the second model, where level of arousal promotes a particular courtship action or set of actions, but the

execution of each action is gated individually by its own acute contextual requirements, such as proximity or velocity of the target, or the presence of an acute sensory cue.

To distinguish between models of action selection based only on arousal versus models involving gating or suppression of actions, it will be important to understand the specificity of courtship inhibition. If action selection requires gating or suppression, then there should be neurons whose activity correlates with suppression of single actions or subsets of actions. In chapter 2, we demonstrated that the activity of aDT2 is necessary and sufficient to suppress all courtship actions that we quantified (orienting, following, wing extension). It remains unclear, however, whether aDT2, a cluster with more than 30 cells per hemisphere, is homogenous or heterogeneous with respect to its influence on specific actions. Homogenous effects of aDT2 (a non-specific suppression of all courtship) may suggest that aDT2 activity reduces arousal. Heterogeneous effects of aDT2 (suppression of specific actions by subsets of aDT2) may suggest that aDT2 acts as a gating mechanism to suppress specific actions. To address this question, it will be necessary to manipulate the activity of subsets of aDT2 (either using genetically-defined subsets or stochastic expression methods) and determine whether behavioural defects can be restricted to specific actions within the suite of courtship behaviours.

The work presented here has laid the groundwork to study *Drosophila* courtship behaviour as a model of a complex and dynamic behaviour. We demonstrated temporal uncoupling of stimulus and behaviour that suggests that engagement in courtship behaviour is maintained by arousal. We speculated that

execution of courtship during arousal requires gating or suppression of behaviours, and identified a class of neurons that suppress courtship. With knowledge of how courtship behaviour is sustained and controlled, we hope to continue to deepen our understanding of how animals design and execute the complex behaviours that we observe in nature.

References

- Aston-Jones, G., Rajkowski, J., Kubiak, P., & Alexinsky, T. (1994). Locus coeruleus neurons in monkey are selectively activated by attended cues in a vigilance task. *The Journal of Neuroscience : the Official Journal of the Society for Neuroscience*, *14*(7), 4467–4480.
- Chuong, A. S., Miri, M. L., Busskamp, V., Matthews, G. A. C., Acker, L. C., Sørensen, A. T., et al. (2014). *Noninvasive optical inhibition with a red-shifted microbial rhodopsin*. *Nature Neuroscience* (Vol. 17, pp. 1123–1129). doi:10.1038/nn.3752
- Inagaki, H. K., Jung, Y., Hoopfer, E. D., Wong, A. M., Mishra, N., Lin, J. Y., et al. (2013). Optogenetic control of *Drosophila* using a red-shifted channelrhodopsin reveals experience-dependent influences on courtship. *Nature Methods*, 1–11. doi:10.1038/nmeth.2765
- Jing, J., Gillette, R., & Weiss, K. R. (2009). Evolving concepts of arousal: insights from simple model systems. *Reviews in the Neurosciences*, *20*(5-6), 405–427.
- Kitamoto, T. (2001). Conditional modification of behavior in *Drosophila* by targeted expression of a temperature-sensitive shibire allele in defined neurons. *Journal of Neurobiology*, *47*(2), 81–92. doi:10.1002/neu.1018
- Kohatsu, S., Koganezawa, M., & Yamamoto, D. (2011). Female Contact Activates Male-Specific Interneurons that Trigger Stereotypic Courtship Behavior in *Drosophila*. *Neuron*, *69*(3), 498–508. doi:10.1016/j.neuron.2010.12.017
- Lau, P.-M., & Bi, G.-Q. (2009). Reverberatory Activity in Neuronal Networks. In K. Josic, J. Rubin, M. Matías, & R. Romo, (Vol. 3, pp. 61–75). Springer Series.
- Lechner, H. A., Baxter, D. A., Clark, J. W., & Byrne, J. H. (1996). Bistability and its regulation by serotonin in the endogenously bursting neuron R15 in *Aplysia*. *Journal of Neurophysiology*, *75*(2), 957–962.
- Seeds, A. M., Ravbar, P., Chung, P., Hampel, S., Midgley, F. M., Mensh, B. D., & Simpson, J. H. (2014). A suppression hierarchy among competing motor programs drives sequential grooming in *Drosophila*. *eLife*, *3*, e02951.
- Teyke, T., Weiss, K. R., & Kupfermann, I. (1991). Activity of identified cerebral neuron correlates with food-induced arousal in *Aplysia*. *Neuroscience Letters*, *133*(2), 307–310.

Curriculum Vitae

Daniel E. Bath

Personal information

Address: Howard Hughes Medical Institute, Janelia Research
Campus, USA
Email: danbath@gmail.com
Date & place of birth: 27th of May, 1986; Wainfleet, Canada
Nationality: Canadian

Education

2011-2014
Doctorate
The University of Vienna
Vienna, Austria

2008-2010
Masters, Molecular Biology
The University of Western Ontario
London, Canada

2004-2008
Honours Bachelor, Genetics
The University of Western Ontario
London, Canada

2004-2008
Highschool
E. L. Crossley Secondary School
Pelham, Ontario, Canada

Research Experience

2011-2014
"Characterization of the neuronal mechanisms that
mediate temporal control of courtship behaviour in
Drosophila melanogaster."
Dr. Barry J. Dickson
Research Institute for Molecular Pathology, Vienna,
Austria
and

Janelia Research Campus, Ashburn, USA

2008-2010

“The role of post-translational modification in regulating the activities of Fushi Tarazu, a pair-rule segmentation protein in *Drosophila melanogaster*.”

Dr. Anthony Percival-Smith
The University of Western Ontario
London, Canada

2007-2008

“Characterization of the functional protein domains of Fushi Tarazu, a pair-rule transcription factor in *Drosophila melanogaster*.”

Dr. Anthony Percival-Smith
London, Canada

Conferences

2013

Talk: “FlyMAD: A novel technique for acute neuronal manipulation in freely-walking *Drosophila*.”
Cold Spring Harbor meeting for *Drosophila* neurobiology
Cold Spring Harbor, New York, USA

2013

Poster: “FlyMAD: A technique for rapid activation of neurons in freely-walking flies”
Cell symposium for Genes, Neurons and Circuits
Toronto, Canada

2010

Talk: “Post-translational modifications mediate the opposing regulatory roles of Fushi tarazu, a pair-rule transcription factor in *Drosophila melanogaster*.”
Genetics Society of Canada Annual Meeting
Hamilton, Canada

2009

Poster: “Mapping the phosphorylation sites of Fushi tarazu.”
European *Drosophila* Research Conference
Nice, France

2009

Poster: “The role of tyrosine in negative and positive regulation by Fushi tarazu, a pair-rule transcription factor in *Drosophila melanogaster*.”
The Genetics Society of America’s *Drosophila* Conference

Chicago, USA

Scholarships

2011-2013

Postgraduate Scholarship
Natural Sciences and Engineering Research Council of
Canada

2009-2010

Canadian Graduate Scholarship
Natural Sciences and Engineering Research Council of
Canada

2009

Ontario Graduate Scholarship
The Government of Ontario, Canada

2008

Undergraduate Summer Research Award
Natural Sciences and Engineering Research Council of
Canada

Publications

Daniel E. Bath, John R. Stowers, Dorothea Hörmann, Andreas Poehlmann, Barry J. Dickson and Andrew D. Straw (2014). FlyMAD: Rapid thermogenetic control of neuronal activity in freely-walking *Drosophila*. *Nature Methods*. *11*(7), 756–762.